NTNU

Norwegian University of
Science and Technology

Comparative Evaluation of the Performance of a Trimaran Seismic Vessel

Oda Myklebost

Marine Technology
Submission date: January 2016
Supervisor: Sverre Steen, IMT

Norwegian University of Science and Technology
Department of Marine Technology

NTNU Trondheim
Norwegian University of Science and Technology
Department of Marine Technology

MASTER THESIS IN MARINE TECHNOLOGY

AUTUMN 2015

FOR

Oda Myklebost

Comparative evaluation of performance of trimaran seismic vessel

The aim of the thesis is to evaluate the performance of a trimaran seismic vessel design, suggested by LMG Marin, in terms of seakeeping and operability. It shall be performed as a comparative study, where the performance is compared to a conventional monohull design. It is recommended to perform the following steps:

- Derive the criteria to be used for evaluation of the ship concepts. This is expected to require listing possible criteria, and discussing their relevance for the actual use of these ships. Weighting the different criteria might be required, and should therefore be discussed.
- Decide how to evaluate the criteria – what types of analysis are applicable and sufficient. What is the required level of accuracy, and what accuracy can be expected from the different candidate methods.
- Model the trimaran and the reference vessel in the softwares that is found suitable (and available) in the previous point.
- Perform the evaluations, compare the ships, identify and implement improvements to the trimaran design as far as time allows.

In the thesis the candidate shall present her personal contribution to the resolution of problem within the scope of the thesis work.

Theories and conclusions shall be based on mathematical derivations and/or logic reasoning identifying the various steps in the deduction.

The thesis work shall be based on the current state of knowledge in the field of study. The current state of knowledge shall be established through a thorough literature study, the results of this study shall be written into the thesis. The candidate should utilize the existing possibilities for obtaining relevant literature.

The thesis should be organized in a rational manner to give a clear exposition of results, assessments, and conclusions. The text should be brief and to the point, with a clear language. Telegraphic language should be avoided.

NTNU Trondheim
Norwegian University of Science and Technology
Department of Marine Technology

The thesis shall contain the following elements: A text defining the scope, preface, list of contents, summary, main body of thesis, conclusions with recommendations for further work, list of symbols and acronyms, reference and (optional) appendices. All figures, tables and equations shall be numerated.

The supervisor may require that the candidate, in an early stage of the work, present a written plan for the completion of the work. The plan should include a budget for the use of computer and laboratory resources that will be charged to the department. Overruns shall be reported to the supervisor.

The original contribution of the candidate and material taken from other sources shall be clearly defined. Work from other sources shall be properly referenced using an acknowledged referencing system.

The thesis shall be submitted electronically (pdf) in DAIM:

- Signed by the candidate
- The text defining the scope (signed by the supervisor) included
- Computer code, input files, videos and other electronic appendages can be uploaded in a zip-file in DAIM. Any electronic appendages shall be listed in the main thesis.

The candidate will receive a printed copy of the thesis.

Supervisor : Professor Sverre Steen
Start : 10.08.2015
Deadline : 26.01.2016

Trondheim, 10.08.2015

Sverre Steen
Supervisor

Preface

This thesis is the final work for the M.Sc. degree in Marine Technology. It was written during the fall semester 2015 at the Department of Marine Technology at the Norwegian University of Science and Technology.

The topic of this thesis is a seakeeping study of a new trimaran concept proposed by Oilcraft AS, who are collaborating with the design and engineering company LMG Marin. I was introduced to this project through an internship I had with LMG Marin during the summer of 2015. I immediately got interested in this project as it meant that I would get to be apart of the development of an innovative design. At the same time I was pleased with the opportunity of doing a seakeeping study to summarize my specialization within the field of hydrodynamics. This also allowed a practical approach to scientific research. However, the choice of topic for the M.Sc thesis at that point in time meant that I had to start from scratch as my pre-master project was on a completely different topic.

Most of the work load has been concentrated around learning the different softwares that were needed to perform the seakeeping analysis. I had no experience from Wasim when this work was initiated, and it turned out to be a time consuming affair to model and run analyzes on five different versions of the trimaran in parallel. During the process I ran into complications related to the software limitations, which I spent numerous hours trying to rectify. However, these challenges benefited in a greater learning outcome opposed to an unproblematic analysis.

I would like to thank my supervisor Sverre Steen, for sharing his valuable time to give guidance throughout the semester. I would also like to express my gratitude towards Robert Weir for pitching the idea of the topic for this thesis and to Per Martin Martinussen for his guidance and commitment to my work. I also want to thank my colleague Endre Sandvik, who also started learning the computer software Wasim at the beginning of this semester. Our collaboration gave a boost to the learning curve which I am sure saved me many hours of frustration.

Further, I would like to thank my family for their unconditional support and my fellow students for making these five years at NTNU a memorable and joyful experience. Lastly but not least, I would like to thank Kristian Mollestad. You always have my back.

Oda Myklebost

Trondheim, January 26th 2016

Summary

The scope of this thesis is proposed by the naval architect and maritime engineering company LMG Marin. Currently, they are in the early design phase of a new trimaran concept intended for the seismic industry. This new trimaran concept differs from other trimaran ships in both purpose area and hull configuration. Therefore it is in the interest of LMG Marin and the project initiator, OilCraft AS, to investigate how this hull configuration will affect the trimaran's seakeeping behaviour. The design process of a multi-hull allows the designer to be creative in his decision of hull layout. Therefore, different hull configurations had to be assessed. The main purpose of this study is to verify the potential advantages of the trimaran concept. In addition, this work aims to provide an insight into how the design process should proceed with respect to the main particulars of the three hulls.

The wave-vessel interaction problem was solved by use of numerical tools. Because the flow around the adjacent hulls will be more complicated opposed to a conventional monohull, it was decided that 2D strip theory method is not sufficiently sophisticated to treat hydrodynamic hull interaction. As the design process is still in the development stage, model trials were not an option. CFD analysis would provide satisfactory amount of information about the flow. However, CFD analysis was not considered an option due to the author's lack of experience with such tools. It was found unrealistic to obtain enough experience to implement the models and carry out the analysis within the allocated time. A literal review of previous research work revealed that 3D potential panel methods can be a good option when analyzing multi-bodied floaters. Such methods are able to describe the reflection of waves between adjacent floaters. Therefore, it was decided to run the simulations in the DNV software Wasim, which is based on a Rankine panel method. The disadvantage of potential theory methods is that viscous effects are neglected, meaning that an important contribution to the wave damping is lacking. When a 3D potential theory method is used to analyse a trimaran, the amplitude of the trapped wave between the hulls will be highly overestimated close to the resonance frequency. As a consequence, the results corresponding to wavelengths in proximity to the resonance frequency have a poor credibility. However, it was found by empirical approximation that the gap wave natural periods will be small compared to the periods of interest. In other words, a 3D potential theory can be justified for moderate to high sea states.

As the trimaran concept is intended for the seismic industry, a set of criteria based on the vessel's purpose were defined. Hospitable working conditions are desired as the ship will be a platform where geophysicists and observers perform assignments that require a high level of precision. Therefore, criteria for motion sickness incidence are included. The ship is also a platform where crew operate seismic equipment and it is required that these tasks can be conducted safely. Therefore, a criterion concerning motion induced

interruption of deck operations is included. As seismic surveys often last for very long periods, it is practical that the vessel can launch and recover a helicopter. For this reason, a helicopter operation criterion is included. Due to the additional hulls, it was found highly relevant to include the hydrodynamic hull interaction in the verification. All additional vibrations and noise will interrupt the seismic data quality. It is therefore important to avoid water impact on the cross-deck structure. It was not found any existing criteria specifically for seismic vessels. Therefore, a conventional seismic vessel has been included in the analysis for comparison.

Analysis problems were encountered when running simulations in Wasim in the case of forward speed. The gap wave amplitude increased without boundaries due to the lack of viscous damping. This was expected, but the solution strategy to exclude periods corresponding to the gap wave natural periods from the frequency set was not successful. Wasim models the incoming regular waves as a single irregular wave form, which makes it difficult to filter out the problematic frequencies. Therefore, an alternative plan was set: The criteria that are derived directly from the vessel's global motions were assessed by utilizing the 2D strip theory software Veres. The questions related to relative motion were answered based on Wasim results corresponding to zero forward speed.

Overall, it was found that the trimaran concept shows better seakeeping abilities than the comparison ship. The trimaran will be a more stable work platform in higher sea states. The disadvantage of this feature is that the trimaran has more prominent occurrence of motion induced interruptions (MII) during small sea states. Even then, the results are quite satisfying. The trimaran concept also showed good results with respect to motion sickness incidence (MSI). Most of the hull configurations that were assessed were superior to the mono-hull. A special feature of the hull configurations that were investigated in this work is that they have a very large beam. Also, the side hulls are very long compared to other trimarans and contribute to a large part of the total displacement. It was found that these attributes result in quite similar roll and pitch natural periods. This implies that the trimaran will show a "cork-screw" motion that is a characteristic of many catamarans. However, this can be avoided by making the side hulls shorter and half planing. Due to the analysis problems, it was difficult to make a definite conclusion regarding the relative motion between wave and vessel in the gap. However, the results imply that the tunnel height should be at least four meters to avoid cross-deck water impact. However, the results indicate that viscous effects will affect the results and should be taken into account to obtain better results. It is therefore recommended to perform model tests to investigate the relative motion. The alternative is to perform an URANS-VOF simulation to include both viscous and rotational effects in the flow and free surface waves.

Sammendrag

Ideen til denne oppgaven er foreslått av selskapet LMG Marin, som har lang erfaring innen utvikling av skip og maritime konstruksjoner. For tiden er de i utviklingsfasen av et nytt trimarankonsept rettet mot seismikkindustrien. Dette nye trimarankonseptet skiller seg fra andre trimaranskip både i bruksområde og skrogutforming. Derfor er det av interesse for LMG Marin og prosjektets initiativtaker, OilCraft AS, å undersøke hvordan denne skrogutformingen vil påvirke trimaranens sjøegenskaper. Fordi en designer står fritt til å være kreativ i sin avgjørelse av skrogenes utforming er det nødvendig å undersøke ulike skrogutforminger. Hovedmålet med denne oppgaven er å verifisere de potensielle fordelene til trimarankonseptet. I tillegg forsøker denne oppgaven å gi innsikt i hvordan designprosessen bør fortsette med tanke på bestemmelse av trimaranens hoveddimensjoner.

Problemet som tar for seg interaksjonen mellom bølge og fartøy har blitt løst ved bruk av numeriske verktøy. Strømningen rundt de nærliggende skrogene vil være mer komplisert sammenlignet med et enkeltskrog. Derfor ble det bestemt at en metode som benytter 2D stripeteori ikke er tilstrekkelig sofistikert til å behandle hydrodynamisk skroginteraksjon. Siden designprosessen fortsatt er i utviklingsfasen har det ikke vært aktuelt å gjøre modellforsøk. En CFD analyse ville ha gitt en tilfredsstillende beskrivelse av strømningen. Fordi forfatteren har manglende erfaring med slike verktøy ble det ikke ansett som et alternativ å benytte CFD. Det ble ansett som urealistisk å tilegne seg nok erfaring til å kunne modellere skipene og gjennomføre analysene i løpet av den tilgjengelige tiden. Et litterært søk gjennom tidligere forskingsarbeid avdekket at 3D potensialteorimetoder kan være et godt alternativ når man skal analysere flytere bestående av flere skrog. Slike metoder er egnet til å beskrive refleksjonen av bølger mellom skrogene. Derfor ble det besluttet å kjøre simuleringer i programvaren Wasim, utviklet av DNV, som baserer seg på en Rankine panelmetode. Ulempen med potensialteori er at viskøse effekter neglisjeres. Dette betyr at et viktig bidrag til bølgedemping ikke blir tatt i betraktning. Når potensialteori brukes til å analysere en trimaran vil bølgene mellom skrogene bli sterkt overestimert nær resonansfrekvensen. Som en følge av dette vil resultatene knyttet til bølgelengder i nærheten av resonansfrekvensen ha liten troverdighet. Imidlertid ble det funnet ved bruk av empiriske anslag at bølgen mellom skrogene vil ha en egenperiode som er liten i forhold til de mest interessante periodene. Med andre ord kan 3D potensialteori forsvares under forhold med moderat til høy sjø.

Siden trimarankonseptet er ment for den seismiske industrien ble det definert et sett med kriterier basert på fartøyets spesifikke formål. Bekvemme arbeidsforhold er ønsket. Dette fordi skipet vil fungere som en plattform der geofysikere og observatører skal utføre oppgaver som krever et høyt presisjonsnivå. Derfor er kriterier for sjøsyke inkludert. Skipet skal også være en plattform der mannskap opererer seismisk utstyr. Det er viktig at disse oppgavene kan gjennomføres trygt. Derfor er det inkludert et

kriterium som omfatter forstyrrelse av dekkoperasjoner på grunn av skipets bevegelser. I og med at seismiske undersøkelser ofte varer i svært lang tid vil være praktisk at et helikopter kan lette og lande fra skipet. Av den grunn er det inkludert et kriterium som tar for seg helikopteroperasjon. På grunn av sideskrogene ble det funnet svært relevant å inkludere den hydrodynamiske skroginteraksjonen i verifiseringen. All støy og alle slags vibrasjoner vil være med på å forstyrre den seismiske datakvaliteten. Det er derfor viktig å unngå at vann slår opp i konstruksjonen som knytter sideskrogene til hovedskroget. Det ble ikke funnet noen eksisterende kriterier som gjelder spesifikt for seismikkfartøy. Derfor har et konvensjonelt seismisk fartøy blitt inkludert i analysen til sammenligning.

Det oppstod analyseproblemer da simuleringene ble kjørt i Wasim i de tilfellende hvor skipet har fremdriftshastighet. Amplituden til bølgen mellom skrogene økte uten grenser på grunn av mangel på viskøs demping. Dette var som forventet, men løsningsstrategien som gikk ut på å fjerne perioder nær egenperioden var ikke vellykket. Wasim modellerer de regulære innkommende bølgene som en enkel uregelmessig bølgeform. Dette gjorde det vanskelig å filtrere ut de problematiske frekvensene. Det ble derfor satt opp en alternativ plan: Kriteriene som utledes direkte fra skipets globale bevegelser ble vurdert ved å benytte programvaren Veres, basert på 2D stripeteori. Spørsmålene knyttet til relativbevegelse ble basert på Wasim-resultater fra kjøringer der skipet ikke har fremdriftshastighet.

Totalt sett ble det funnet at trimarankonseptet viser bedre sjøegenskaper enn sammenligningsskipet. Trimarankonseptet vil være en mer stabil arbeidsplattform ved høye sjøtilstander. Ulempen med denne egenskapen er at trimaranen har mer fremtredende forekomst av avbrutte dekkoperasjoner grunnet skipets bevegelse (MII) ved mindre sjøtilstander. Selv da er resultatene nok så tilfredsstillende. Trimarankonseptet viste også gode egenskaper når det kommer til forekomsten av sjøsyke (MSI). De fleste skrogutformingene viste overlegne resultater sammenlignet med det konvensjonelle skipet. Et særegent trekk ved de skrogutformingene som ble undersøkt er at de har meget bred hekk. I tillegg er sideskrogene relativt lange og skrogene bidrar til en større del av oppdriften enn det som er vanlig for trimaraner. Det ble funnet at disse egenskapene bidrar til relativt like egenperioder i rull og stamp. Dette innebærer at forholdene ligger til rette for at trimaranen vil ha en såkalt skrukorkbevegelse, noe som ofte er sett hos katamaraner. Dette kan imidlertid unngås ved å ved å gjøre sideskrogene kortere og gi dem en halvplanende skrogform. På grunn av analyseproblemer, var det vanskelig å gi en endelig konklusjon angående relativbevegelsen mellom bølge og fartøy i gapet mellom skrogene. Resultatene antyder at tunnelhøyden bør være minst fire meter for å unngå at vann slår opp i konstruksjonen. I og med at resultatene også viser at viskøse effekter vil ha en betydelig påvirkning på resultatene bør disse bli tatt med i betraktningen for å oppnå bedre resultater. Det anbefales derfor å gjøre modellforsøk for å undersøke relativbevegelsen. Alternativet er å utføre en URANS-VOF simulering for å inkludere viskøse- og rotasjonseffekter i strømningen og bølgene på den frie overflaten.

Contents

List of Figures

List of Tables

Nomenclature

Symbols and abbreviations are generally defined the first time they appear in the text.

Abbreviations

CFD	Computational fluid dynamics
GM	Metacentric height
MII	Motion induced interruptions
MSI	Motion sickness incidence
RAO	Response amplitude operator
RMS	Root mean square
URANS	Unsteady Reynolds-averaged Navier–Stokes
VOF	Volume of fluid
2D	Two dimensional
3D	Three dimensional
4D	Four dimensional

Greek letters

β	Frequency ratio
β	Stability parameter
Δ	Weight of vessel
Δ^*_{SH}	Percentage of the total displacement supported by each side hull
$\vec{\delta}$	Displacement vector
ϵ	Stochastic phase angle
ζ	Wave elevation
η	Vessel response
θ	Wave direction
μ	Empirical parameter

ξ	Critical damping ratio
ρ	Density
σ	Empirical parameter
σ	Standard deviation
ϕ	Wave potential
φ	Phase angle
ψ	Spline coefficient
ω	Wave frequency
ω_d	Damped natural frequency
ω_e	Encounter frequency
ω_n	Natural frequency
Ω	Rotation

Roman Letters

A_{jk}	Coupled added mass coefficient
$\bar{a}$	The time integral of the absolute value of acceleration imparted in each half-wave cycle
B	Width of hull
B_G	Width of gap between side hull and main hull
B_{jk}	Coupled damping coefficient
B_{SH}	Width of side hull
B_1	Linear roll damping coefficient
B_2	Quadratic damping coefficient
B_v^{crit}	Critical damping in roll
b_1	Linear non-dimensional damping coefficient
b_2	Quadratic non-dimensional damping coefficient
c	Phase velocity
C_b	Block coefficient
C_{jk}	Coupled restoring coefficient
$\ddot{D}_2$	Lateral acceleration

$\ddot{D}_3$	Vertical acceleration
$E(\eta_{max})$	The expected maximum of the response
F_j	Hydrodynamic exciting loads
f	Frequency
$\mathcal{F}_h$	Grid froude number
$\mathcal{F}_n$	Froude number
G_j	Hydrodynamic loads due to the body motions
G_{Li}	Lateral force estimator
g	Gravitational acceleration
H_j	Hydrodynamic forces and moment amplitudes
H_s	Significant wave height
$H(\omega)$	Transfer function
$\|H(\omega)\|$	RAO
h_x	Smallest panel length in the longitudinal direction
k	Wave number
L_{oa}	Length over all
L_{pp}	Length between perpendiculars
L_{SH}	Length of side hull
L^*_{SH}	Length of side hul in percentage of main hull
$^l/_h$	Tipping coefficient
L_1	The length of the side hull affected by hull interaction
M_i	Number of total MII's during a task with a duration of T_T
m_k	The kth spectral moment
M_{jk}	Generalized mass matrix
p	Pressure
r	Radius of gyration
S_B	The submerged portion of the hull
$S_{\bar{B}}$	The mean submerged portion of the hull
S_F	Border defining the surface of the sea
S_∞	The border of the sea infinitely distant from the vessel

$S(\omega)$	Wave spectrum
$S_R(\omega)$	Response spectrum
T	Draft
T	Period
T_{GLi}	Zero up-crossing period of GLi
T_{jk}	Hydrodynamic force or moment in the jth direction due to a unitary displacement in the kth direction
T_n	Natural period
T_T	Time duration of a specific task
T_z	Zero up-crossing period
Δt	Time step
U	Average forward speed
V	Slip speed
$\vec{W}$	Mean velocity field
$X(\omega)$	Transfer function for excitation loads

CHAPTER 1

Introduction

A trimaran ship concept has been proposed by OilCraft AS. The main idea of the ship design is to take advantage of two outrigger hulls to increase the width of the stern. By utilizing three slender hulls, the ship will have a lower resistance than the equivalent monohull.

The concept is intended for the seismic industry where there is a demand for wide ship types. The proposed trimaran concept has a width that is almost twice the width of a conventional seismic research vessel. This means that the trimaran will be able to tow a large number of cables and secure sufficient spread. The trimaran will have a large deck area as a consequence of the connecting structure between the side- and main hull. The large deck area will provide enough storage space for the seismic equipment and provide good working conditions for the crew that operates the equipment.

The concept of trimaran ships is not new. There exists many sailing yachts, naval ships and passenger ferries with three hulls. A common feature for most of the trimaran concepts that exist today is that they are designed to operate with high speeds and have side hulls that are very small compared to the main hull. The trimaran concept that is the subject of investigation in this thesis has a hull configuration that differs from typical trimaran designs. The side hulls have a significant contribution to the displacement which makes it necessary to investigate the influence on the transverse stiffness and accelerations. The operability criteria will also differ from existing designs in terms of speed and purpose area.

The potential advantages towards the seismic industry are clear. The objective of this thesis is to perform an initial feasibility study to verify the seakeeping abilities of this new trimaran concept. The introduction of two additional hulls allows the designer to be flexible in the choice of hull configuration. It is therefore necessary to evaluate how this choice will affect the hydrodynamic performance of the trimaran. Another consequence of the two side hulls is that the flow around the hulls will be more complicated. An important question to be answered is how the choice of hull configuration will affect the interaction between the hulls.

In order to derive the criteria to be used for the evaluation of the trimaran concept a review of the seismic industry will be conducted. The objective is to identify the purpose area and desired characteristics of seismic vessels. Based on the findings from this review, a set of criteria will be established. The wave-vessel interaction problem will be solved with means of numerical tools. Due to the complexity of the trimaran, a review of available tools is necessary. The objective is to determine what type of analysis that is sufficient, applicable and also possible to utilize with respect to the available time and prerequisites of the author. Different hull configurations will be analyzed with reference

to the specified criteria to provide insight views on the configuration choice for the trimaran concept.

An essential question that will not be answered in this thesis is about the construction- and operating costs. Good sales arguments are obtained if it can be proved that this new concept has favorable seakeeping characteristics opposed to conventional vessels. However, experience shows that ship owners are hesitant to innovate designs and often settle for projects that have low investment costs. A potential benefit of the trimaran concept is reduced operational costs due to lower ship resistance. In addition, a cost analysis must focus on the possible savings due to the increased amount of acquired seismic data per sail line. If ship owners can be convinced that the increased construction costs can be justified by the low operational costs, this new concept will definitely create an interest.

The structure of this thesis is described in the following. Chapter 2 gives a presentation of the trimaran concept, including the different hull configurations that is to be evaluated. Chapter 3 provides an overview of the main aspects of the seismic industry. The operational criteria are presented in chapter 4. Chapter 5 describes the method of evaluating the criteria. This includes a literature review of the available analysis tools and arguments the choice of method. Chapter 6 describes the underlying theory and features of the software that was chosen to solve the wave-vessel interaction problem. This chapter also describes how the model was implemented in the software. Chapter 7 describes the challenges related to the analysis execution and the alternative approach that lead to the results. Chapter 8 contains the results and the discussion of the findings. The conclusions are given in chapter 9 together with recommendations for further work.

CHAPTER 2

The Trimaran Concept

The initiator of the trimaran that is the subject of this thesis is the design company OilCraft lead by Stian Teige. OilCraft has recently teamed up with the naval architect and maritime engineering company LMG Marin that has a broad experience since 1943. This is reflected in the involvement in more than 1000 ships. Together they have established LMG OilCraft that offers a combination of the innovative and create design solutions of OilCraft together with the solid engineering experience provided by LMG Marine.

The main intention of the trimaran concept is to meet the demand for a functional design with a wide stern that is seen in the seismic market. With the proposed design OilCraft LMG aims offer a preferred solution in terms of streamer capacity, stability, fuel efficiency and motion characteristics. An increased streamer capacity generates a need for a large deck space for storing of equipment. This need is met by taking advantage of the cross-structure and a large longitudinal extension of the side hulls.

At the current time, the trimaran project is still in the development stage. The main question of this study is suggested by LMG Marin. The objective is to investigate the motion characteristics of the preliminary hull configuration, which is yet to be fixed.

As a first approach to the verification of the trimaran a calm water resistance evaluation was initiated by OilCraft (Berchiche, 2014). This evaluation was performed by the means of CFD simulations in order to obtain the drag force as well as the wave elevations at speeds ranging from 5-25 knots. The CFD study was performed by MARINTEK. It was found that the vessel presents reasonable calm water resistance performance, with a very small wave resistance and side hull resistance at speeds of 5 and 10 knots. However, at larger speeds is was found that the contribution to the total resistance from the side hulls was too prominent. It was argued that the large resistance could be partially explained by the deep submergence of the side hulls.

As a continuation of this first approach, LMG Marin has suggested five different versions of the trimaran. The hull forms are represented graphically by line drawings together with 3D drawings. These can be seen in section 2.1 through 2.5. The main dimensions of the main hull and side hulls of each version are summarized in table 2.1. As can be seen from the figures and table 2.1, the versions differ in the fullness of the main hull and side-hulls and the draft of the side hulls. All the versions have the same extreme width, which means that the gap between the outriggers and the main hull will vary. With reference in the CFD report it can be argued that a small draft is preferred in order to reduce the resistance. It is also known that a slender hull will have improved frictional resistance compared to a ship of equal length but larger displacement (Steen,

2011). Steen (2011) also explains that a reduction in the fullness will reduce the resistance at the expense of the transverse stability. However, one of the benefits of a trimaran is that the the hulls can be made more slender without violating the stability requirements. This can be explained by the additional restoring forces that are related to the displacement of the side hulls and the up-righting arm that spans from the roll centre and the buoyancy centre at the outriggers.

The main dimensions of the versions are based on the general arrangement drawings done by OilCraft. The general arrangement is designed according to the requirements for storage volume and storage space with respect to the number of streamers and other seismic equipment. The objective of comparing this set of hull configurations is to obtain a good idea of how the distribution of volume displacement will affect the seakeeping abilities. Based on the discussion above, it is clear that each of these versions will have varying resistance performance. Another significant difference that must be taken into account will be the building costs. Roughly speaking, the most expensive version to build will be the version that requires the most steel. However, a cost analysis is beyond the scope of this work.

As mentioned, the presence of side hulls will have an important influence on the transverse stability compared to a monohull with same dimensions as the main hull. The restoring moment will increase with the distance between the side-hull and main hull. As the righting moment is influenced by the instantaneous buoyancy, the shape of the side hull will affect the roll motion. It is important that a vessel has sufficient stability such that there is minimal risk of capsizing. However, there exist vessels with a very high stability, i.e large GM values, which means that the vessel will return abruptly to upright position when exposed to a heeling moment. This case has been experienced for catamaran vessels (Zhang, 1997). Such stiff rolling motion can lead to discomfort and motion sickness among the passengers. Because the trimaran has the potential to show similar behaviour, the passenger's well-being should be given attention when comparing the five different versions of the trimaran survey vessel.

Apart from the triple hull configuration, the width-to-length[1] ratio of the trimaran vessel differs from conventional ships. As can be seen from table 2.1, the width-to-length ratio is 0.54 for version 1, 2 and 5, while version 3 and 4 have a width-to-length ratio of 0.42. These values are quite extreme compared to conventional mono-hull survey vessels which normally have a width-to-length ratio in the range 0.15-0.25. This characteristic of the trimaran concept gives rise to a hypothesis about the seakeeping behaviour. According to NATO (2000), an effect of slender hulls is that the vessel will have reduced resistance to pitching, especially at head seas, compared to a mono hull. When this effect is combined with the high stability and stiff roll motion, the end result can be synchronised roll and pitch natural periods. The relation between natural pitch and roll periods will lead to a "corkscrew" motion that is reported to be very uncomfortable for the people

[1]The width-to-length ratio it is calculated as $\frac{b}{l}$, where b and l are the width and length of the hull.

aboard. This corkscrew motion is typical for catamarans and it has been a challenge to overcome this problem, because the hull separation has to be quite small in order to keep sufficient separation between roll and pitch motion (NATO, 2000). It is claimed in many sources that trimarans have the advantages of a catamaran in terms of large deck area and stability, but at the same time show seakeeping abilities more similar to a monohull. See for instance Fang and Too (2006), Zhang (1997) and Yun and Bliault (2012). This is summarized in the maritime trade journal Ship&Offshore:

> "The vessel's unique trimaran hull form combines the softer roll of monohulls with the low resistance, stability and carrying capacity of catamarans. (...) Most importantly, the trimaran's lower roll speed means lower accelerations experienced by passengers, significantly reducing passenger seasickness. Studies show that motion sickness on the trimaran will be approximately 56 per cent lower than on a 100 metre catamaran operating in head seas. Even larger benefits are realised in other headings."

In order to achieve such superior advantages for a specific trimaran design it is important that the hull configuration is chosen properly. This is a consideration that should be kept in mind during a verification of a new trimaran concept, especially when the design has a pioneering hull configuration. The OilCraft trimaran concept differ from existing trimaran designs in the large width-to-length ratio. See table 2.2 in Zhang (1997) for examples of principal characteristics for a number of trimaran displacement ships. In addition, the side hulls of the OilCraft trimaran are longer compared to the examples in Zhang (1997). It should also be noted that the OilCraft trimaran concept has a fuller main hull, see table 2.1 "main hull". The five OilCraft trimaran versions have a width-to-length ratio in the range of 0.17-0.23, while the examples found in Zhang (1997) is in the range of 0.055-0.08. This can also be reflected in the block coefficient, C_b, that is in the range of 0.63-0.74 for the OilCraft trimaran while the example ships have block coefficients in the range of 0.39-0.56. Blanchard and Ge (2007) state that the corkscrew motion will be avoided for a trimaran because the pitch period can be tuned to make the trimaran behave more like a monohull. To make this statement applicable it is assumed that the main hull is very long and slender. Based on this discussion it is important to investigate the relation between the pitch and roll period for the various versions of the OilCraft trimaran concept.

It is also important to have in mind that the presence of side hulls will make the flow around the ship more complicated compared to a monohull (Zhang, 1997). When a multi-bodied vessel is interacting with waves, each body will scatter waves. The waves scattered by one body will contribute to the response of another body and vice versa (Chen and Fang, 2001). Factors that are important for the effect of wave interaction between the hulls of a trimaran are the speed of the vessel and the distance between the main hull and the side hulls. In general the wave interaction will be more important

when the side hulls are close to the main hull. For high speeds the scattered waves from one body will be passed by the vessel before they reach the adjacent bodies. However, seismic vessels normally operate at low speeds unlike most trimaran concepts which are often classified as high-speed vessels. Because the OilCraft trimaran has relatively small clearance between the main hull and the side hull it is indeed relevant to investigate the hull interaction. A concern related to hull interaction is the relative motion between the water surface and the cross-deck structure. The relative vertical velocities between the water and ship may lead to wet-deck slamming, which is a problem with respect to safety and structural integrity. Blanchard and Ge (2007) states that wet-deck slamming is more often a problem for catamarans than it is for trimarans, due to the fact that the leading edge of the trimaran cross-structure can be located fairly well aft. As mentioned, the length of the side hulls of the OilCraft trimaran extend relatively far towards the front of the ship. As can be seen from table 2.1 the length of the side hull is ranging from 54.5%-63.6% of the main hull, which means that the leading edge of the cross structure will be located such that probability of wet-deck slamming can not be neglected.

The designer of a trimaran vessel has the advantage of flexibility when it comes to hull configuration and volume distribution. However, it is clear from the discussion above that the hull configuration will influence many aspects of the hydrodynamical performance. Because this thesis aims to verify a design that is still in the early development stage, it is convenient to include several alternatives of hull configurations in the verification study. As a consequence, the comparison will give an indication of which direction the design process should proceed.

Table 2.1: Main particulars of the five different versions of the trimaran concept. (Δ^*_{SH} denotes the percentage of the total displacement supported by each of the side hulls. L^*_{SH} denotes the length of the side hull expressed in percentage of the main hull)

		VERSION 1	VERSION 2	VERSION 3	VERSION 4	VERSION 5
				MAIN HULL		
L_{oa}	[m]	110	110	120	120	110
L_{pp}	[m]	99.3	99.3	109.3	109.3	99.3
B	[m]	25	25	23	20	20
T	[m]	7.5	7.5	7.5	8.0	8.0
Δ	[t]	12 091	14 139	13 404	12 895	11 321
C_b	[-]	0.63	0.74	0.69	0.72	0.69
B/L	[-]	0.23	0.23	0.19	0.17	0.18
				SIDE HULL		
L_{SH}	[m]	60	60	70	70	70
B	[m]	7.4	6.0	4.0	4.0	6.0
T	[m]	7.5	3.5	3.5	4.0	5.0
Δ	[t]	1 707	646	502	689	1 507
C_b	[-]	0.5	0.5	0.5	0.6	0.7
B/L	[-]	0.12	0.1	0.06	0.06	0.08
Δ^*_{SH}	[%]	11.0	4.2	3.5	4.8	10.5
L^*_{SH}	[%]	54.5	54.5	58.3	58.3	63.6
				TOTAL VESSEL		
B	[m]	50	50	50	50	50
Δ	[t]	15 504	15 431	14 409	14 272	14 335
B/L	[-]	0.54	0.54	0.42	0.42	0.54

2.1 Version 1

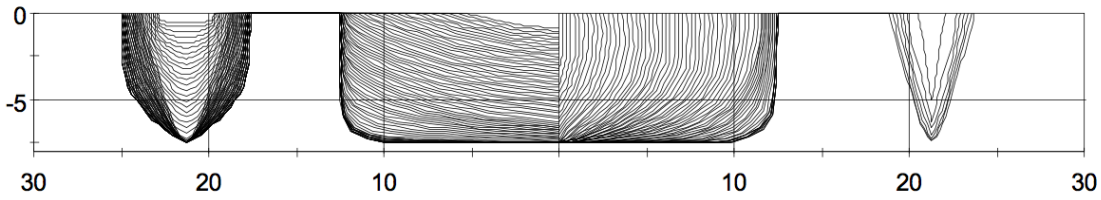

Figure 2.1: Veres plot of Trimaran Version 1

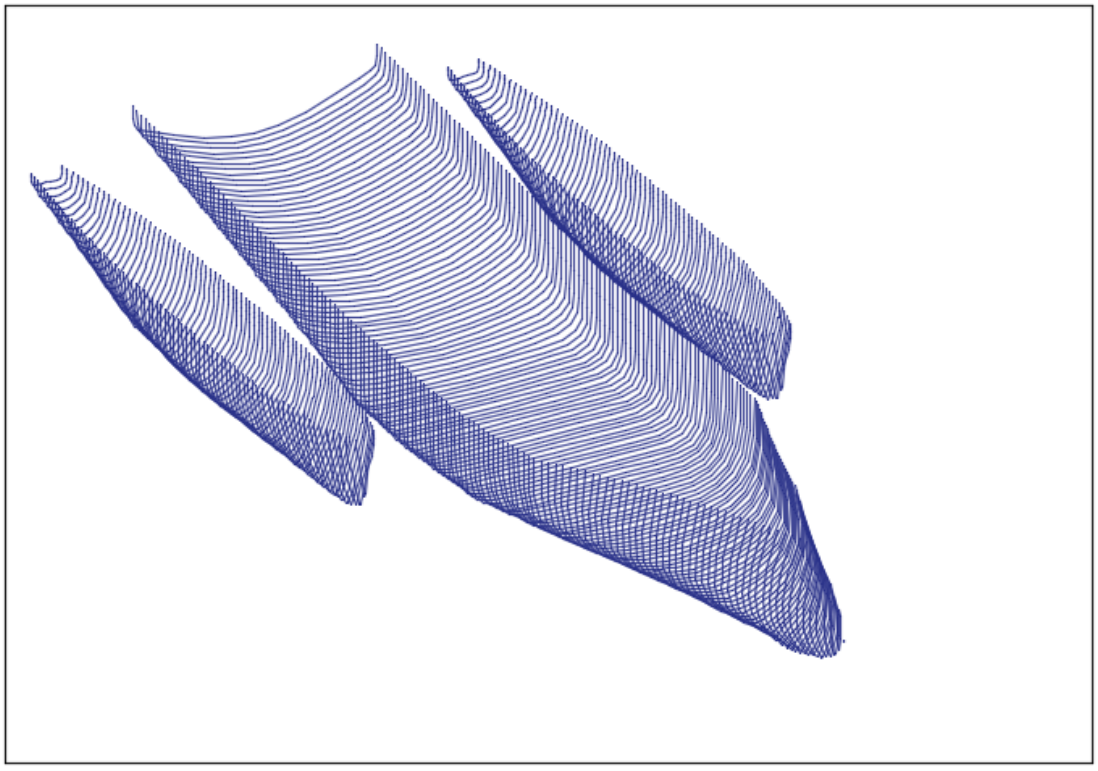

Figure 2.2: 3D view of Trimaran version 1

2.2 Version 2

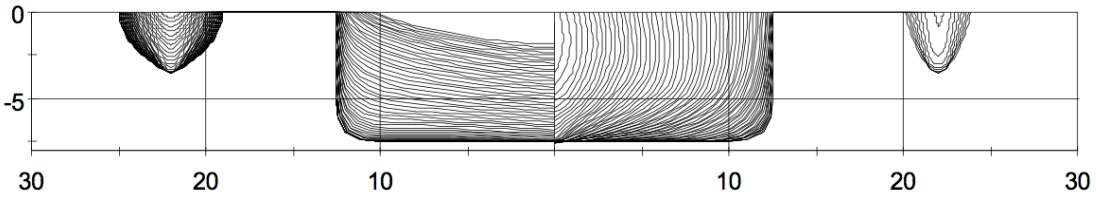

Figure 2.3: Veres plot of Trimaran Version 2

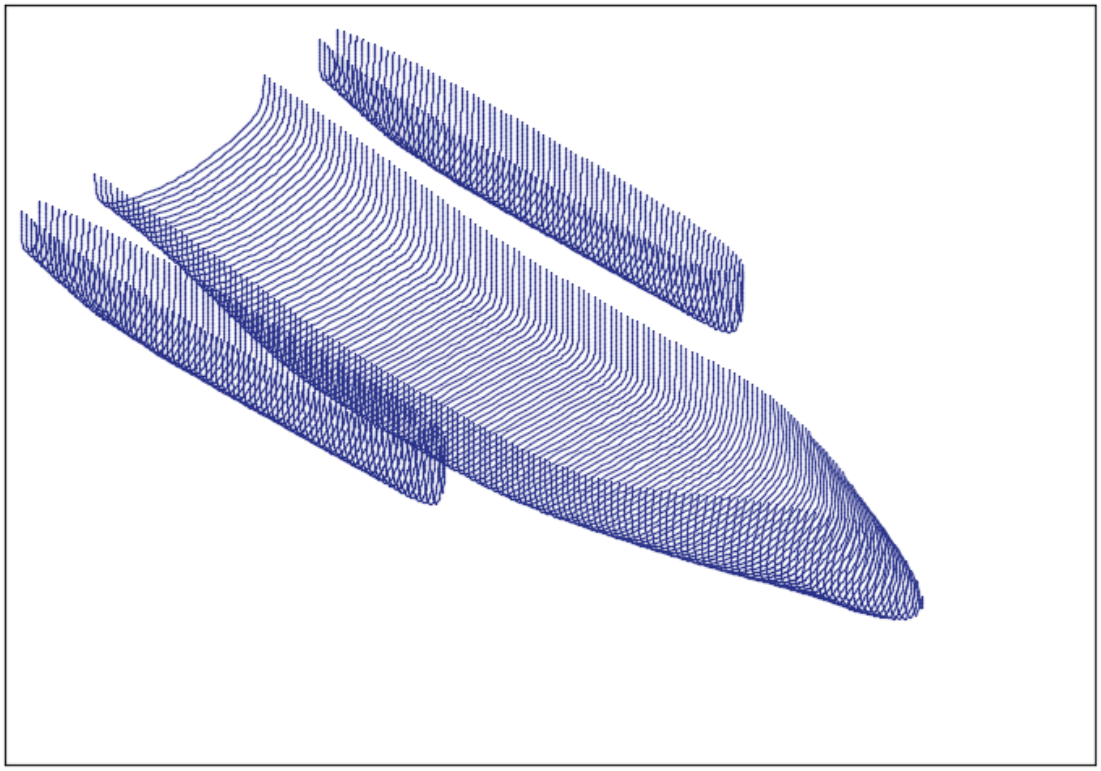

Figure 2.4: 3D view of Trimaran version 2

2.3 Version 3

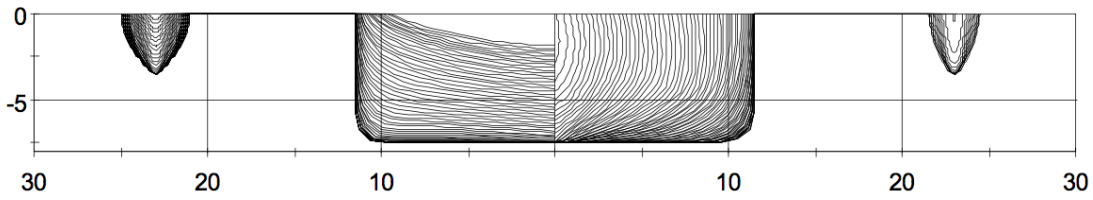

Figure 2.5: Veres plot of Trimaran Version 3

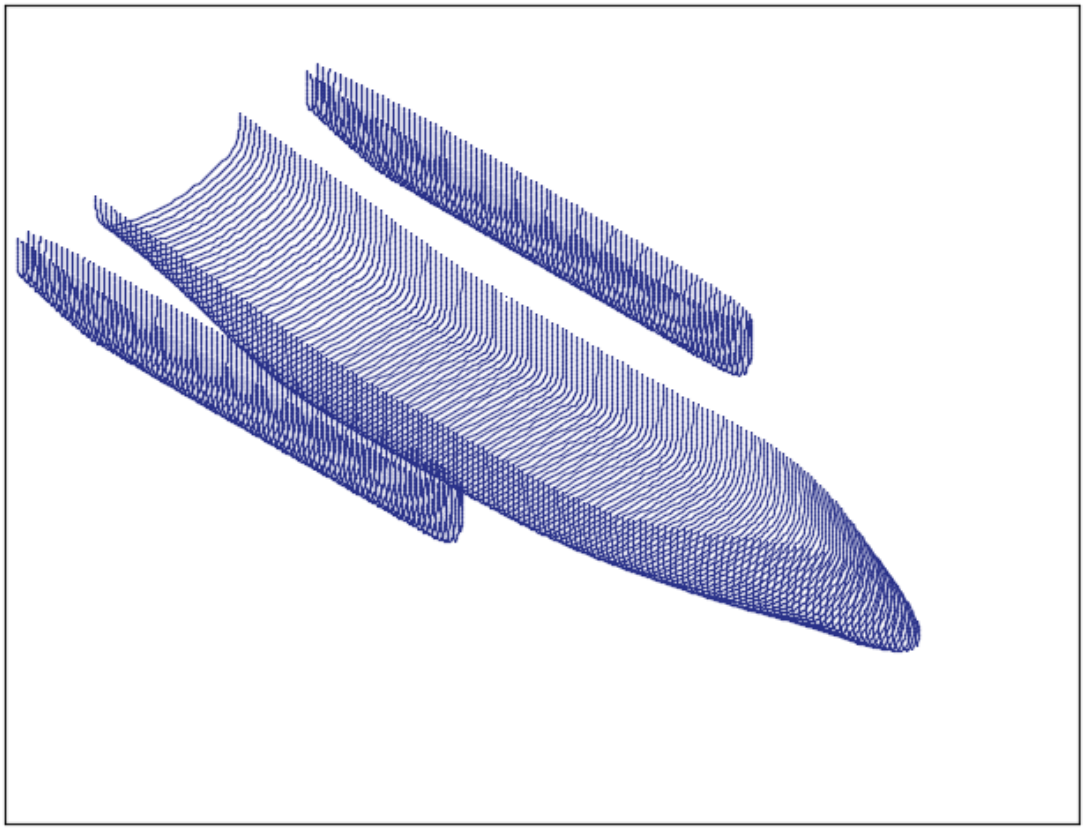

Figure 2.6: 3D view of Trimaran version 3

2.4 Version 4

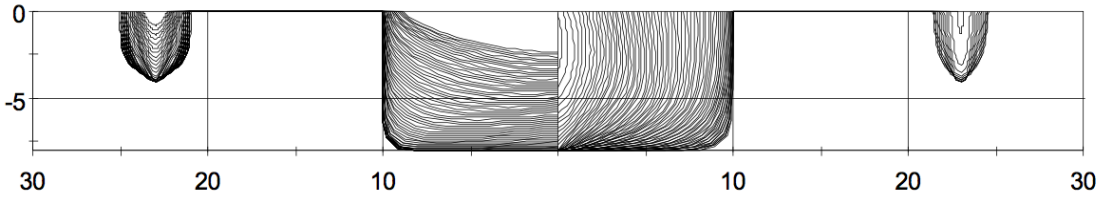

Figure 2.7: Veres plot of Trimaran Version 4

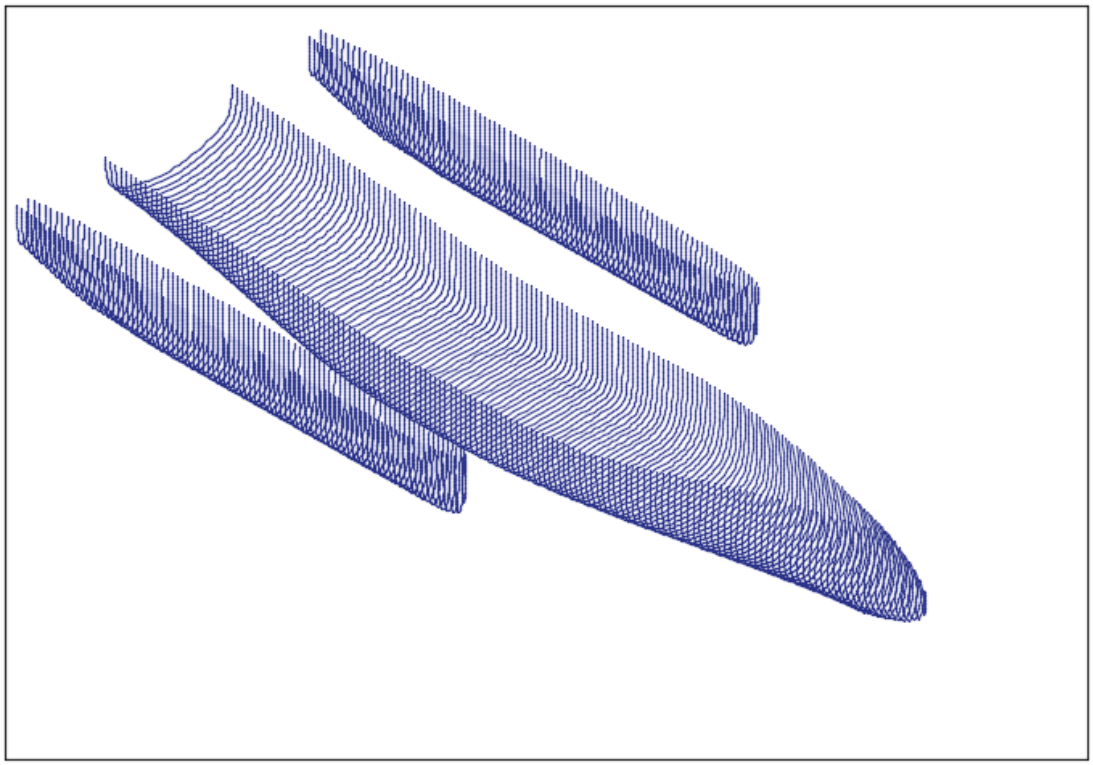

Figure 2.8: 3D view of Trimaran version 4

2.5 Version 5

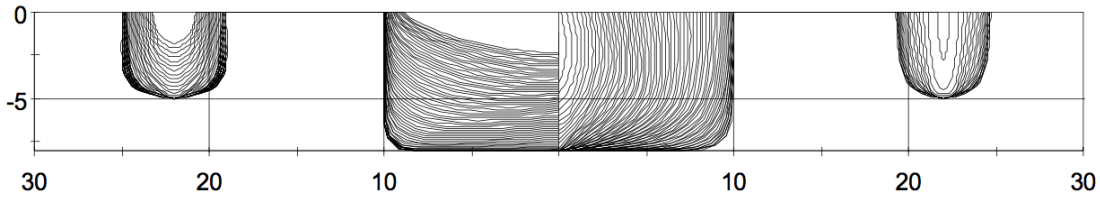

Figure 2.9: Veres plot of Trimaran Version 5

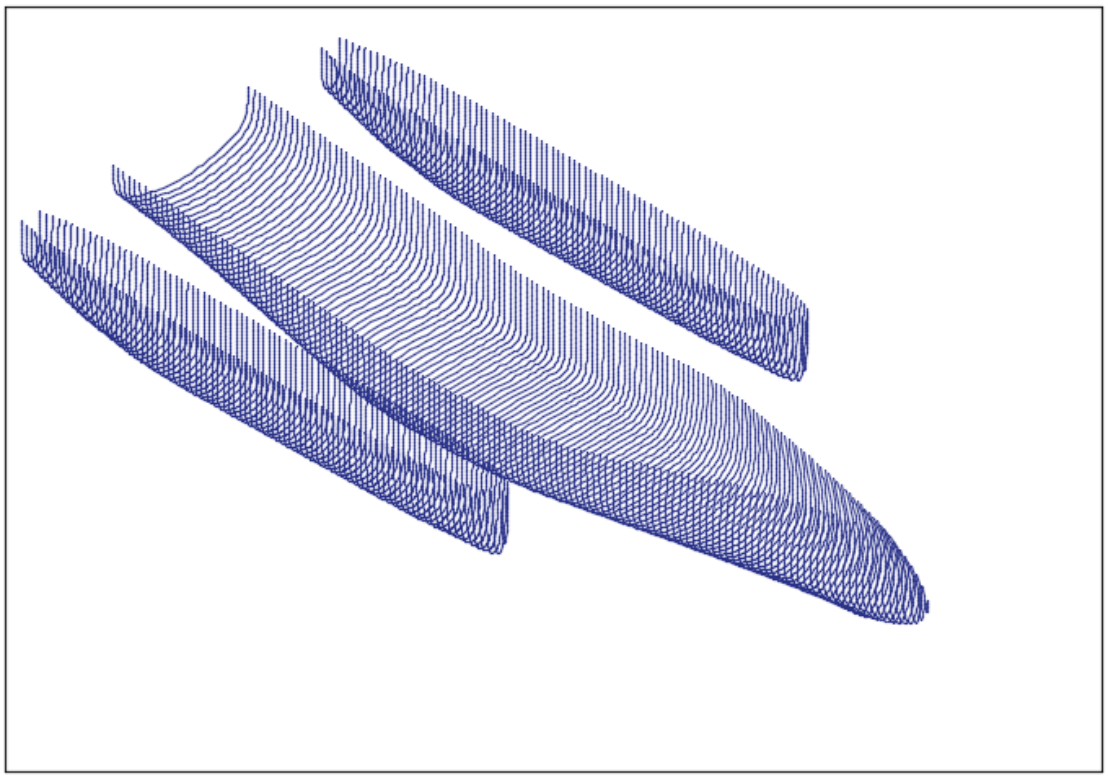

Figure 2.10: 3D view of Trimaran version 5

2.6 Comparison ship

When the framework of this project was set together with LMG Marin, a goal was set to collect operational criteria for a trimaran. When it was discovered that there are limited to no existing information about seakeeping criteria specifically for seismic operations it was proposed to include a comparison ship in the study. LMG Marin has done a project in the past regarding a conventional seismic ship. This ship was included in the analysis to obtain seakeeping results for a vessel that is known to perform seismic operations.

Naturally, it is expected that the motion characteristics of the trimaran will be quite different than the mono-hull as the main dimensions are not comparable. However, it is of interest to include the comparison ship in this study to see if there are any outstanding deviations with respect to maxima values of the criteria that are being evaluated. In addition, the result from the seakeeping evaluation of the comparison ship can be used to evaluate the correlation between the pitch and roll natural periods with respect to the so-called cork-screw motion that were discussed in the above.

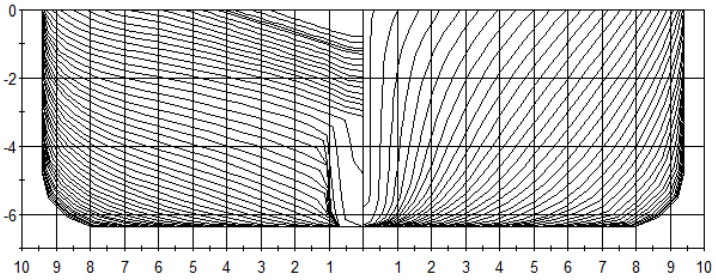

(a) Veres plot of comparison ship

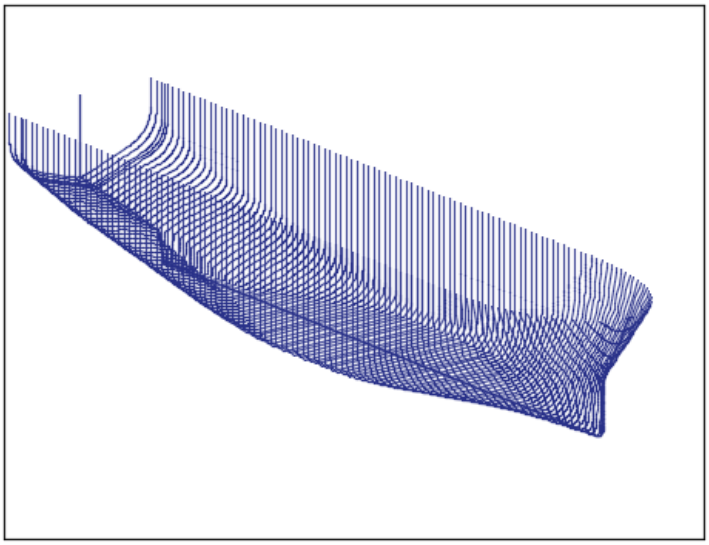

(b) 3D view of comparison ship

CHAPTER 3

Marine Geophysical Exploration

Whenever a possible presence of hydrocarbons is found in a certain area, the next step is to perform a seismic survey. A seismic survey is more cost efficient and generates more widespread information than the alternative of drilling, which is expensive and only provides information at discrete locations (Kearey et al., 2002). This reflects the development of the geophysical industry that always seeks to improve the efficiency, reliability and the quality of the geophysical data.

3.1 Marine seismic operations - an overview

There are a variety of surveys used by the oil and gas industry. The applied method depends on the stage in the exploration and the wanted granularity of the information about the subsurface. Marine seismic surveys also differentiate in the geometry and in the type of equipment that is used. Figure 3.1 illustrates some of the diversities in seismic operations.

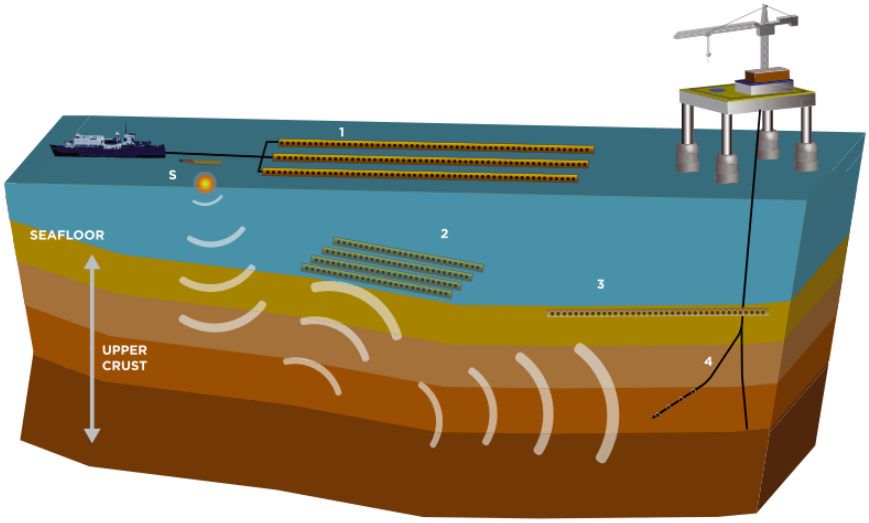

Figure 3.1: An illustration of towed receiver cables or streamers (1), receiver cables fixed at the seafloor (2), buried receivers (3) and a vertical seismic profile with the receivers positioned in the well (4). All marine seismic surveys involve a source towed behind the vessel (S). (OPG, 2011)

The fundamental principles of all marine seismic survey are the same. Controlled acoustic energy is transmitted into the earth from an energy source (often an array of air guns) towed by the vessel. The energy will be reflected back from the boundaries in the subsurface and detected by the receiver sensors. The sensors can be either fixed at the

seafloor, towed behind the vessel or even buried. The sound waves that are reflected back to the recording system will differ in energy and in the time elapsed during the two-way travel. Interpreting the attributes of the returning energy gives an understanding of the different layers in the earth's soil, (CGG, nd).

In an early stage, the objective is to cover a large region to obtain a general understanding of the region's geological structure. If an area of this region appears to have the characteristics of a probable hydrocarbon reservoir, more detailed and reliable information are needed before drilling can take place. Once an oilfield is in production it is necessary to track the developments of the reservoir to be able to extract as much as possible of the available hydrocarbons. In this aspect it is relevant to differentiate between the density of the measurements. The available options are 2D, 3D and 4D seismic surveys. (2015, Roar Lunde, personal communication, July 8th, 2009)

3.1.1 2D seismic

As the name implies, a 2D seismic survey is resulting in a two-dimensional image of the subsurface. Only one array of receivers and one source is towed behind the survey vessel. Hence, a 2D survey does not give rise to any special criteria in terms of vessel design, as space and towing capacity are not limiting. The concept will be described briefly anyway, as it is the forerunner to newer technologies.

The 2D seismic data will be a single vertical plane that is extended in the horizontal path of the vessel. This type of seismic survey is less sophisticated and than 3D and 4D exploration. A preliminary survey is more about regional reconnaissance and the data must be acquired, processed and interpreted efficiently. Before high density- and detailed data are necessary, a 2D seismic survey is more cost efficient than a 3D seismic survey. As a consequence, the 2D technique will not be fully replaced by the 3D technique and will therefore maintain on the market.

3.1.2 3D seismic

Before drilling is initiated, the search company must try to increase the odds of this high risk activity. Millions of dollars of investments in capital and resources are at stake and improved information about the location of development wells is necessary. At this stage a 3D survey is beneficial and is often required in exploration contracts before drilling can take place, (Beckett et al., 1995). The cost of a 3D seismic survey with data processing is considerable less than the cost of drilling. The survey will be worth the investment if it provides the necessary information to eliminate dry wells (Boreham et al., 1991).

Boreham et al. (1991) gave the following simple explanation of the 3D technique: If the 2D technique is applied multiple times over an area, the many vertical planes can be assembled to create a 3D representation of the substructure. Hence, 3D seismic data can be produced by a vessel traversing an area in parallel lines with only one streamer and a single air gun. This is not the practice today, as it is found to be more cost efficient to

tow multiple streamers behind one vessel. Figure 3.2 illustrates the difference between 2D- and 3D seismic operation. In this case, the number of streamers in the 3D survey is six, which was the absolute towing capacity of a common seismic vessel 15-20 years ago (Amundsen and Landrø, 2008). In the following years the capacity limit was moved to 8 streamers and later 12 streamers. Today, there exist vessels specifically designed for seismic survey with the capacity of towing up to 24 streamers. The historical progress in 3D seismic survey is described in more detail in section 3.5.

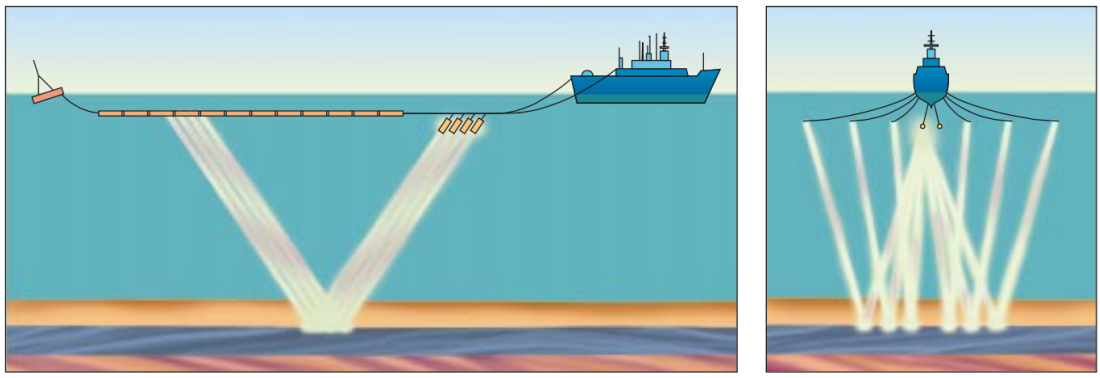

Figure 3.2: 2D seismic survey with one streamer (side view) to the left and 3D seismic survey (front view) with six streamers producing six times the amount of data. (Beckett et al., 1995).

The ship traverses the survey area creating a grid pattern. The distance between two adjacent ship tracks is typically 1 km or greater for a 2D survey. If a ship with multiple streamers were to follow the same track, a much denser data set would be obtained in the same amount of time. According to OPG (2011) a small 3D survey area is on the order of 300 square kilometres, while a large 3D survey may cover 1000 to 3000 square kilometres.

The duration of a survey can be in the order of months and depends on many factors. Some factors can be accounted for like the presence of oil rigs, vessels operating in the area and other obstructions. Other factors that can affect the efficiency of the survey are tides, wind and rough weather. Every interruption is connected to high costs and the retrieval of seismic equipment is very time consuming and difficult in high sea states. Instead, the vessel can either tow the streamers to a sheltered area or ride out the storm at the site. A supply ship, also known as the chase vessel, provides the seismic ship with fuel and other supplies and allows the ship to stay at site throughout the survey.

3.1.3 4D Seismic

By acquiring seismic data at different stages during the production life, the fluid changes in the reservoir can be monitored by interpreting these time-lapse snap shots. Such information is necessary to optimize the extraction of hydrocarbons. In this perspective a fourth dimension is involved, which is referred to as a 4D seismic operation. The

fourth dimension is, of course, time. If the 4D technique can help operators to extend the useful life of a field, the extra costs of a such a survey will indeed be profitable (Pedersen et al., 1996). A 4D seismic survey is therefore similar to a 3D survey in terms of setup of equipment and planning of the operation.

There are several other approaches of carrying out a seismic survey, as demonstrated in figure 3.1. Both 2D, 3D and 4D seismic data can also be accessed by placing seismic nodes attached to a cable on the sea bottom. In this case the survey vessel is only required to tow the air guns which means that a conventional ship is sufficient for the operation. Only seismic operations where there is a demand for a large deck area and width of the aft is of interest in this thesis. The trimaran concept will be associated with higher building costs compared to conventional hulls. A conclusion of this is that the trimaran concept will be of interest in connection with high density 3D and 4D seismic operations where the hydrophones are towed behind the ship. The study of seismic operation will therefore only consider aspects related to this class of operation.

3.2 The seismic crew

The seismic field crew consists of geophysicists, observers, mechanics and navigators (PGS, nd).

The geophysicists analyze, investigate and quality control the seismic data. The observers are responsible of the operation of the seismic recording instruments. They check the data quality, and makes sure that the signal is not disturbed too much by other noise sources. Both the geophysicists' and observers' assignments must be performed with a high level of precision and requires concentration. A seismic ship must therefore house a recording room with satisfactory working conditions.

The maintenance and operation of the mechanical related equipment are kept by the mechanics. They are responsible of the deployment, retraction and in-sea positioning of the streamers and air guns. In order for the mechanical crew to perform their work tasks, the vertical and lateral motions at the streamer deck must be kept at a minimum.

The navigator has the responsibility of the planning of the seismic shooting and ensuring that the vessel follows the right track. He or she works either from the recording room or the bridge.

3.3 Maneuvering and speed

During the seismic shooting the vessel has to follow a certain pattern to achieve the wanted density and quality of the data. When the ship is towing many streamers and more than one source, the acquisition of a large area can be completed in one sail line. Figure 3.3 illustrates how the seismic data is acquired. This strategy has two advantages: it is easier and thus time saving to turn the ship due to the larger radius, and adjacent lines are recorded in the same direction.

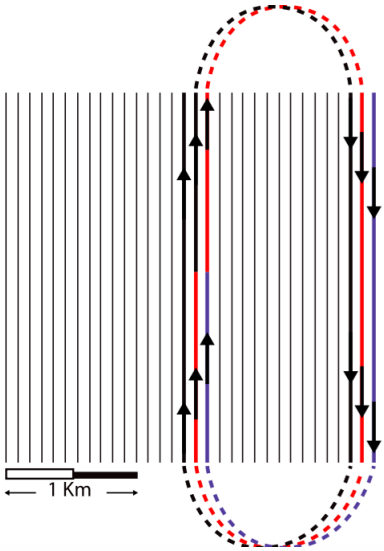

Figure 3.3: Each line represent a sail line. The ship will track down one sail line, but instead of turning and track down the adjacent sail line it skips a number of lines, shoots a new line, before it heads back to the skipped lines, (OPG, 2011).

By looking at figure 3.3 it is clear that the vessel does not have the option to face the weather in the direction that minimizes the motion. Keeping a straight course is important for the quality of the data, which means that the ship must show good seakeeping abilities in all headings during the shooting.

The speed that must be kept throughout the survey is influenced by several factors. If the speed decreases below a certain limit the low tension in the streamers will cause them to sink and tangle. The latter is catastrophic, due to the high cost of the streamers. The reflected seismic data is of very low amplitude and therefore sensitive to noise from the surrounding environment (OPG, 2011). One of the reasons that the noise increase with increasing speed is that the flow around the streamers will become turbulent and cause 'turbulent flow noise' (Elboth and Andreassen, 2009). Experience indicates that the challenges regarding noise and streamer tension are best met at a tow speed between 4.5 and 5.0 knots.

3.4 Environment

As mentioned above, it is critical to minimize noise that will influence and disturb the seismic data. In rough sea states the noise level will become unacceptable, and the acquisition must be postponed. Hence, a seismic survey relies on calm weather. Increasing the tow depth of the streamers can cancel some of the weather and wave noise. However, increasing the tow depth will also affect the resolution of the data in a negative way OPG (2011). According to a guide from the Norwegian petroleum directorate, the limiting wave height is 2 - 4 m (Oljedirektoratet, 2013), depending on

the contract specifications concerning the required data quality. When the wave height exceeds this limit, the survey will be put on hold until the weather allows continuation.

This means that areas with rough winters can only be accessed for seismic survey during the summer half of the year. A scenario for a research vessel could therefore be to operate in the North Sea during the summer, and then sail to the coast of Africa for the winter. A seismic vessel will therefore have to spend significant time in transit, in order to keep busy throughout the year. Due to this fact, it is relevant to evaluate the trimaran concept during transit. By searching in vessel databases like Marine Traffic and Searcher Seismic it can be seen that most vessels that are in transit keeps a speed of 10-12 knots. This was confirmed by Roar Lunde from Magseis (2015, personnal communication, July 8th). However, it can be necessary to exceed the speed that is economical favorable. The top speed in transit for a survey vessel does generally not exceed 16 knots.

3.5 Opportunities in the market

Figure 3.4 demonstrates how the scope of seismic survey has evolved over the years. It is clear that 3D seismic is dominating over 2D seismic. Another important trend that can be seen from the figure is that although the amount of acquired seismic data (measured in kilometers of acquired data) has increased drastically, the number of sailed boat-kilometers has not. As pointed out by Oljedirektoratet (2013), this is due to the fact that the streamers nowadays are longer and the survey vessel tows a higher number of streamers. Hence, a lot more seismic data can be gathered during one sail line. In other words, it is more cost efficient to increase the width of the data swath by increasing the number of streamers towed behind one vessel opposed to using two or more vessels with fewer streamers. It means that a vessel with a wide transom compared to conventional hulls will create an interest in the market. The extremely wide transom of the trimaran concept has the potential to tow 20 cables, which will result in an efficiency step-up and increased data density.

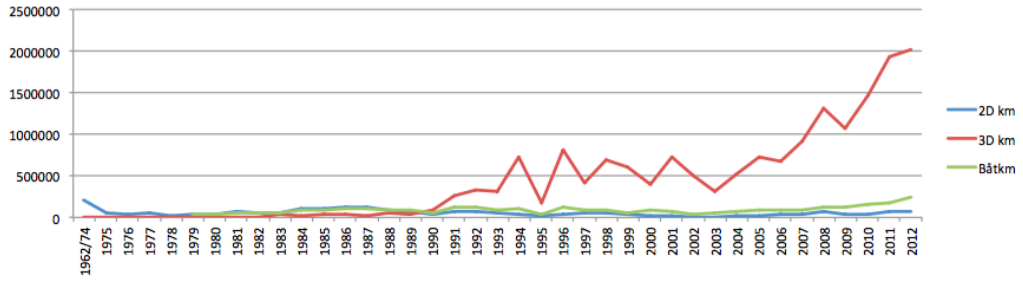

Figure 3.4: Development of the amount of aquired seismic data over the years. The red and blue line represents kilometers of aquired data from 3D and 2D survey, respectively. The green line represents the number of sailed boat kilometers. (Oljedirektoratet, 2013)

CHAPTER 4

Operational Criteria

The most important criterion for all ships and offshore units is to ensure the safety of the crew on board. If the working environment enter a state where a member of the crew can no longer perform his or her tasks, the operation will be interrupted. A shut-down is very expensive and frustrating for all parties involved. Hence, it is in the interest of both the crew and the contractor to increase the operating window as much as possible.

Some criteria are weighted equally, regardless of the corresponding ship's purpose. The safety of the crew is equally important whether the ship in question is an anchor handler or a bulk ship. On the other hand, the operating environment for a specific project can be very different compared to another. As discussed in chapter 3, a seismic operation will not be executed when the wave height exceeds 4 meters. This exemplifies an aspect that is unique for a seismic survey vessel, and will indeed influence the weighting of different operational criteria. The purpose of this chapter is to enlighten the most important criteria for a seismic survey vessel. The objective is to have a set of well argued criteria in order to prove or decline the success of the design in question.

4.1 Crew comfort

The well being of the people on board is crucial for the operation of any type of vessel. If the incidence of motion sickness exceeds unacceptable levels, the operation may even be cancelled. However, the nonacceptance limit will vary according to how well the crew is adapted to ship motion.

The crew on board a seismic vessel consist of seafarers who operates the ship and a seismic crew that are responsible for all the tasks related to the seismic shooting, see section 3.2. The assignments carried out by the geophysicists and observers must be performed with high precision. In other words, they are more sensitive to motion sickness which means that the habitability in the recording rooms must be examined. The same can be reasoned for the working environment at the bridge. In addition, a location in the living areas should be checked.

4.1.1 Motion sickness incidence (MSI)

To evaluate the incidence of motion sickness, the effect of ship motions on humans must be understood. This was examined by O'Hanlon and McCauley in a research supported by the Bureau of Medicine and Surgery of the U.S Navy in 1973. The result of the research was the concept of MSI which is a quantifiable measure of motion sickness.

Before the work of O'Hanlon and McCauley (1973) began it was established in other studies that the periodic vertical motion is the primary factor inducing human fatigue.

The objective of O'Hanlon and McCauley were to show how the the motion sickness varies as a function of the components of vertical periodic motion. The concept of MSI as proposed by O'Hanlon and McCauley (1973) is explained in the following.

The MSI is defined as the percentage of a group of people who will experience emesis (vomiting) by a 2 hour exposure of a given wave frequency ω and acceleration $\bar{a}$. $\bar{a}$ is the time integral of the absolute value of acceleration imparted in each half-wave cycle. It was discovered that for each level of ω, the MSI showed a monotonic increase $\bar{a}$. The MSI as a function of the acceleration $\bar{a}$ and the frequency is given in the following expression:

$$\mathrm{MSI} = \int_{-\infty}^{\log \bar{a}} \frac{100}{\sigma\sqrt{2\pi}} \quad \mathrm{e}^{-[(x-\mu)^2/2\sigma^2]} \, \mathrm{d}x \tag{4.1}$$

where x is a unit of integration in units of log $\bar{a}$. Both μ and σ have values that are determined empirically.

The parameter μ is a function of the frequency and gives a measure of how the acceleration affects the MSI value at a given frequency level. If the value of μ is in the lower regime, less acceleration is required to obtain a certain MSI value. This indicates that human fatigue is easier obtained at frequency levels with low μ values. An approximate relationship between the frequency and μ was obtained by fitting the quadratic equation to the data obtained from the research of O'Hanlon and McCauley:

$$\mu = 0.659 + 3.840 \ \log f + 2.467 \ (\log f)^2 \tag{4.2}$$

where f is in Hz.

Equation 4.1.1 shows an important trend about motion sickness that has been confirmed in later studies (Lawhter and Griffin, 1987). This is that the sensitivity to acceleration reach a sharp peak at a certain frequency range. For high frequencies the sensitivity to acceleration will be reduced.

It should be noted that the people who participated in the research trials where not adapted to the motions. It is a common experience amongst seafarers that one will be more resistant to motion sickness after a while at sea. However, this is a phenomenon that is harder to describe with a mathematical model.

In 1976 a refined mathematical model was developed through an expanded research, McCauley et al. (1976). This model incorporates more data for angular acceleration and frequencies for vertical motion than equation 4.1.1. In addition, the duration of exposure is included as a variable in the refined model. This allows for a calculation of the percentage of MSI for a certain exposure time.

4.1.2 Definition of criteria

According to NATO (2000), the criterion of motion sickness incidence should be set to 20% during a 4 hour sea state. However, this is a strict criterion as it applies to naval ships. Therefore, the comparison ship will be included in the assessment.

Normally, the ship will operate in calm weather sea states with a forward speed of maximum 5 knots. A significant wave height 4 meters will therefore be used in the calculations. The transit speed of 16 knots will also be included in the assessment of MSI.

4.2 Cork screw motion

A simple evaluation of the pitch and roll natural periods will be done in order to check if the different trimaran configurations have a possibility of showing the so-called cork-screw motion, ref. chapter 2. It is of interest to check whether the different hull configurations result in a stronger or weaker correlation between the roll and pitch natural periods.

4.3 Motion induced interruption

Work tasks conducted during operations on board a ship are especially demanding due to the moving environment. This section presents the necessary criteria to ensure safe execution of necessary tasks with respect to the expected environmental state.

According to Graham (1990), it is clear that deck operations are limited by the deck inclinations in combination with lateral and vertical accelerations. A typical seakeeping criterion used in combination with deck operations is to use a roll angle of 4° as a limiting measure. However, this approximation is only applicable for a certain type of ships, i.e frigates and destroyers. Graham arguments that this criterion is not sufficient as a general criterion to verify operability performance, because response vary considerably with ship type and size. This argument is indeed valid for a trimaran due to the shape and distribution of the submerged volume. The large width will increase the effect of the roll angle with respect to vertical translation. In addition, the submerged volume added by the side hulls increase the lateral stiffness, and the effect of vertical acceleration must be included.

The research of Graham (1990) had the objective to describe the conditions that cause the crew to loose their balance. As a result of the research, a set of criteria to describe deck operability were suggested. This research is an extension of another research done by Baitis et al. (1984), where the quantity MII (motion induced interruptions) was established in order to assess the deck operability. The research describes a method to calculate the MII during an arbitrary deck operation, that is the number of loss-of-balance events during the operation. Graham extended the calculation method of MII to include not only lateral accelerations, but also vertical accelerations.

The conditions for loss balance explained by (Graham, 1990) are given by the following equalities:

$$\Big[- g\eta_4 - \ddot{D}_2 - \frac{l}{h}\ddot{D}_3 \Big] > g\frac{l}{h} \tag{4.3}$$

$$\Big[g\eta_4 + \ddot{D}_2 - \frac{l}{h}\ddot{D}_3 \Big] > g\frac{l}{h} \tag{4.4}$$

Where $\ddot{D}_2$ and $\ddot{D}_3$ are the lateral and vertical acceleration at the location. η_4 is the roll angle and g is the acceleration due to gravity. $^{l}/_{h}$ is named the tipping coefficient, and has the value of 0,25 for a person standing upright on a dry deck. The expression inside the square brackets of equality 4.3 and 4.4 are the general lateral force estimators, named $GL1$ and $GL2$. The number of MII's during the time T_T it takes to complete a task is given in the following expression:

$$M_i = \frac{T_T}{T_{GLi}} P[GLi > g\frac{l}{h}] = \frac{T_T}{T_{GLi}} exp\Big[- \frac{1}{2}\Big(\frac{^{l}/_{h} \cdot g}{GLi_{RMS}}\Big)^2 \Big] \tag{4.5}$$

GLi_{RMS} is the root mean square value of GLi, while T_{GLi} is the zero up-crossing period of Gli. $M_1 + M_2$ will give the number of total MII's during the task.

There is no typical time duration, T_T, of a seismic operation. The project can last for several months or years and the equipment will not be retracted as long as the weather conditions allow it. The equipment must be maintained while deployed and constantly monitored during the survey. Graham (1990) has suggested a standard deck operation for comparison purposes, which will be applicable for the verification of the trimaran concept. The unit MIIs per minute was introduced along with a table of risk levels, reproduced in table 4.1.

Table 4.1: MII Risk Levels

RISK LEVEL	MIIS PER MINUTE
1. possible	0.1
2. probable	0.5
3. serious	1.5
4. severe	3.0
5. extreme	5.0

4.3.1 Definition of criteria

When the number of MIIs exceeds one per minute the crew will face significant interruptions while performing their tasks. Hence, a one minute deck operation with a tipping coefficient of 0.25 will be used as a standard deck operation. One MII per minute will serve as a benchmark for comparison. The comparison ship will also be included in the assessment.

As discussed in chapter 3, the limiting wave height for a survey is 4 meters. Hence, it is relevant to assess the criteria for deck operations under these conditions. The limiting sea state may lead to a stop in the seismic data assembly, but for practical reasons the streamers are towed until the survey is resumed. It is crucial that the mechanics are able to work under difficult conditions to avoid damage on the equipment. For this reason the criteria for deck operations will also be assessed at higher sea states.

The MII is a parameter that is very position-dependent. The MII will be calculated at several positions at the streamer deck. Multiple positions are included to make a fair comparison between the trimaran concept and the comparison ship. It is also necessary to check different positions to identify where the MIIs are prominent. Figure 4.1 and 4.2 illustrates location where the MIIs are calculated. The coordinates of the positions are given in table 4.2.

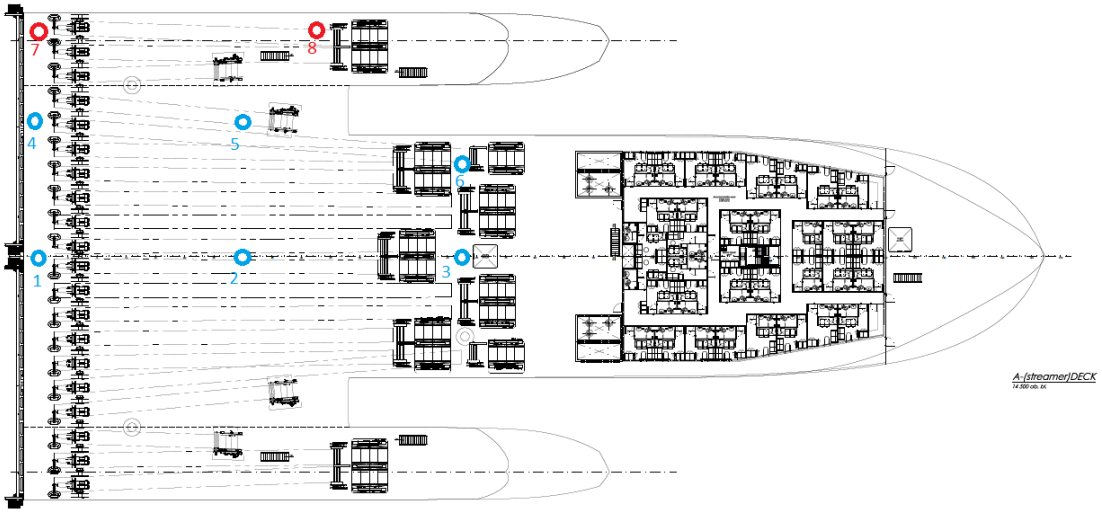

Figure 4.1: Position 1-4 are included for comparison of MIIs, while position 7-8 are included due to the large distance from the roll centre.

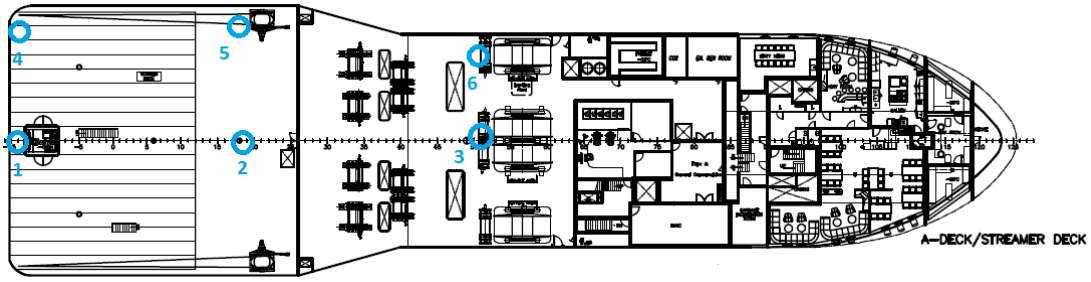

Figure 4.2: Locations for comparison of MIIs.

Table 4.2: Coordinates for MIIs. X-position is meters forward of AP, Y-position is meters off the center-line (positive at starboard side) and Z-position is meters above the base-line.

	TRIMARAN			COMPARISON SHIP		
POSITION	X	Y	Z	X	Y	Z
1	0	0	14.5	0	0	11.7
2	25	0	14.5	20	0	11.7
3	45	0	14.5	40	0	11.7
4	0	12	14.5	0	10	11.7
5	25	12	14.5	20	10	11.7
6	45	10	14.5	40	8	11.7
7	0	22	14.5	-	-	-
8	30	22	14.5	-	-	-

4.4 Helicopter operation

Because a seismic ship often operates at site for several months without returning to shore, it is necessary that the ship has the opportunity to launch and recover a helicopter. This enables efficient crew change and replenishment of provisions and spare parts, even when the ship is far away from shore.

The criteria for helicopter operations are given according to NATO (2000). Limitations are defined to permit safe vertical takeoff, short takeoff and vertical landing. A generic criteria was developed by Comstock et al. (1982) by a comparative seakeeping assessment of nine air capable ships. The study covered a wide range of size and hull forms to establish a default criteria that could be used in any design study. The limiting criteria for pitch, roll and vertical velocity at the helicopter deck are given in table 4.3.

Table 4.3: Performance limitations for helicopter operation. Roll, pitch and vertical velocity are given in terms of root-mean-square amplitude.

MOTION	LIMIT	LOCATION
Roll	2.5°	-
Pitch	1.5°	-
Vertical velocity	1 m/s	Landing spot

The location of the helicopter deck for trimaran version 1, 2 and 5 is 28 meters above the base line and the centre of the deck is located 76.5 meters forward of the stern. The location of the helicopter deck for version 3 and 4 is not yet specified. It will be assumed that the location of the deck centre is 86.5 meters forward of the stern, as version 3 and 4 are 10 meters longer in total than version 1, 2 and 5.

4.5 Hull interaction

The additional hulls of a trimaran involve a possibility of a trapped wave between the hulls. For multi-body vessels with a narrow gap between the bodies the phenomena of fluid resonance may take place. This will lead to increased wave oscillation amplitudes and large loads on the cross-structure. The wave elevation between the hulls relative to the motion of the hull gives an understanding of the impact between the water and cross-structure. For seismic surveillance vessels it is particularly important to avoid water-vessel impact, as slamming will cause vibration and noise that interferes with the recording of sound waves. Because this phenomenon has a significant importance to the choice of hull configuration it must be included in the verification of the trimaran.

There are no defined criteria that treat this matter. As the LMG Oilcraft trimaran is still in the early design stage, the tunnel height has not yet been specified. A way to evaluate the hull interaction is therefore to compare the expected maxima value of the relative motion for the five trimaran versions. This will also serve as a guide in the decision of the magnitude of the tunnel height.

The gap between the side- and main hull for the five trimaran versions have varying size. In addition, the longitudinal extent of the side hull is also different. The goal is to identify which hull configuration that is beneficial with regards to hull interaction.

CHAPTER 5

Evaluation of Criteria

The purpose of this chapter is to describe the methods of evaluating the criteria that were described in section 4. The description will include the advantages and drawbacks of the available methods and a decision of which method to be used for the evaluation. The decision is made by having in mind that the trimaran design is an unconventional design compared to slender mono-hulls. Since the design in question is a multihull, it is crucial to treat the challenges related to hull interaction. It is therefore necessary to investigate the ability of the different methods to treat the phenomena related to hull interaction.

MII, MSI and criteria for helicopter operations are derived directly from the ship's response characteristics by evaluating the global motion transfer functions. There are several methods for determining ship responses. These include theoretical methods, model experiments and full scale trials. The choice of method includes an assessment of costs and the complexity of the outcome of the analysis or experiment. There has been great progress in the development of computational tools for evaluation of seakeeping problems. Therefore it is not common to perform model experiments in the early design stage, and have not been considered an option for this study. The theoretical methods include 2D potential strip formulations, 3D potential panel methods and CFD methods.

5.1 CFD

CFD methods are very powerful as complex effects may be included in the analysis. CFD are the preferred method when detailed information about the flow processes are necessary because viscous effects may be included in the problem. It means that bodies with arbitrary geometries can be analysed with higher accuracy than potential theory methods, in that the flow separation can be modelled with high accuracy. Further, a better description of roll damping can be obtained by the use of CFD. Roll damping is known to be highly dependent on viscous effects which means that potential theory provides a limited representation of the reality. However, the use of CFD in this study would require that the user possess wide experience with such methods. Time is an important limitation as such method requires a large computational effort. The author of this thesis has no previous training in CFD. Hence, the option of performing the motion analysis with CFD was not considered feasible with respect to the available time.

5.2 2D strip theory

2D strip theory methods are the least expensive in terms of computational time. Only limited details of hull definition are required. The computation of the hydrodynamic

coefficients and exciting wave loads are performed in 2D by dividing the ship hull in 20-30 cross sections. The three-dimensional values are obtained by a numerical integration over the length of the hull.

As the strip theory takes advantage of linearisation techniques, it explicitly assumed that the wave steepness is small. Accordingly, this assumptions also holds for the amplitudes of the ship responses. It means that responses in extreme sea states, where non-linear effects are relevant, are out of the scope of strip theory methods. However, strip theory is strictly valid for long waves in the order of the beam. Strip theory also shows good results for wave lengths in the order of the ship length, NATO (2000). The method is less accurate when computing the 2D hydrodynamic coefficients in heave at low frequencies. For ships with forward speed, the effect of encounter frequency will reduce the frequency at following and quartering seas. The method will therefore give better results at head and bow sea waves. However, the method can be justified as the vertical motions are dominated by restoring forces in the long wave range, Salvesen et al. (1970). Strip theory is also a low Froude number theory and should be applied with care for $\mathcal{F}_n >\approx 0.4$, Faltinsen (1990). The Froude number for the trimaran concept does not violate this condition.

Another important limitation of strip theory is the assumption of a long and slender body. The trimaran has a very large width-to-length ratio, but the individual hulls are slender. This makes the trimaran applicable for strip theory. However, the side hulls are shorter than the main hull, meaning that the flow around the hull will be more complicated than the flow around a mono-hull or catamaran with identical hulls. Strip theory assumes that the variation in the cross-sectional plane is much larger than the variation of the flow in the longitudinal direction, Faltinsen (1990). Because the strip theory treats each section individually, the lengthwise interaction will be neglected. This can not be justified for a trimaran with side hulls of finite length.

Another consequence of a 2D method is that the effects of interaction between the main hull and side hulls is lost. Each hull will radiate waves that will interact with another hull. This interaction will affect the sea-keeping behaviour and the effect will increase as the size of the outriggers increase. In strip theory, the loads are computed on each hull as if the other hulls are not present and the contributions are superimposed. Hence, all interaction effects are neglected. A study has been conducted to investigate the correlation between the result of the strip theory program Veres and model test results of multi-hull vessels, (O'Dea, 2005). According to this study, Veres is able to predict the seakeeping behaviour of trimarans with a good precision. It was concluded that the loads due to interaction have relatively minor effect on the overall motion of the total configuration. However, the side hulls in this study were small compared to the main hull. The Oilcraft Trimaran has a significant size on the side hulls which makes the conclusion in O'Dea (2005) questionable.

According to NATO (2000), the heave and pitch motion hardly shows non-linear effects

and can therefore be predicted with means of strip theory methods with good results. However, the non-linear effects are more pronounced for heave and pitch velocities and accelerations. The non-linearities are important in the case when time histories and extreme values are of interest, but are of less importance when the statistical values such as RMS amplitudes are considered. Based on this discussion, a strip theory method can be considered as an adequate method when evaluating criteria that are less sensitive to the prediction method, e.g MII, MSI and criteria for helicopter operations. Criteria that are based on relative motions between ship hull and wave surface should be evaluated by a method that takes the wave-body interaction into account. Due to the fact that hull interaction is a 3D effect, strip theory can not be used to investigate this phenomena.

5.3 3D potential theory

Three dimensional methods uses panels to evaluate the hydrodynamic forces on the ship, which means that hydrodynamic interactions can be accounted for both transversely and longitudinally. This subsection will give a further explanation on the treatment of hull interaction in 3D potential theory methods.

There are two different interaction effects due to the presence of side hulls which is called wave interference and wave interaction, (Faltinsen, 2010):

Wave interaction is when the waves radiated from one hull reaches another hull and diffraction occurs. The diffracted waves include reflected and transmitted waves. The degree of wave interaction is dependent on the gap between the hulls, the heading of the incident waves and the forward speed of the vessel. Faltinsen (2010) presents a simple method to assess the importance of hull interaction by considering the Kelvin angle for one hull to see if the waves inside the Kelvin angle will be incident to the other hull. The length, L_1, of the side hull that is affected by the other hull can be given as in expression 5.1. Here L is the length of the main hull, B_G is the width of the gap and B_{SH} is the width of the side hull.

$$\frac{L_1}{L} = 1 - \left(\frac{B_G + 0.5B_{SH}}{L} \right) 2 \frac{\omega_e U}{g} \tag{5.1}$$

Equation 5.1 shows that the for a given frequency of encounter, ω_e, the wave interaction will decrease as the forward speed, U, increases. Also, the wave interaction will decrease as the width of the side hull and the gap increase.

Wave interference concerns the effect of a superimposed wave elevation in the gap due to wave generation from each hull. The wave interaction between the hulls will be increased if the wave motion exerts resonant behaviour. This effect will be worst in the case of zero forward speed, while 3D effects and forward speed will have a reducing impact. 3D potential theory methods are able to describe this behaviour. However, as potential theory neglects viscous effects, an important damping mechanism of the wave elevation

is lost. Lu et al. (2010) have done a study that discusses fluid resonance in narrow gaps supported by numerical simulations based on both a viscous fluid model and a potential flow model. The numerical results are compared to experimental results. The study concludes with that potential theory is able to determine the resonant frequency of the gap wave. However, the amplitude of the wave is highly overestimated close to the resonance frequency. The response agrees well with experimental results in cases where the incident wave frequency is far away from the resonance frequency, see fig. 5.1.

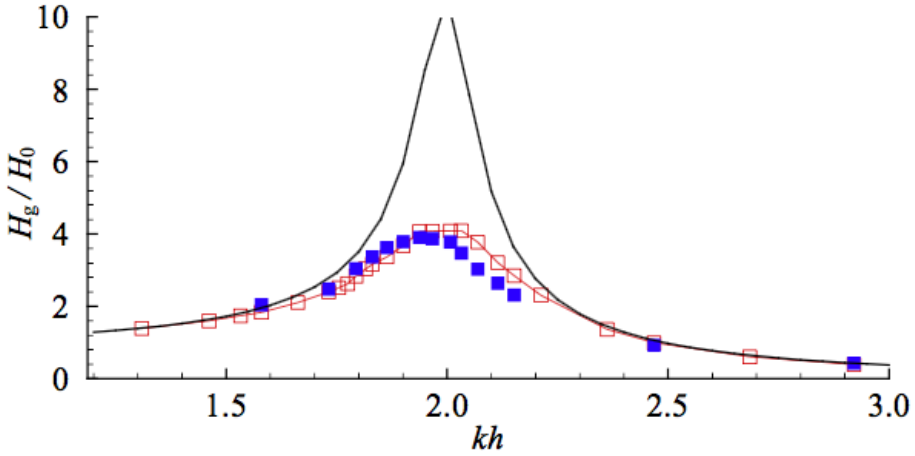

Figure 5.1: Response of the wave elevation in a narrow gap between two floaters. The viscous and potential model is represented by the red and black line, respectively. The blue line shows the experimental data. (Lu et al., 2010)

Based on the discussion above, a three dimensional theory is more suitable than a two dimensional strip theory for computation of hydrodynamic forces and motions for the trimaran. It is necessary to use a three dimensional theory to evaluate the criteria related to hull interaction. It is therefore decided to carry out the simulations in Wasim, which performs the calculations with a Rankine panel method. A more detailed description of Wasim is given in chapter 6.

5.4 Calculation of ship responses

As implied in the introduction of this chapter, the starting point of evaluating the criteria is to obtain the motion transfer functions. It is the first order wave loads that are in the center of attention in this work, meaning that the problem can be solved by the frequency response method. In a case where transient- or non-linear effects are considered, the response must be solved in time domain. This section will describe how the criteria can be evaluated by the frequency response method.

5.4.1 The frequency response method

For an oscillating linear system under steady state conditions the response will be linearly related to the exciting force or input. It means that the response to each input variable can be considered separately and the total contribution may be found by superposition. Each input variable can be described as a sinusoidal wave with constant amplitude and a fixed frequency of oscillation.

$$f(t) = f_0 \cos \omega t \tag{5.2}$$

As a consequence of the linear relationship, the response must also be a sinusoidal wave with a constant amplitude and oscillate with the same frequency with phase angle φ.

$$u(t) = u_0 \cos(\omega - \varphi) \tag{5.3}$$

The amplitude ratio $^{f_0}/_{u_0}$ and the phase angle, φ, defines the transmission characteristics or the transfer function of the system for a given frequency. The dynamic characteristics of the system can be completely defined if the amplitude ratio and phase angle are found for a set of closely spaced frequencies ranging from zero to infinity:

The relation between the input and output is found by solving Newton's second law of equation, which is a second order differential equation:

$$m\ddot{u} + b\dot{u} + cu = f(t) \tag{5.4}$$

The general solution to equation 5.4 is a sum of a particular and a homogeneous solution, $u(t) = u_h(t) + u_p(t)$. The homogeneous solution is often referred to the as the transient term and will appear as an initial term which will die out with time. The particular solution is referred to as the steady state term and will dominate the solution as the transient term is damped out.

The homogeneous solution is found by considering a damped system that is free to oscillate with no excitation forces:

$$m\ddot{u} + b\dot{u} + cu = 0 \tag{5.5}$$

The solution to this equation depends strongly on the damping ratio $\xi = c/2m\omega_e$. For different values of the damping ratio, three different types of solutions are possible. The damping may be critical, supercritical or subcritical, where a subcritical damping is the most common case. In this case the homogeneous solution will take the following form.

$$u_h(t) = \exp^{-\xi\omega_e t}(a_1 \cos \omega_d t + a_2 \sin \omega_d t) \tag{5.6}$$

Here ω_d is the damped natural frequency, which is given as $\omega_d = \omega_e\sqrt{1-\xi^2}$. Figure 5.2 shows a damped oscillatory response according to equation 5.6.

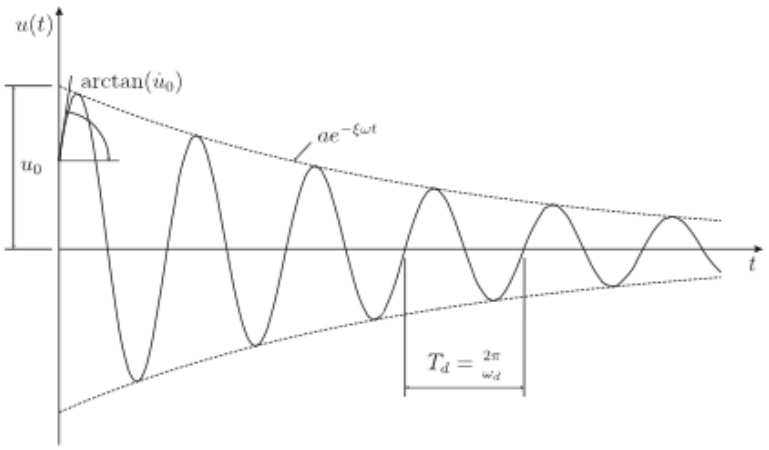

Figure 5.2: Example of subcritically damped oscillatory response, (Naess and Moan, 2012). The oscillation amplitude decays with time and will eventually vanish, depending on the amount of damping relative to the restoring and inertia, i.e the damping ratio, ξ.

The particular solution is found by considering dynamic equilibrium when the system is excited by a harmonic force, f.

$$m\ddot{u} + b\dot{u} + cu = f_0 \cos \omega t \tag{5.7}$$

The solution to 5.7 can be found by assuming that the solution has the following form:

$$u_p(t) = b_1 \cos \omega t + b_2 \sin \omega t \tag{5.8}$$

By substitution into equation 5.7 the following equations are obtained:

$$-m\omega^2 b_1 + b\omega b_2 + cb_1 = f_0 \tag{5.9}$$

and

$$-m\omega^2 b_1 - b\omega b_2 + cb_1 = 0 \tag{5.10}$$

Solving these equations with respect to b_1 and b_2 will result in the following expressions:

$$b_1 = \frac{f_0}{c} \cdot \frac{1-\beta^2}{(1-\beta^2)^2 + (2\xi\beta)^2} \tag{5.11}$$

and

$$b_2 = \frac{f_0}{c} \cdot \frac{2\xi\beta}{(1-\beta^2)^2 + (2\xi\beta)^2} \tag{5.12}$$

Where β is the frequency ratio $\beta = \omega/\omega_e$.

Based on the previous derivation, the particular solution will take the following form:

$$u_p(t) = \frac{f_0}{c} \cdot \frac{1}{(1-\beta^2)^2 + (2\xi\beta)^2}((1-\beta^2)^2 \cos\omega t + 2\xi\beta \sin\omega t), \tag{5.13}$$

which can be written on the equivalent form:

$$u_p(t) = b\cos(\omega t - \varphi) \tag{5.14}$$

where

$$b = \sqrt{b_1^2 + b_2^2} = \frac{f_0}{c} \cdot \frac{1}{((1-\beta^2)^2 + (2\xi\beta)^2))^{\frac{1}{2}}} \tag{5.15}$$

and

$$\varphi = \arctan(b_2/b_1) = \arctan\left(\frac{2\xi\beta}{1-\beta^2}\right) \tag{5.16}$$

As can be seen from equation 5.15 the response will increase strongly as the excitation frequency approaches the natural frequency of the system, i.e $\beta \to 1$.

It is common to introduce the complex transfer function, $H(\omega) = |H(\omega)| \exp^{-i\varphi}$, which contains all information about the amplitude ratio and phase angle between the output and input. Hence, it defines the system response to a given harmonic excitation. The non-transient part of the response can now be written:

$$u_p(t) = |H(\omega)| f_0 \cos(\omega t - \varphi) \tag{5.17}$$

From equation 5.14 and 5.15 it follows that $|H(\omega)|$ can be expressed as in equation 5.18. $|H(\omega)|$ gives the response amplitude operator, or RAO, which is the transfer function of the body motions relative to the exciting force.

$$|H(\omega)| = \frac{1}{c\sqrt{(1-\beta^2)^2 + (2\xi\beta)^2)}} \tag{5.18}$$

The frequency response method only considers the particular solution of the dynamic problem. Hence, it is assumed that all transient effects have been damped out so that the homogeneous solution can be excluded. The frequency response method is presented for a simple harmonic load. As a result of the linearization of the problem, any type of loading can be solved for as long as the loading show a periodic behaviour. Because the principle of superposition holds, the periodic loading can be represented by a Fourier series.

In the case of a freely floating body, the problem will be expanded from a single degree of freedom problem to a multi-degree of freedom problem. Depending on the geometry of the body, the motions will be coupled or uncoupled. There are six degrees of freedom and the dynamic equation can be written as in equation 5.19, using the complex notation $\eta_k = \eta_{ka} e^{i\omega t}$, Greco (2012). X_j is the transfer function for the excitation loads for a wave with frequency ω and direction θ.

$$\sum_{k=1}^{6}[-\omega^2(M_{jk} + A_{jk}(\omega)) + i\omega B_{jk}(\omega) + C_{jk})]\eta_{ka} = \zeta_a X_j(\omega, \theta), \quad j = 1, ..., 6 \tag{5.19}$$

where $\eta_{ka} = |\eta_{ka}|e^{i\varphi_{nk}}$ and $X_j = |X_j|e^{i\varphi_{x_j}}$ gives the amplitude and phase of the body motions and the excitation loads, respectively. The direction of the excitation loads is defined by θ. The transfer function will provide the motions amplitude per unit incident wave amplitude and the phase of the motions relative to the incident waves:

$$\boldsymbol{H}(\omega, \theta) = \boldsymbol{\eta}_a/\zeta_a = [-\omega^2(\boldsymbol{M} + \boldsymbol{A}(\omega)) + i\omega\boldsymbol{B}(\omega) + \boldsymbol{C}]^{-1}\boldsymbol{X}(\omega, \theta) \tag{5.20}$$

The main effort of estimating the transfer functions lies in finding the hydrodynamic coefficients, $\boldsymbol{A}(\omega)$ and $\boldsymbol{B}(\omega)$. Assuming that these quantities are solved for, the RAOs can be plotted against the frequency of the incoming wave loads for each degree of freedom with respect to a fixed heading, θ. The RAOs will contain all the necessary information needed to evaluate the criteria described in chapter 4. Figure 5.3 shows an example of a RAO in heave for zero forward speed. Similar plots can be found for the remaining degrees of freedom at different vessel speeds.

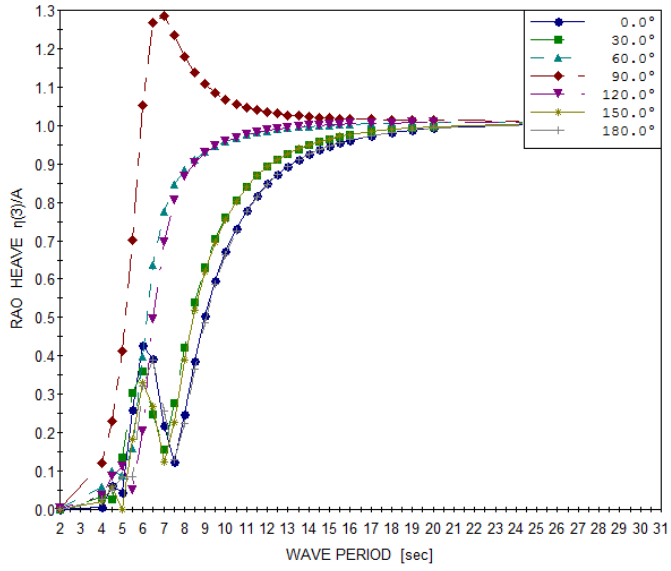

Figure 5.3: Example of RAOs

5.4.2 Environmental loads

Subsection 5.4.1 describes how the response can be found by the frequency response method. The result is the transfer function that describes the response as a function of a regular sinusoidal wave load. Such waves are rarely seen in nature as ocean waves are irregular and of random nature. To give a better representation of the reality, the irregular and random nature must be taken into account. The ocean climate is continuously changing, meaning that the wave loads are also non-stationary. Because the frequency response method assumes steady state conditions it is not possible to directly solve for non-stationary wave loads. Therefore it is common practice to treat the the random processes as stationary for limited periods of time. The stationary periods are often limited to three hours and are referred to as the short-term description of the wave field. In the short-term perspective the characteristics of the wave field will therefore be constant. In the long term perspective these characteristics will change. A normal assumption to describe the short-term wave process is that the sea surface can be represented by a Gaussian random variable. This subsection will describe how the short term wave elevation can be described by a wave spectrum. It is assumed that the irregular waves propagate in the same direction, θ. In this case the free surface elevation can be expressed as in equation 5.21.

$$\sum_{n=1}^{N} \zeta_{an} \cos\left(\omega_n t + \epsilon_n\right) \tag{5.21}$$

The phase, ϵ, is a independent stochastic variable which represents the random nature of the surface elevation. The total energy in a sea state can be described as the sum of the energy contribution from each wave component per unit area:

$$\frac{E}{\rho g} = \sum_{n=1}^{N} \frac{1}{2} \zeta_{an}^2(\omega_n) \tag{5.22}$$

The wave spectrum or energy spectrum, $S(\omega)$, is defined such that the area within a small frequency range $\Delta\omega$ equals the energy contribution from all the wave components within this range:

$$\frac{1}{2}\zeta_{an}^2 = S(\omega_n)\Delta\omega \tag{5.23}$$

It means that the total energy in the sea state can be found by integration over the entire frequency range when the number of wave components approaches infinity, $N \to \infty$, and $\Delta\omega \to 0$:

$$\frac{E}{\rho g} = \frac{1}{2}\zeta_a^2 = \int_0^\infty S(\omega) d\omega \tag{5.24}$$

The wave spectrum contains all the necessary information about the statistical properties of the surface elevation, $\zeta(t)$, as the variance of the surface elevation is given as $\sigma^2 = \int_0^\infty S(\omega)d\omega$. The wave spectrum describes how much energy within the sea state that is related to a given wave length.

A standardized wave spectrum must be chosen as there is no information about the true wave spectrum at the location where the ship is going to operate. In the case of the trimaran it is not specified a fixed location where the ship will conduct the seismic operations. The ship will probably operate in the North Sea during the summer season and at a location with smaller sea states during the winter season. Therefore it has been decided by the author to use the Pierson-Moskowitz spectrum. The PM spectrum holds for a fully developed sea states at the open sea and can be expressed by the significant wave height, H_s, and the zero up-crossing period, T_z, as follows:

$$S_{PM}(\omega) = \frac{4\pi^3 H_s^2}{T_z^4} \cdot \frac{1}{\omega^5} \cdot \exp\left(- \frac{16\pi^3}{T_z^4} \cdot \frac{1}{\omega^4} \right) \tag{5.25}$$

5.4.3 Response spectrum

The short term statistics of the responses are needed to evaluate the criteria. These are found by combining the transfer functions with the wave spectrum to obtain the response spectrum as a function of the wave frequency. The definition of the RAO was given in section 5.4.1:

$$|H(\omega, \theta)| = \frac{\eta_a}{\zeta_a} \tag{5.26}$$

Equation 5.26 is rewritten on the equivalent form:

$$\frac{1}{2}\eta_a^2 = |H(\omega, \theta)|^2 \frac{1}{2}\zeta_a^2 \tag{5.27}$$

By substituting of equation 5.23 into equation 5.27, the following expression is obtained:

$$\frac{1}{2}\eta_{an}^2(\omega_n) = |H(\omega_n, \theta)|^2 \frac{1}{2}\zeta_{an}^2 = |H(\omega_n, \theta)|^2 S(\omega_n)\Delta\omega_n \tag{5.28}$$

The response spectrum, $S_R(\omega)$, is defined in the same manner as the wave spectrum was defined:

$$S_R(\omega_n) = \frac{1}{2}\eta_{an}^2(\omega_n)\Delta\omega \tag{5.29}$$

Finally, the relationship between the response spectrum and the wave spectrum can be established:

$$S_R(\omega) = |H(\omega,\theta)|^2 S(\omega) \tag{5.30}$$

The linear relationship between load and response has been utilized such that the same probability distributions that were used to describe the wave environment can be used to describe the response. Now that the response spectrum is known, the statistical properties can be found from the moments. The kth moment of the response is given by:

$$m_k^{\eta_a} = \int_0^\infty \omega^k S_R(\omega) d\omega \tag{5.31}$$

The standard deviation of the response process is given from the area of the response spectrum, i.e $\sigma_{\eta_a} = \sqrt{m_0^{\eta_a}}$. This is also known as the root-mean square value or RMS value. The variance can be used to express the significant value of the response. This value is given as $\eta_s = 4\sigma_{\eta_a}$. The zero crossing period, T_z, can also be found from the moments:

$$T_z^{\eta_a} = 2\pi\sqrt{\frac{m_0^{\eta_a}}{m_2^{\eta_a}}} \tag{5.32}$$

Figure 5.4 shows how the response spectrum is obtained from the combination of the transfer function and the wave spectrum. The figure also shows how the response spectrum can be integrated to obtain the RMS-value of the response.

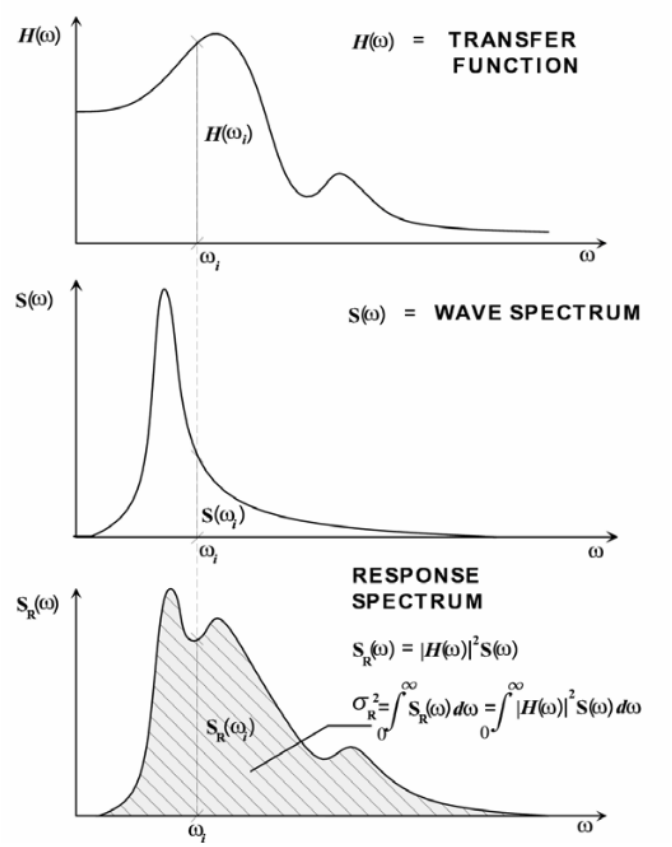

Figure 5.4: Proceedure to obtain the response spectrum and the zero'th order moment corresponding to the variance of the response, Fathi (2004).

The expected maximum value, $E(\eta_{max})$, in a sea state with a duration of T hours can be found if the probability distribution function for the maxima of responses is known. It can be assumed that the maxima of responses is Rayleigh distributed and an expression for the expected maximum can be formulated:

$$E(\eta_{max}) = 2\sigma_{\eta_a}\left[\sqrt{2\ln N} + \frac{0.5772}{\sqrt{2\ln N}}\right], \qquad N = \frac{T \cdot 3600}{T_z^{\eta_a}} \tag{5.33}$$

Note that the result from expression 5.33 is the double amplitude of the expected maximum response.

5.4.4 Coupling of motions

The MSI and MII criteria are evaluated at specified locations on the ship. They are derived from the acceleration that comes from combining the motion relative to each degree of freedom.

The displacement, velocity and acceleration at a critical position are the result of the coupling of motions. If all the translations and rotations are solved for, the motion of any point on the body can be found from the following expression:

$$\vec{\delta} = (\eta_1 + z\eta_5 - y\eta_6)\vec{i} + \eta_2 - z\eta_4 + x\eta_6)\vec{j} + (\eta_3 + y\eta_4 - x\eta_5)\vec{k} \tag{5.34}$$

Surge, sway and heave is denoted by η_1, η_2 and η_3, respectively. Similarly roll, pitch and yaw is denoted by η_4, η_5 and η_6. $\vec{i}$, $\vec{j}$ and $\vec{k}$ are unit vectors along the x-, y- and z-axis, respectively.

To evaluate the criteria related to hull interaction, the relative displacement , η_{rel}, between the vertical ship motion and the surface elevation must be found. In order to find the relative displacement, the following expression is used:

$$\eta_{rel} = |\zeta_{loc} - \eta_{ver}| \tag{5.35}$$

Here ζ_{loc} represents the water surface elevation at a defined location between the hulls and η_{ver} represents the vertical displacement of the ship at this location. Now the RAO for the relative displacement can be found to obtain the response spectrum, eq. 5.36. In turn, the short term statistics of the response can be found as described in section 5.4.3.

$$|H_{rel}(\omega, \theta)| = \left| \frac{\zeta_{loc} - \eta_{ver}}{\zeta_a} \right| \tag{5.36}$$

It should be emphasized that expression 5.36 implies that the criteria related to hull interaction is more sensitive to the chosen computation method than the criteria related to MII, MSI and helicopter operation. The reason is that since ζ_{loc} is included in the expression, the result is dependent on the deformation of the incoming waves by diffraction and radiation.

CHAPTER 6

Wasim

Wasim is a part of the SESAM suite of programs and is integrated in the Sesam HydroD Software. The Sesam program package is owned and distributed by DNV GL. Wasim is used for linear and non-linear hydrodynamic analysis of vessels moving with any forward speed. The program can also be used to analyze both fixed and floating vessels.

The fully 3-dimensional radiation/diffraction problem is solved by a Rankine panel method. The simulations are performed in the time domain, but a Fourier transformation makes it possible to obtain the results in the frequency domain.

The Rankine panel method requires panels both on the hull and on the free surface. The built-in mesh generator handles the free surface mesh but the hull meshing must be carried out by the user. This is done by creating a geometry model that is meshed by means of the mesh generator. According to Kim et al. (2008), the Rankine panel method that Wasim is based on was first implemented in the computer program SWAN2 at MIT by Kring (1994). The theory presented in the following section is based on Kring (1994).

6.1 Theory of Wasim

Consider a body travelling at constant forward speed with rotation Ω about an inertial frame (x_0, y_0, z_0). The forward speed can be decomposed into a x-component, U, and y-component, V, in the reference frame (x, y, x), see figure 6.1. Further, a mean velocity field in the body fixed reference frame can be defined, $\vec{W} = (U - \Omega x)\vec{i} + (V - \Omega y)\vec{j}$. The Gallilean transform relates the inertial and reference frame, where $\frac{d}{dt}$ represents the time rate of change in the inertial frame and $\frac{\partial}{\partial t}$ represents the time rate of change in the reference frame:

$$\frac{d}{dt} = \frac{\partial}{\partial t} - \vec{W} \cdot \nabla \tag{6.1}$$

To obtain the hydrodynamic loads, the wave flow about the ship must be examined. Wasim utilizes the velocity potential to find the fluid motion and pressure field. In addition to satisfying the Laplace equation, a set of boundary conditions must be imposed. The boundary value problem governs the wave propagation on the hull and the pressure distribution on the hull. The exact boundary value problem is linearized and decomposed into the basis flow, the local flow, the memory flow and the incident wave flow, ref. eq 6.2. The local flow decomposition is introduced as a means of numerical stability. The memory flow accounts for all wave propagation and has the form of an initial boundary value problem. The basis flow is assumed to be the largest part of the total flow. The incident wave potential represent the incoming wave.

$$\phi_{TOT} = \phi_I + \phi_B + \phi_L + \phi_M \tag{6.2}$$

Here ϕ_{TOT} is the total disturbance potential, ϕ_I is the incident wave potential, while ϕ_B, ϕ_L and ϕ_M is the basis-, local- and memory potential.

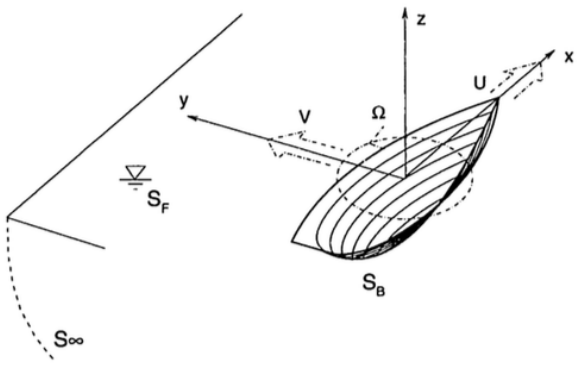

Figure 6.1: A surface piercing vessel where S_B represents the submerged part of the hull. The vessel is travelling at a constant forward speed, U, slip speed, V, and rotation, Ω, with respect to an intertial frame, (x_0, y_0, z_0). The ship is interacting with the surface waves and the waves generated by the vessel, which is represented by S_F. S_∞ represents the border of the sea infinitely distant from the vessel. The vessel is free to translate or rotate about a reference frame, (x, y, z), meaning that it has six rigid-body degrees of freedom. Kring (1994)

A summary of how the boundary value problem is treated is given in the following. The reader is referred to Kring (1994) for more details.

The purpose of the basis flow is to account for the presence of the hull. It does not satisfy the actual boundary condition of the ship because a normal mass flux is allowed to extrude from the stern of the ship to simulate a transom stern. This is done by imposing the following flux condition on the body, eq. 6.3.

$$\frac{\partial \phi_B}{\partial n} = (1 - f(x, y, z))\vec{W} \cdot n \qquad on\ S_{\bar{B}} \tag{6.3}$$

The function f controls the flux such that the flux is zero over most of the body and reduces the problem to the Double-body linearization. At the stern f attempts to produce a pressure approaching zero and reduces the problem to the Neumann-Kelvin basis flow. At the free surface and sea bottom the vertical velocity component of the basis flow is zero, $\frac{\partial \phi_B}{\partial z} = 0$.

The instantaneous fluid response is represented by the local potential, ϕ_L, that transfers the unsteady forcing from the body boundary condition to the free surface condition for the memory flow. It satisfies the boundary conditions on the actual hull. Basically, it represents the response of the ship. Because this component equals zero on the free surface, the local flow is not dependent on frequency but only the motion of the ship. The entire unsteady forcing is balanced by the local potential, eq. 6.4. The vertical component is equal to zero on the sea bottom, $\frac{\partial \phi_L}{\partial z} = 0$.

$$\frac{\partial \phi_L}{\partial n} = \sum_{j=1}^{6} \left(\frac{\partial \eta_j}{\partial t} + \eta_j m_j \right) \ on \ S_{\bar{B}} \tag{6.4}$$

where

$$\begin{aligned} (n_1, n_2, n_3) &= \vec{n} \\ (n_4, n_5, n_6) &= \vec{x} \times \vec{n} \\ (m_1, m_2, m_3) &= (\vec{n} \cdot \nabla)(\vec{W} - \nabla \phi_B) \\ (m_4, m_5, m_6) &= (\vec{n} \cdot \nabla)(\vec{x} \times (\vec{W} - \nabla \phi_B)) \end{aligned} \tag{6.5}$$

The m-terms, m_j, provide a coupling between the basis flow and the unsteady wave solution. $\phi_L = 0$ at the free surface. Hence, the z=0 plane has a condition of zero pressure but allows a flux. This vertical flux transfers the body forcing to an inhomogeneity in the initial boundary value problem that will be taken care of by the memory flow.

The memory flow represents the reflections of waves on the hull, ie. it represents the solution for the steady, radiated and scattered wave patterns, ζ_M. Its purpose is to cancel the effect of incoming waves at the hull, and make sure that the free surface conditions are satisfied. The solution of this wave flow requires that the basis and local flows are found. The initial boundary value problem is given in equation 6.6 and balances the forcing arising from steady motion on the mean body position $S_{\bar{B}}$.

$$\frac{\partial \phi_M}{\partial n} = (\vec{W} - \vec{\phi_B}) \cdot \vec{n} - \frac{\partial \phi_I}{\partial n} \ \ on \ S_{\bar{B}} \tag{6.6}$$

The linearized kinematic and dynamic free surface conditions are given in equation 6.7 and 6.8, respectively. The formulation of the free surface conditions expanded to account for incident waves, ζ_I, is given in Luo (2013).

$$\frac{\partial \zeta_M}{\partial t} - (\vec{W} - \nabla \phi_B) \nabla \zeta = \frac{\partial^2 \phi_B}{\partial z^2} (\zeta_M + \zeta_I) + \frac{\partial \phi_L}{\partial z} + \frac{\partial \phi_M}{\partial z} - (\nabla \phi_B \cdot \nabla \zeta_I) \ \ on \ z{=}0 \tag{6.7}$$

$$\frac{\partial \phi_M}{\partial t} - (\vec{W} - \nabla \phi_B) \nabla \phi_M = -g \zeta_M + [\vec{W} \cdot \nabla \phi_B - \frac{1}{2} \nabla \phi_B \cdot \nabla \phi_B] - \nabla \phi_B \nabla \phi_I \ \ on \ z{=}0 \tag{6.8}$$

where ϕ_M, $\frac{\partial \phi_M}{\partial z}$ and ζ_M are unknown a priori. The vertical component of the memory potential, $\frac{\partial \phi_M}{\partial z}$, is zero at the sea bottom. The radiation condition is satisfied by the implementation of a numerical beach.

The hydrodynamic forces and moment amplitudes is found by integrating the linearized pressure over the mean submerged portion of the hull:

$$H_j = \int \int_{S_{\bar{B}}} p \cdot n_j \, dS \quad \text{for} \quad j = 1, ..., 6 \tag{6.9}$$

where H_1, H_2 and H_3 are force components along the x, y and z direction respectively. H_4, H_5 and H_6 are components of moment about the x, y and z axis respectively. The linear pressure is decomposed into the Froude-Krylov, p_{FK}, local, p_l, the memory, p_m and the zero-speed hydrostatic, p_c, pressure components. Hence, $p = p_{FK} + p_l + p_m + p_c$. A further decomposition is imposed on the local potential such that terms for acceleration, velocity and displacement can be collected. This decomposition results in the local force coefficients, i.e the added mass, damping and restoring coefficients.

The boundary value problems are transformed into boundary integral equations by application of Green's second identity, eq. 6.10.

$$2\pi\phi_{TOT}(\vec{x}) - \int \int_{S_F \cup S_U} \frac{\partial \phi_{TOT}(\vec{x'})}{\partial n} G(\vec{x'}; \vec{x}) dx' + \int \int_{S_F \cup S_U} \phi_{TOT}(\vec{x'}) \frac{\partial G(\vec{x'}; \vec{x'})}{\partial n} dx' \tag{6.10}$$

where $G(\vec{x}'; \vec{x})$ is the Rankine source potential, eq. 6.11.

$$G(\vec{x}; \vec{x}) = \frac{1}{|\vec{x} - \vec{x}'|} \tag{6.11}$$

The basis- and local flows can be determined by using any general source or potential based panel method. Wasim utilizes the fundamental Rankine source. The Rankine source only satisfies the Laplace equation in the fluid domain and no boundary conditions. Thus, sources have to be distributed on all the boundaries, which causes a high number of unknowns and an increased memory cost. The numerical approach to solve the memory flow boundary value problem is to discretize the body boundary and free surface. In Wasim, the sea bottom boundary conditions is satisfied by mirroring, meaning that no mesh is needed here. The unknown global quantities, ζ_M, ϕ_M and $\frac{\partial \phi_M}{\partial n}$ are discretized by a biquadratic spline representation and the geometry is discretized by grids of quadrilateral facets or panels. This representation of the geometry gives rise to the name "panel method". The B-spline representation takes advantage of a basis function or a shape function to determine the continuity of the global quantities between panels. At each panel, the basis function is magnified by the associated time-dependent

spline coefficient, $(\zeta_M)_j(t)$, $(\psi)_j(t)$ and $(\psi_z)_j(t)$. The spline coefficients can be considered the spatially discrete unknowns. The global quantities are found by summation of the basis functions, B_j, centered at the jth panel, weighted by the spline coefficient. By distributing Rankine sources and dipoles over the free surface and the wet hull surface, the Laplace equation within the fluid and the condition at infinity, S_∞, are satisfies. The remaining conditions are explicitly satisfied through the boundary integral formulation, eq. 6.10, and the set of time evolution equations, eqns. 6.7 and 6.8. The solution of the integral equation provides the initial conditions for the evolution equations. The kinematic condition uses the past solution for vertical flux to update the wave elevation. The dynamic condition used the present solution for the wave elevation to update the potential.

6.2 Features of Wasim

This section will describe the features of Wasim that is necessary to review before conducting the analysis. Wasim is able to perform linear- and non linear analysis, both in time domain and frequency domain. This section will only treat the relevant subjects for this work. For a complete description of Wasim, the reader is referred to DNV (2011).

6.2.1 Definition of waves

Wasim defines the incoming waves as presented in equation 6.12, where k is the wave number, the wave direction is defined by θ and the phase angle is given by φ.

$$\zeta(x, y, t) = \zeta_a \cos[(k \cos\theta)x + (k \sin\theta)y - \omega t + \varphi] \tag{6.12}$$

In a Wasim frequency domain analysis, the regular wave components are described by defining a frequency set and direction set. The input to the wave load analysis is a sum of these wave components. As mentioned in section 6.1, Wasim solves the wave-vessel interaction problem in time domain. Each analysis is divided into a number of runs, depending on the density of the mesh, the size of the time step and the size of the direction- and frequency set. Each run uses a limited number of the frequencies from the set. However, many of the frequencies appear in multiple runs. By looking at the time series from a selected run, it can be seen that the input signal appears as an irregular wave form, see figure 6.2. It is possible to represent the regular wave set in this manner due to the linear relationship between the input signal and the response.

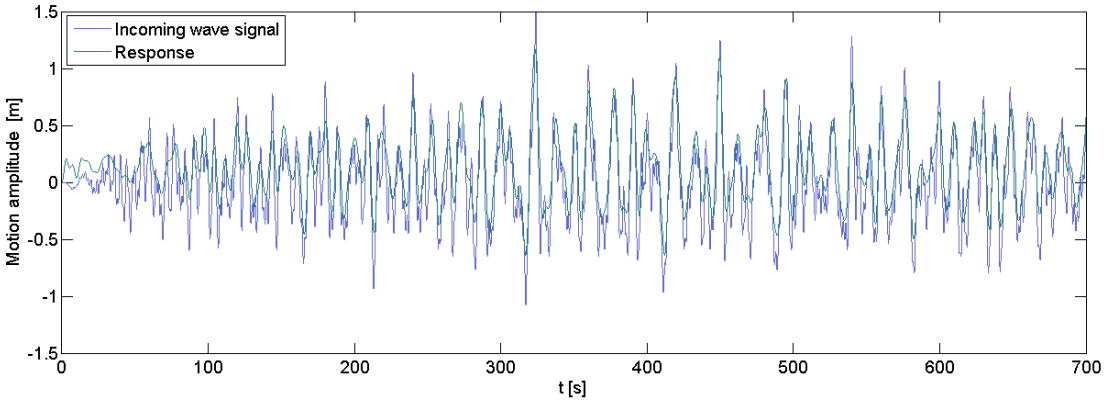

Figure 6.2: It is seen from this example run that the incoming wave signal is modelled like an irregular wave. This irregular wave is a superposition of the regular wave components defined in the frequency set.

6.2.2 Coordinate system

Wasim defines the global coordinate system, used internally for all calculations, as in figure 6.3.

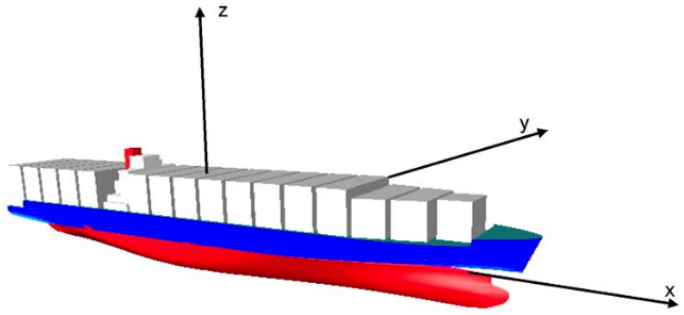

Figure 6.3: The global coordinate system in Wasim defines the mean free surface by the xy-plane and the symmetry plane by the xz-plane. The axis-origin is located at mid-ship, which is defined as the mean of the two perpendiculars given in the geometry file. The x-axis is directed towards the bow of the ship, the y-axis is positive at port side and the z-axis is directed upwards, (DNV, 2011).

The waves are propagating in the positive x-direction, eq. 6.12. As the x-axis is directed towards the bow a heading of $\theta = 0^\circ$ corresponds to following seas, while a heading of $\theta = 180^\circ$ corresponds to head seas. When $\theta = 90^\circ$ the ship will experience beam seas with the port side as the lee side.

6.2.3 Stability and accuracy

In order to obtain a stable solution it is crucial to choose a sufficiently small time step for the algorithm. The limiting time step will be dependent on the shape and orientation of the individual panels in the mesh. DNV (2011) has presented a method to theoretically analyze the stability for a uniform grid with rectangular panels. A stability diagram can be used to find the relation between the stability parameter β and the grid Froude number $\mathcal{F}_h$.

The stability parameter is defined in mathematical terms by expression 6.13, while the grid Froude number is defined in expression 6.14.

$$\beta^2 = \frac{h_x}{g(\Delta t)^2} \tag{6.13}$$

$$\mathcal{F}_h = \frac{U}{\sqrt{gh_x}} \tag{6.14}$$

Here h_x is the smallest panel length in the longitudinal direction. The stability diagram is presented in figure 6.4

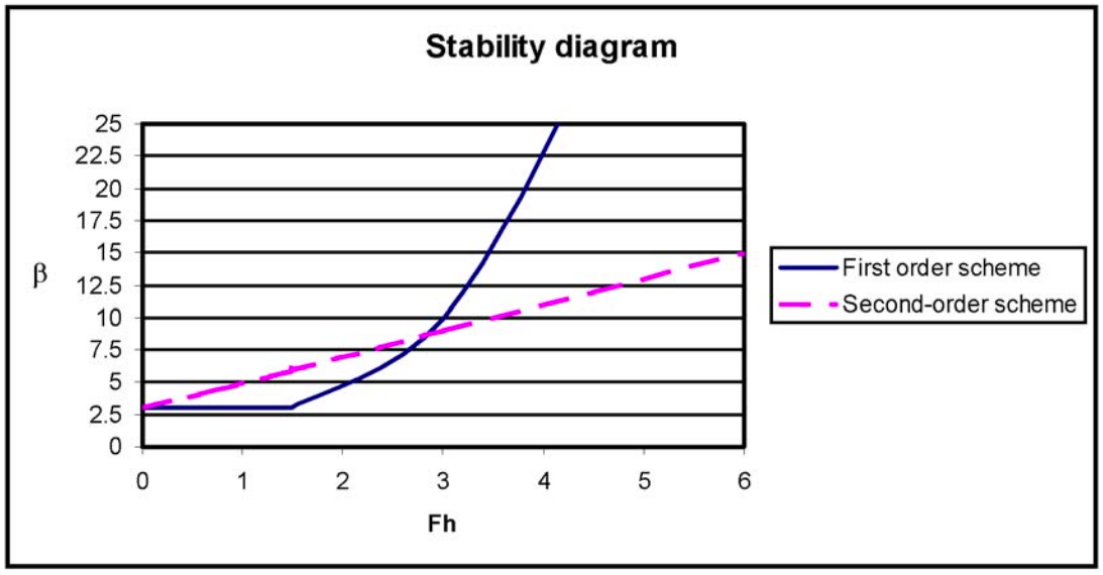

Figure 6.4: The stability diagram describes the relationship between the free surface grid number β and the grid Froude number $\mathcal{F}_h$. The sufficient time stepping, Δt, for the time domain solution of the wave-vessel interaction problem can be found with support in this diagram (DNV, 2011).

The first step to find the sufficient time step, Δt, is to determine the smallest panel length in the x-direction, h_x, and solving for the corresponding grid Froude number by

equation 6.14. Further, the free surface grid number, β, can be read from the stability diagram in order to solve for Δt by equation 6.13. The solution is stable if β is chosen to be larger than the limiting value.

It should be noted from figure 6.4 that a large Froude number will result in a large free surface grid number and a small time step. In other words, for high speed cases the stability will be a dominating issue.

It should be noted that the stability requirement defined by DNV (2011) does not guarantee stability for all frequencies. As stated in Xiang and Faltinsen (2011), each oscillation period should include at least 40 time steps for the case that is presented in their study. In this study the smallest oscillation period included is $T = 2s$. If 40 time steps is used the time stepping size will be $\Delta t = 0.05s$ instead of the necessary condition defined by DNV (2011), which gives $\Delta t = 0.08$ for the case of a grid froude number of $\mathcal{F}_h = 2$ with the grid size $h_x = 1.7$.

For the case of low to moderate grid froude numbers the stability requirement is less limiting. See figure 6.4. Because stability can be achieved for a relatively large time step size there will be a risk of a non-accurate solution. The kinematic and dynamic free surface condition must be satisfied at each time step. The kinematic condition uses the past solution at $t = t_n$ for vertical flux to update the wave elevation, which is applied to update the potential for the dynamic condition, see section 6.1. If the time step size is sufficiently small the solution will be accurate. If not, the wave energy will be over- or underestimated. In practice a sufficient time step size can be found by running a convergence test for a limited set of frequencies and directions before the complete analysis is initiated.

6.2.4 Motion control

Another issue that can cause instability in a time domain simulation is the treatment of the horizontal motions. In a frequency domain analysis, the degrees of freedom are treated as harmonic responses, while this is not the case in time domain. The heave, roll and pitch motion will be controlled by the natural restoring forces induced by the changing buoyancy. The surge, sway and yaw motion have no stiffness and if these motions are not controlled the response will grow to extreme values if the ship is drifting off.

In Wasim, there are two different methods to handle control of the horizontal motions. One option is to use a rudder and autopilot. If applied correctly this method has the benefit of producing a model that is a good representation of the real problem. To use this method a set of coefficient must be provided to describe the rudder model. To find a set of coefficient that also gives a stable solution is difficult and normally no set of coefficient will provide stability for all speeds and wave directions. Because the trimaran ship must be evaluated at a range of wave directions at different speeds this method will

be a poor choice and is therefore avoided.

The other available option is to use a soft spring system that will provide stiffness for the horizontal motions. The setup of the soft spring system is presented in figure 6.5

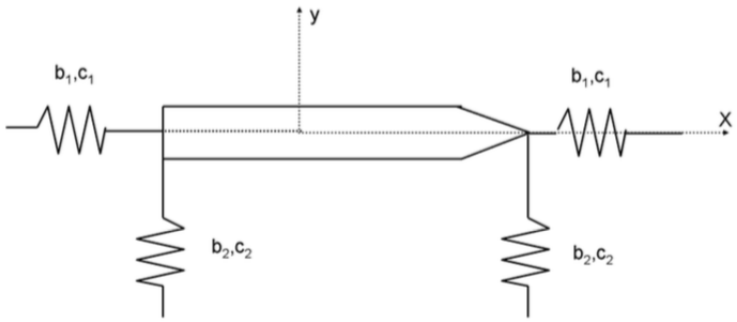

Figure 6.5: The soft spring system is designed to control the horizontal motion to obtain stability of the solution. The stiffness coefficients, c_1 and c_2, and the damping coefficients, b_1 and b_2, are implicitly defined by the user. (DNV, 2011).

The stiffness coefficients are defined by specifying the natural period of surge, sway and yaw. The damping coefficients are defined by specifying the fraction of critical damping. Hence, the it is not required to define the damping- and restoring coefficients directly. It is important to avoid unwanted interference with the roll motion, so the natural periods of the horizontal motions should be much longer than the natural periods of roll. According to DNV (2011), typical values are in the range 60-120 s for conventional vessels. High speed vessels will have natural periods in the range 30-60 s.

6.2.5 Roll damping

Unlike the pitch motion that is dominated by potential damping, the roll damping is dominated by viscous damping. It is therefore necessary to include a damping model in the analysis to account for viscous effects. The roll damping model that is used in Wasim is a quadratic damping model:

$$B_{44} = B_1 + B_2|\dot{\eta}_4| = \left(b_1 + b_2\frac{|\dot{\eta}_4|}{\omega_4}\right)B_4^{crit} \tag{6.15}$$

B_{44} is the roll damping coefficient and B_1 is the linear damping coefficient. B_4^{crit} is the the critical damping in roll. B_2 is the quadratic damping coefficient and is only relevant in non-linear analyzes. In a linear analysis the user only has to specify the non-dimensional coefficient b_1, which is given as a fraction of the critical damping.

6.2.6 Hull interaction

The 3D potential theory that is implemented in Wasim is able to account for the interaction between the side- and main hull. However, this method assumes that intertial and gravity forces will dominate the wave propagation and therefore the flow within the fluid volume is assumed to be invicid, irrotational and incompressible. This simplification can be justified if only the global motions are of interest. In the case of multi-hulled vessels this assumption can lead to unphysical results. An important interaction effect is a near resonance wave that is trapped between the hulls. This wave will excite sway and roll motions. Due to the lack of viscous wave damping, this wave will build up and become unphysical. This will be seen as resonant peaks in the transfer functions for sway and roll motions, (DNV, 2014). Resonance peaks will also appear for the heave and pitch motions, due to the coupling between motions.

According to DNV (2014) the eigenfrequency of a trapped wave in a narrow wave between two floaters will be in the range given in equation 6.16, where G is the gap between the floaters and T is the draft of the floaters.

$$1 + \frac{2}{\pi} \cdot \frac{G}{T} < \frac{\omega_0^2 T}{g} < 1 + \frac{\pi}{2} \cdot \frac{G}{T} \tag{6.16}$$

Care must be taken if the wavelengths of interest are in this range. Equation 6.16 can be used as a guide to predict the eigenfrequency of the trapped wave for each version of the trimaran, see table 6.1. According to equation 6.16, the natural period of the gap wave has a stronger dependence on the side hull draft compared to the gap size. Although version 5 has a relatively large gap size compared to version 2 it can be seen that the gap wave natural periods are in approximately the same range. This is due to the large draft of the side hulls of version 5 compared to version 2

Table 6.1: Natural period range of gap found by utilizing equality 6.16

NATURAL PERIOD RANGE OF GAP WAVE					
Version 1	3.8 s	$<$	T_n	$<$	4.6 s
Version 2	3.0 s	$<$	T_n	$<$	3.8 s
Version 3	1.8 s	$<$	T_n	$<$	2.5 s
Version 4	1.7 s	$<$	T_n	$<$	2.4 s
Version 5	2.7 s	$<$	T_n	$<$	3.5 s

To account for hull interaction when comparing the five versions of the trimaran hull, an array of evaluation points have been defined between the main hull and the side hull. It is necessary to define points on both port- and starboard side to take sheltering effects into consideration. Figure 6.6 presents how the evaluation points are specified.

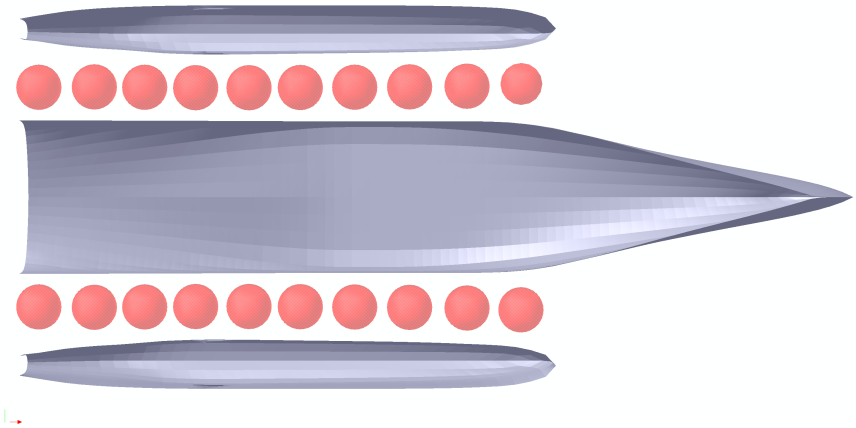

Figure 6.6: Evaluation points for evaluation of hull interaction.

6.3 Input

6.3.1 Modelling

LMG Marin has provided a panel model for each trimaran version that describes the geometry. However, these panel models can not be used as input for the Wasim analysis. A new geometry file for each trimaran version has been created which are are based on the panel models provided by LMG Marin.

The geometry files contains a description of the vessel geometry by a set of hull parts, which are called patches. Each patch contains a number of sections, defined by a set of offset points given from keel to a point located above the water line. The sections are not allowed to intersect each other and must be defined from bow to stern. The sections are only allowed to intersect the free surface once. The patches must be defined in the right sequence to define the water line correctly. For a trimaran, the patches are defined such that the first patch describes the bow region for the port side hull, followed by the middle - and aft region. The next group of patches are defined similarly for the stern side of the side hull. Lastly, the port side of the main hull are defined by the patches arranged from bow to stern. It is recommended to use as few patches as possible, to obtain a good mesh quality. If a patch has irregular geometry the patch must be split up, as in the case of a bulbous bow. Otherwise the meshing tool will not be able to mesh the patch. Wasim uses the user defined sections to describe the hull geometry by interpolating across the sections. It is therefore important to give a sufficient description of irregular geometries by providing enough points on the sections and keeping a small distance between the sections.

6.3.2 Mesh

Most of the effort of obtaining a nice mesh is done if the geometry file is of high quality. The meshing is done by the program Wasim_Mesh/Hydro_Mesh with the geometry file as input. An example of a mesh distribution is shown in figure 6.7.

The user can define the number of grids or panels in the longitudinal- and horizontal direction. It is important to choose a mesh size that is small enough to obtain an accurate solution. In order to find a good mesh distribution it is recommended to run a convergence test. Thus, it can be avoided to use a mesh size that is unnecessary small, which is beneficial because stability will be reached for a larger time step. If a very small time step is used, the solution will be neutrally stable. However, if stability and accuracy can be obtained at a larger time step there will be a lot to save in terms of CPU time for a large run.

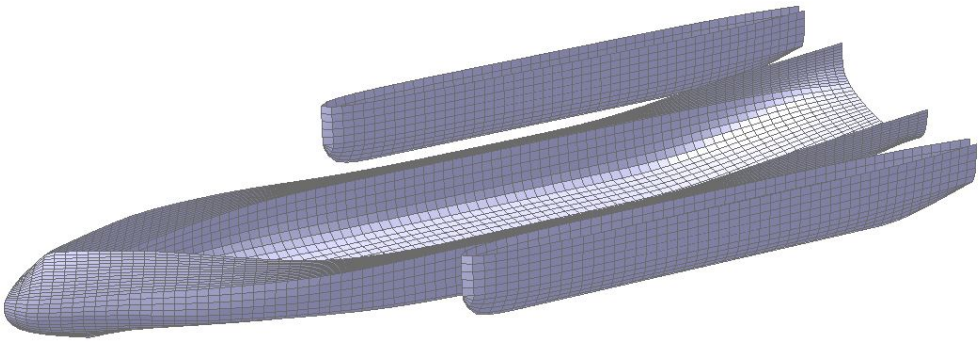

Figure 6.7: Mesh for Trimaran Version 3

It was found that accurate results were obtained for an average panel length $h_x = 1.5$ m. The smallest panel length in this case was chosen as $h_x = 1.2$ m.

6.3.3 Time step

At zero forward speed the stability parameter is $\beta = 2.6$, see figure 6.4. This corresponds to a time step $\Delta t = 0.14$. The time step value used in the analysis was $\Delta t = 0.1$. The necessary time step for 5 and 16 knot was found by the same approach and the result is given in table 6.2.

Table 6.2: Final time step value Δt_{final} used in the analysis, together with grid froude number $\mathcal{F}_h$, stability parameter β and minimum time step value Δt_{min} respecting the stability requirement defined by DNV (2011).

U [kt]	$\mathcal{F}_h$ [-]	β_{min} [-]	Δt_{min} [s]	Δt_{final} [s]
0	0	2.6	0.13	0.12
5	0.75	2.6	0.13	0.1
16	2.40	6.3	0.05	0.04

6.3.4 Location parameters

The density and kinematic viscosity of the water and air surrounding the vessel must be defined. These values are presented in table 6.3. It was chosen to use the default value of 300 meters for the depth.

Table 6.3: Environmental properties

PROPERTY		AIR	WATER
Kinematic viscosity	[m^2/s]	1.19E-06	1.46E-05
Density	[kg/m^3]	1.226	1025

6.3.5 Mass model

The total mass of the model is calculated by Wasim when the loading condition is specified. It is assumed zero trim and heel angle. In addition, the radius of gyration must be specified. These values were provided by LMG Marin and was used as input in the Wasim analysis. The loading condition, defined by the draft T, and radii of gyration is presented for each version in table 6.4. The loading condition is presented as the distance from the base line to the water line.

Table 6.4: Input for the mass model in Wasim

	VERSION 1	VERSION 2	VERSION 3	VERSION 4	VERSION 5
T [m]	7.5	7.5	7.5	8.0	8.0
r_{44} [m]	12.000	10.600	9.870	9.9	11.970
r_{55} [m]	27.400	27.400	29.800	27.325	27.400
r_{66} [m]	27.400	27.400	29.800	27.325	27.400
r_{64} [m]	0	0	0	0	0

6.3.6 Directions of wave propagation

Due to the symmetry of the vessel it is only necessary to evaluate wave directions from 0° to 180°. It is decided to include directions in this range with a step of 30°. Hence the following directions are included: 0°, 30°, 60°, 90°, 120°, 150° and 180°. 180° corresponds to head seas and 0° corresponds to following seas.

6.3.7 Wave periods

To obtain complete information about the motion characteristics it is necessary to include a sufficiently large range of wave periods. In addition, the step between the periods should not be too large, especially close to the natural periods. It was decided to run the analysis for wave periods ranging from T = 2-30 s. Between T = 4-16 s, the range was divided into intervals of 0.5 seconds to obtain a complete RAO. The range between T = 17-20 s was given with an interval of 1 s and the range T = 20 - 30 was given with an interval of 5 second.

In the low period range it was expected that problems related to excitation of a trapped wave between the hulls would occur, ref. eq. 6.16. The only option to treat this challenge is to do trial runs in order to detect the natural period of the trapped wave. A solution strategy to remove the disturbance from the trapped wave is to exclude periods close to this natural period. The influence of this trapped wave turned out to be the largest challenge in this work. Therefore an own chapter has been dedicated for the discussion of this particular event, ref chapter 7.

6.3.8 Motion control springs

According to the discussion in section 6.2.4, a way to provide stiffness for the horizontal motions is to introduce a soft spring system. The input to the soft spring system is the natural period and critical damping ratio for surge, sway and yaw. Table 6.5 shows the input for the motion control springs.

Table 6.5: Input for the motion control system

MOTION MODE	T_n [s]	ξ [-]
Surge	100	0.05
Sway	70	0.05
Yaw	70	0.05

CHAPTER 7

Analysis Problems

7.1 Description of the problem

The analysis for zero forward speed was conducted without any difficulties when the stability requirements were respected. The analysis for version 3 and 4 in the case of a forward speed of 5 knots was also manageable. The results of version 5 were within reasonable values, but the results was affected by some interruptions. The analysis of version 1 at a forward speed of 5 knots resulted in unphysical results throughout the whole frequency range. It was discovered that the wave elevation in the gap between the side- and main hull showed extremely high values and that resonant peaks were occurring for periods in the range 3 - 7 s. It was therefore attempted to avoid the irregular frequencies by removing periods in this range. It was even attempted to remove all periods up to 10 s. None of these methods gave any significant improvement of the results.

Because the problems concerned the whole frequency range it was suspected that the cause could be related to stability issues, ref. section 6.2.3 and 6.2.4. Hence, it was attempted to decrease the time step and increase the mesh size. Many attempts of solving the stability issues were tested, but none of them had any affect on the results. To exclude that the problems were related to stability issues a test run was performed for a model where the side hulls were removed. In this case the analysis was performed without any stability problems and the results was within expected limits. The same was seen for high speeds.

Figure 7.1a presents the heave RAOs for version 1 at 5 knots. Clear resonance peaks corresponding to low periods can be seen. The behaviour after these resonant peaks can not be related to any physical arguments. It is particularly abnormal that the RAO values increase as the periods increase. Except from the local peak values, each RAO has its maximum at $T = 30$ s, where the wave period is far away from the natural period of the gap wave.

Figure 7.1b presents the RAOs for the relative vertical displacement between the surface elevation and the vessel motion. The position where the relative displacement is found is located at the port side of the vessel close to $L_{SH}/2$, where L_{SH} is the length of the side hull. However, the trend that is shown in figure 7.1b is representative for all the positions along the side hull, i.e all positions have extremely high values and natural periods in approximately the same range. It can be seen that the natural periods of the relative displacement RAOs correspond to the natural periods in the heave RAOs. The response is unphysical throughout the whole frequency range.

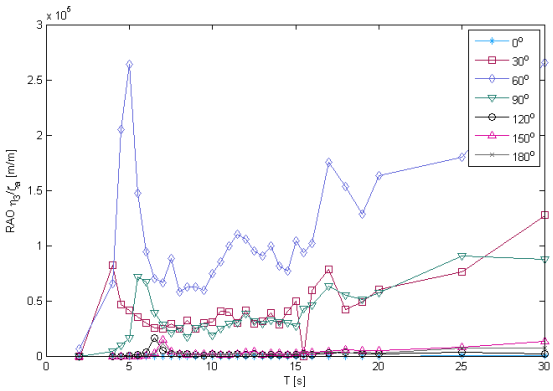

(a) Heave RAOs for Version 1

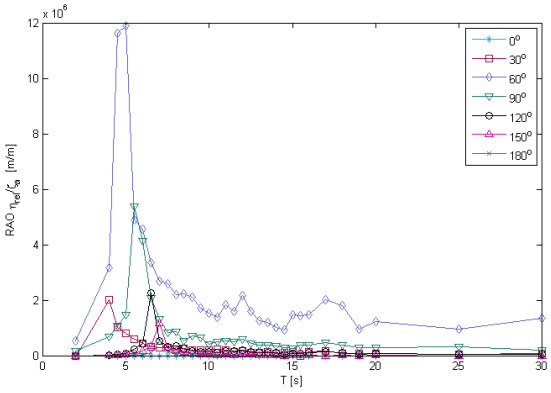

(b) Relative vertical motion RAO

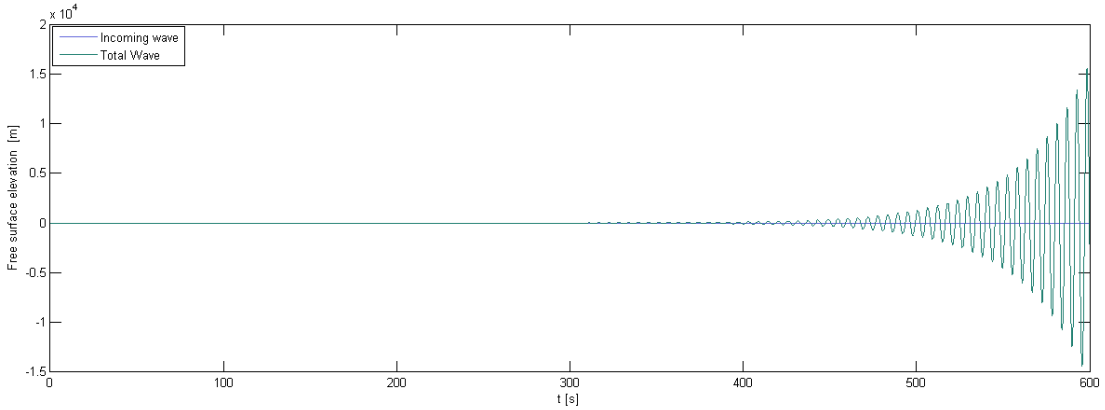

(c) Time development of wave elevation for the incoming wave and the total wave elevation for the complete analysis

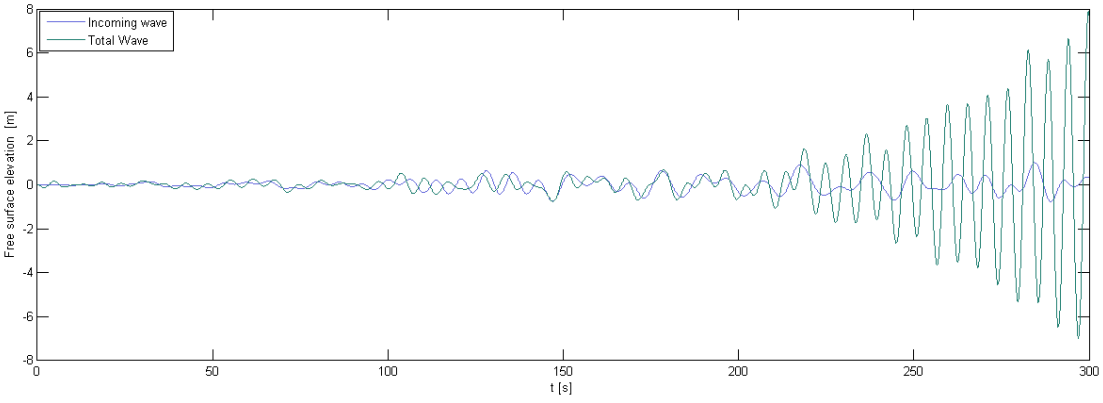

(d) Time development of wave elevation for the incoming wave and the total wave elevation for a shorter time series

Figure 7.1: Presentation of unphysical results obtained for trimaran version 1 at a forward speed of 5 knots

It appears as if the irregular frequencies from the resonant peaks is transmitted on to the remaining frequencies. To understand why this is happening it is necessary to look at the wave elevation at the described position, ref. 7.1c and ref. figure 7.1d. Up until about 200 seconds into the analysis the total wave elevation has reasonable behaviour. As the simulation continues from this point, the total wave elevation start to show illogical behaviour. The lack of viscous damping allows the wave to increase without boundaries. In theory, it should be effective to remove the frequencies which are not possible to control by the damping mechanism caused by 3D effects. It is suspected that this method fails due to the way Wasim models the incident wave, ref. section 6.1. In the cases where the analysis fail, the incoming waves will have a form similar to the one presented in figure 7.1c. When the analysis is complete, Wasim will try to decompose this wave form into regular wave components corresponding to the specified frequency range. As the wave form no longer has a physical shape, the total wave energy will be distributed over the whole frequency range, and the final result will end up as in the case presented in figure 7.1a. If the incident waves were modelled as regular wave components it would be easier to separate the irregular frequency waves from the other waves and thus avoid the transmitted interference. Figure 7.2 presents the heave RAOs of version 1 at 5 knots after a number of periods in the range 2 - 7 have been removed. It is clear that this approach does improve the results. The response amplitudes corresponding to 0° and 30° are now in the order of 10^7, which is an aggravation of the results.

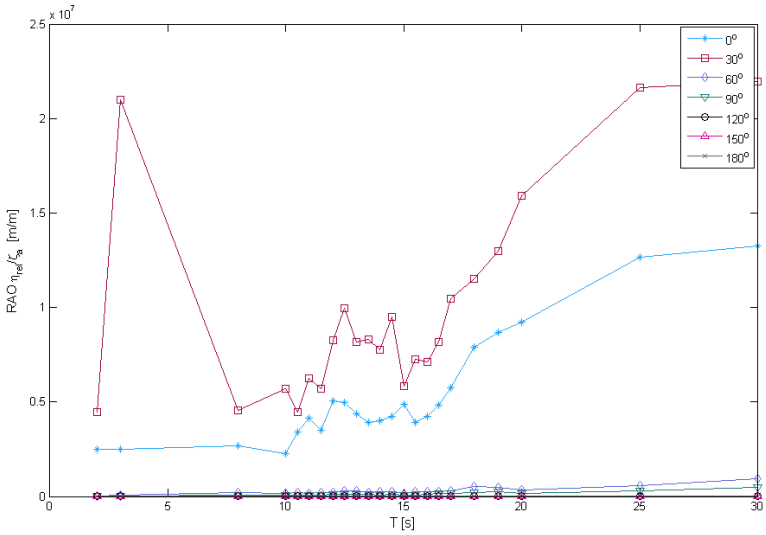

Figure 7.2: Heave RAO for version 1 at 5 knots. It has been attempted to improve the results by removing a number of periods in the range 2 - 7 s.

As mentioned above, reasonable results were obtained for version 3 and 4 at 5 knots. Therefore it was attempted to increase the speed to 16 knots in the simulations. These simulations failed in the same manner as presented in figure 7.1. It became clear that the difficulties related to resonant wave motion are harder to avoid as the speed increases.

A suggested explanation of this is that the resonant frequencies will be more dominant due to the effect of encounter frequency. In other words, the resonant peaks are shifted into the frequency range and causes large disturbances.

It also became clear that version 1 has the most challenging hull configuration, followed by version 2 and version 5. The hull configuration of version 3 and 4 are easier to handle for Wasim. As it was seen in section 6.2.6, the hull configuration of version 1 will lead to the largest gap wave natural period due to the large side hull draft and small gap size. This could be the reason that version 1 is the most challenging hull configuration and also supports the suggested explanation of why the simulation fails at high velocities. Version 3 and 4 have the lowest natural periods due to small draft and large gap size and was well handled by Wasim at 0 and 5 knots.

7.2 Alternative approach - Veres

The initial plan was to perform the complete seakeeping analysis in Wasim. For this reason, the complete transfer functions had to be obtained at the operational speed of 5 knots and the transit speed of 16 knots. This way, it would be possible to account for the effects caused by diffraction due to wave interaction. However, as these results were not obtained it was decided to utilize the software Veres to assess the criteria that are less sensitive to analysis method. I.e the MSI, MII and helicopter operation criteria. The criteria related to relative motion between the wave elevation and the vessel motion will be assessed based on the successful results from Wasim. Due to this deviation from the initial plan, a description of Veres will be given in the following.

ShipX is a hydrodynamic design tool developed by MARINTEK. The workbench is developed to perform systematic design studies using advanced hydrodynamic analysis tools. The advanced functions are built in as “Plug-Ins”, which are managed through an interface that is easy to navigate. The module that will be utilized in this context is the Plug-In named Vessel Responses (Veres). Veres has great advantages in terms of computational effort and user interface.

Fathi (2004) describes Veres as a tool that is suitable in an early design stage. The available outputs from Veres are the motion transfer functions in six degrees of freedom, relative motion transfer functions and global wave induced loads. The post-processor provides a range of wave spectra that can be utilized to obtain short terms statistics of the mentioned output. Further, the post-processor offers the options of calculating long term statistics, slamming pressures and producing operability diagrams. Time simulations of motions and loads allow for assessment of important non-linear effects. The mentioned results can be found for a vessel with zero forward speed or advancing with any forward speed. The direction of the incoming waves can be chosen arbitrarily.

7.2.1 Theory of Veres

Veres uses the strip theory formulation by Salvesen et al. (1970). The strip theory is based on potential theory, meaning that the velocity potential has to satisfy the Laplace equation in addition to the boundary conditions. The decomposition of the total velocity potential is different than the method that was seen in section 6.1. The velocity potential is separated into a time-independent steady contribution due to the forward motion and a time-dependent part associated with the incident wave system and the unsteady body motions, (Fathi, 2004):

$$\phi(x,y,z,t) = [Ux + \phi_S(x,y,z)] + \phi_T(x,y,z)e^{i\omega t} \tag{7.1}$$

The problem is linearized by assuming small oscillatory motions which also allows a convenient decomposition of the time-dependent part of the potential:

$$\phi_T(x,y,z) = \phi_I + \phi_D + \sum_{j=1}^{6} \phi_j \eta_j \tag{7.2}$$

Here ϕ_I is the incident wave potential, ϕ_D is the diffraction potential and ϕ_j is the contribution to the velocity potential from each mode of motion.

By obtaining the fluid pressure from the Bernoulli equation, the hydrodynamic forces and moment amplitudes can be found by integrating the linearized pressure over the mean position of the surface hull:

$$H_j = \rho \int\int_{S_{\bar{B}}} \eta_j \Big(i\omega + U\frac{\partial}{\partial x}\Big)\ \phi_T\ dS,\ \ j = 1,2,...,6. \tag{7.3}$$

Here H_1, H_2, H_3 are the force components in x, y and z direction, while H_4, H_5, H_6 are the moments about the x, y and z-axis. The forces and moments can be divided into exciting loads, F_j, and forces due to the body motions, G_j.

$$F_j = \rho \int\int_{S_{\bar{B}}} \eta_j \Big(i\omega + U\frac{\partial}{\partial x}\Big)(\phi_I + \phi_D)\ dS \tag{7.4}$$

$$G_j = \rho \int\int_{S_{\bar{B}}} \eta_j (i\omega + U\frac{\partial}{\partial x}) \sum_{k=1}^{6} \phi_j \eta_j\ dS = \sum_{k=1}^{6} T_{jk}\eta_k \tag{7.5}$$

Here T_{jk} represents the hydrodynamic force or moment in the jth direction due to a a unitary displacement in the kth motion mode. By separating T_{jk} into a real and imaginary part, the following expression is obtained:

$$T_{jk} = \omega^2 A_{jk} - i\omega B_{jk} \tag{7.6}$$

where A_{jk} is the added mass coefficient and B_{jk} is the damping coefficient. The restoring coefficients, C_{jk} are independent of frequency and forward speed and can be found directly from hydrostatic considerations.

The velocity potential and hydrodynamic coefficients is found by considering a closed surface containing the body surface, the free surface and a control surface far away from the body:

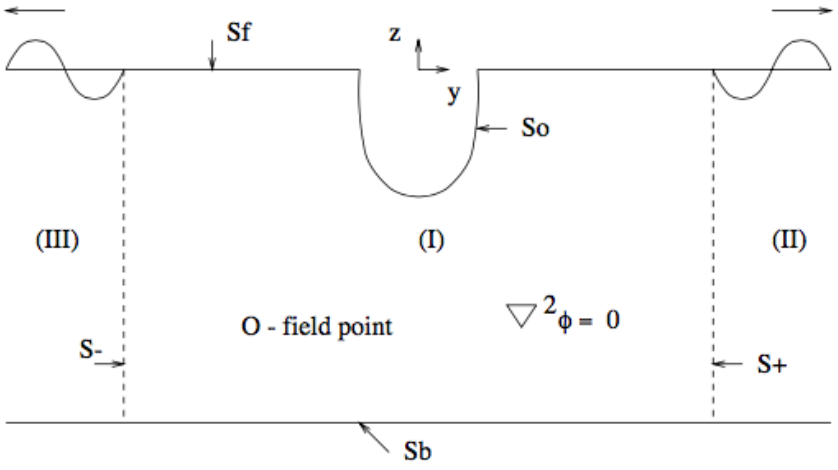

Figure 7.3: Fundamental two-dimensional sources and dipoles are distributed over a closed surface consisting the body surface, the free surface and a control surface far away from the body. (Fathi, 2004).

Green's second identity is applied to represent the velocity potential in terms of sources and dipoles over the control surface, eq. 7.7. The control surfaces are approximated by straight line segments and constant values of the velocity potentials and its normal derivatives are assumed at each segment.

$$-2\pi\phi = \int_S \left(\phi \frac{\partial log(r)}{\partial n} - log(r) \frac{\partial \phi}{\partial n} \right) \tag{7.7}$$

Now that the diffraction and radiation problems are reduced to the two dimensions, the hydrodynamic coefficients, A_{jk} and B_{jk}, can be expressed in terms of two dimensional added mass- and damping coefficients. This also applies for the exciting forces and moments. The strip theory solves the diffraction and radiation problem at a number of sections along the length of the hull, and approximate the 3D solution by integrating the solution at each section over the length of the ship. The described method is applicable both in the low speed and high speed theory, but different theories are used for the integration over the body and for the description of the the boundary conditions. The reader is referred to Fathi (2004) for details.

7.2.2 Coordinate system

The coordinate system in Veres is defined as in figure 7.4

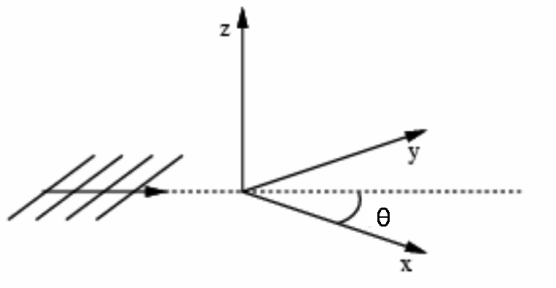

Figure 7.4: The global coordinate system in Veres defines the mean free surface by the xy-plane and the xz-plane coincides with the center-plane, like in Wasim. The axis-origin is located at the center of gravity. The x-axis is directed towards the stern, the y-axis is positive to starboard and the z-axis is directed upwards. (Fathi, 2004).

As the waves are propagating in the positive x-direction, a wave direction of 0° corresponds to head sea waves and 180° corresponds to following seas. A wave direction of 90° corresponds to beam sea waves with starboard side as lee side.

7.2.3 Viscous roll damping

Veres provides the option of including viscous roll damping in the calculations. These values are based on empirical formulations. The reader is referred to Fathi (2004) for a detailed description. In practice, the user has to specify the amplitude of the incident wave. The chosen wave amplitude should be corresponding to the significant wave height used in the short term response calculations. As the short term response in this thesis are found using a significant wave height of $H_s = 4$ m, a wave amplitude of 2 meters is specified in Veres.

CHAPTER 8

Results and Discussion

8.1 Post-processing results

The transfer functions have been obtained by the use of numerical tools. To evaluate the criteria that were specified in chapter 4, the short term statistics must be obtained. The Veres post-processor is very effective and has the option to calculate both MSI and MII values. The initial plan was to obtain the transfer functions from Wasim and utilize the Veres post-processor to evaluate the MII and MSI criteria. In order to use the Veres post-processor together with Wasim result, the transfer functions must be converted into a *.re1-file. However, due to the analysis problems it was decided to run simulations in Veres for the assessment of the MSI, MII and helicopter operation criteria. Therefore, the transfer functions could be imported to the post-processor directly through the ShipX interface.

The results corresponding to the Veres simulations are presented in section 8.3 through 8.9. The results corresponding to the Wasim simulations are presented in section 8.10. Section 8.10 starts with describing how the Wasim results were post-processed.

8.2 Interpretation of results

Wasim and Veres have different definitions of the global coordinate system, ref. section 6.2.2 and 7.2.2. Wasim results are interpreted as follows: 0°, 180° and 90° corresponds to following, head and beam sea with port side as lee side. Veres results are interpreted as follows: 0°, 180° and 90° corresponds to head, following and beam sea with starboard side as lee side.

8.3 MSI at the bridge

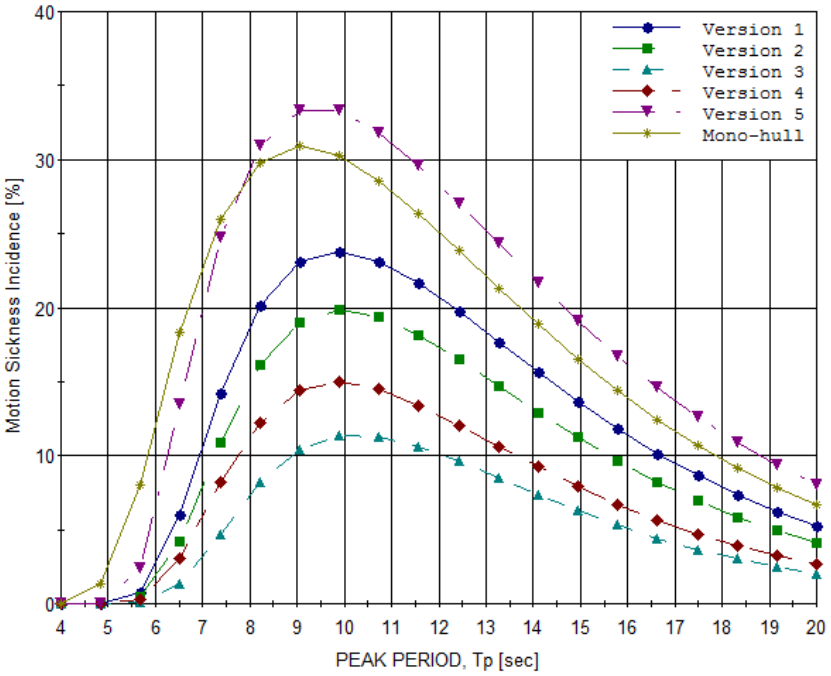

(a) 0 deg heading

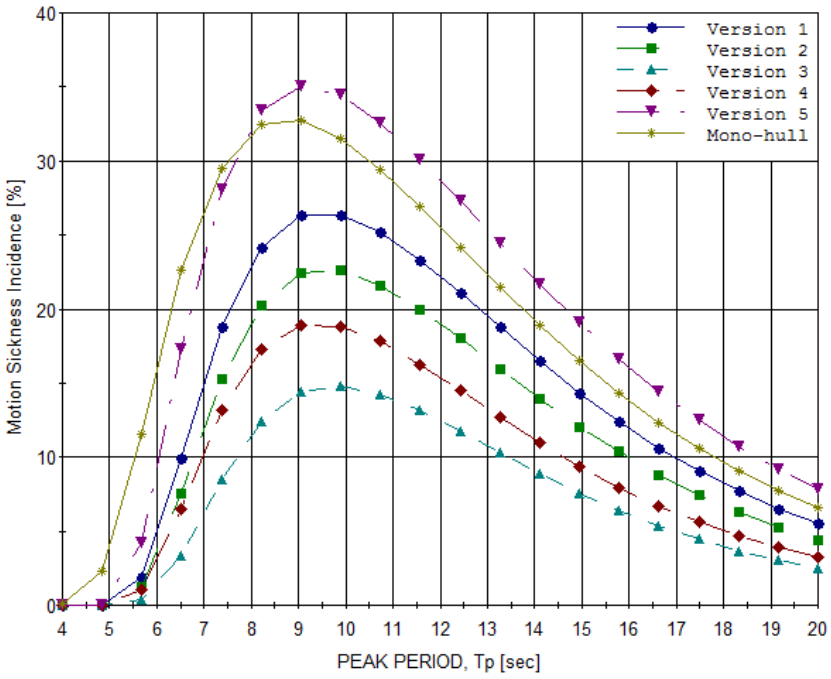

(b) 30 deg heading

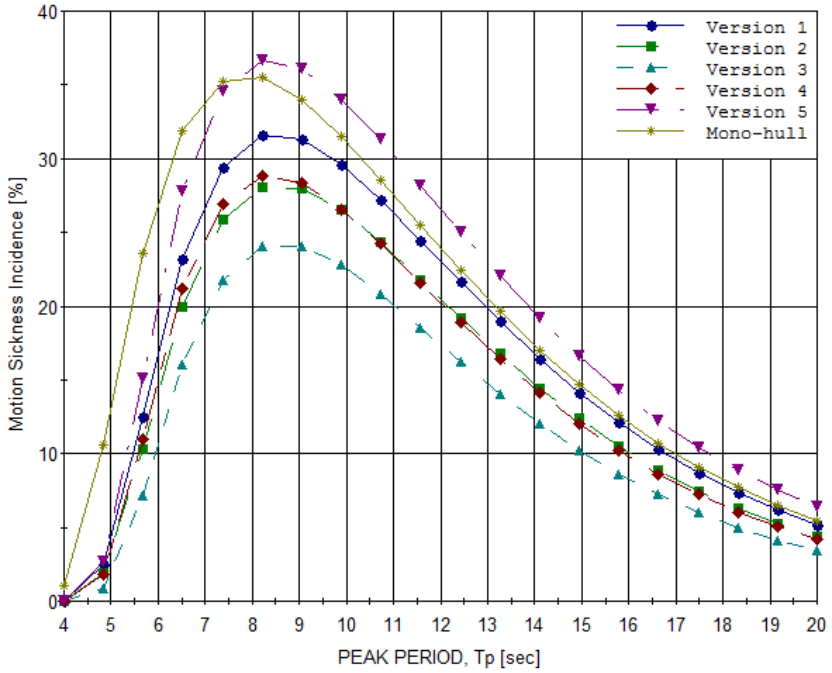

(c) 60 deg heading

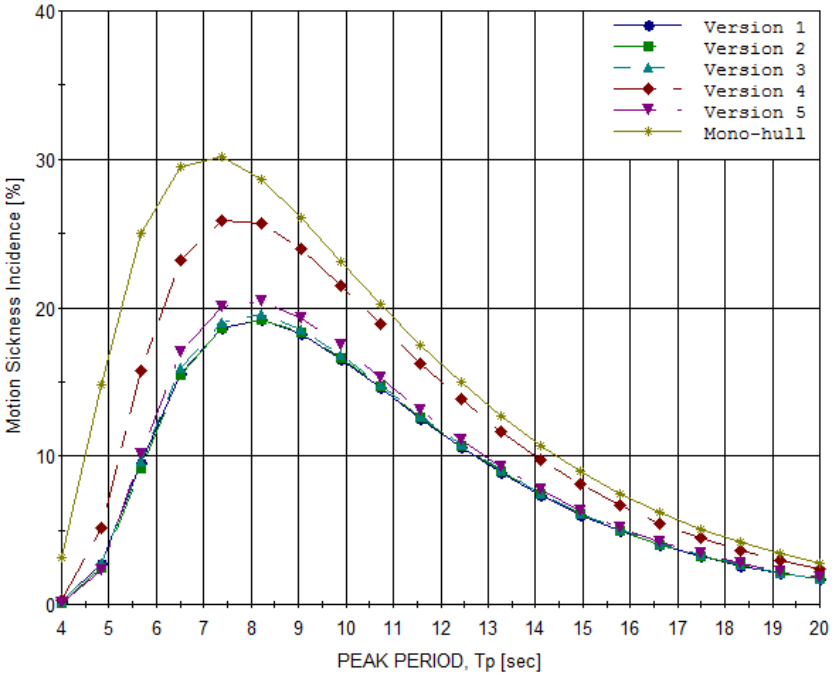

(d) MSI 90 deg

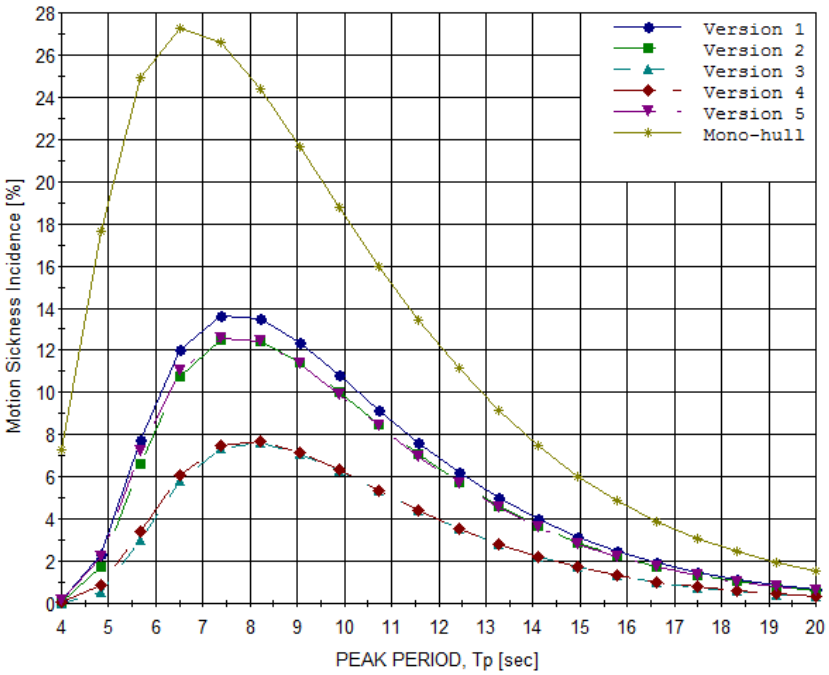

(e) 120 deg heading

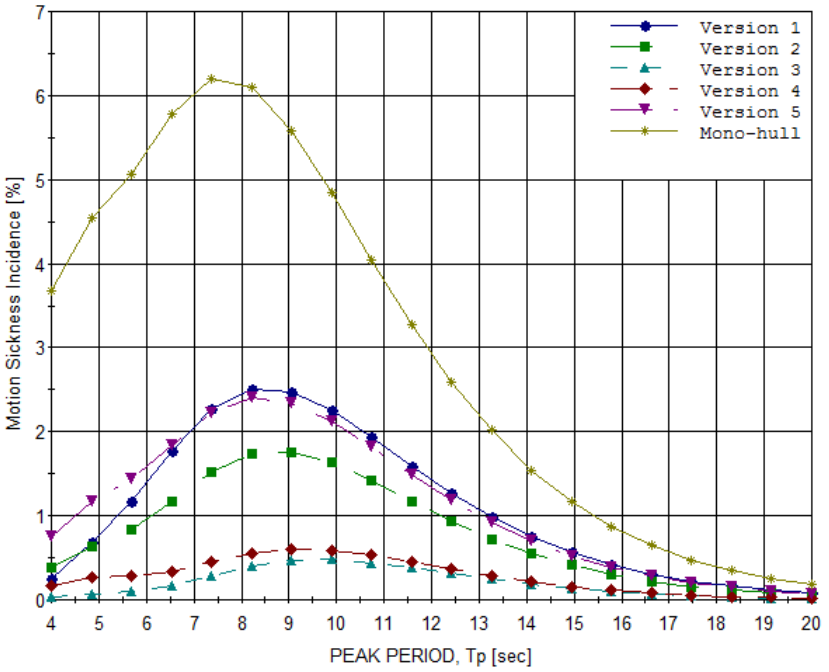

(f) 150 deg heading

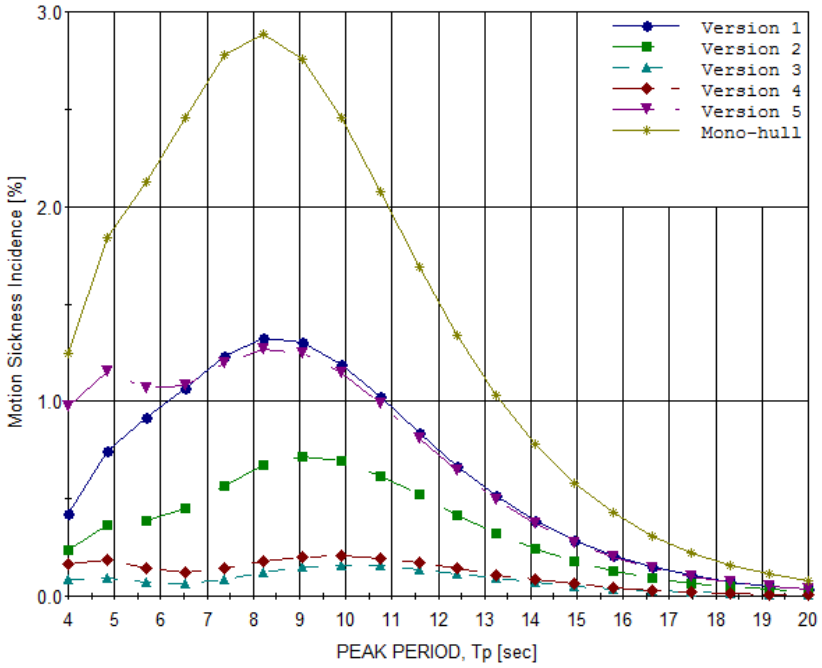

(g) 180 deg heading

Figure 8.1: The percentage occurrence of MSI against the peak period, T_p. $H_s = 4$ m. Each vessel has a forward speed of 5 knots. The position of the MSI is at the bridge.

From the results in figure 8.2 it can be seen that version 5 has the highest occurrence of MSI in the cases of waves with directions of 0°, 30° and 60°. These are also the cases where the percentage of MSI reaches its highest values. In these cases, version 5 has a higher occurrence of MSI than the mono-hull. In all other cases, the largest occurrence of MSI corresponds to the mono-hull. By reviewing the results it becomes clear that version 3 has the lowest MSI values. Version 4 also shows good result compared to the other versions, except from the case of beam sea.

The highest values of MSI at the bridge occurs when the incoming waves have a direction of 60°. The values decrease when the direction angle of the incoming waves increase. The working conditions on the bridge will be favourable in the case of following seas.

8.4 MSI in the recording room

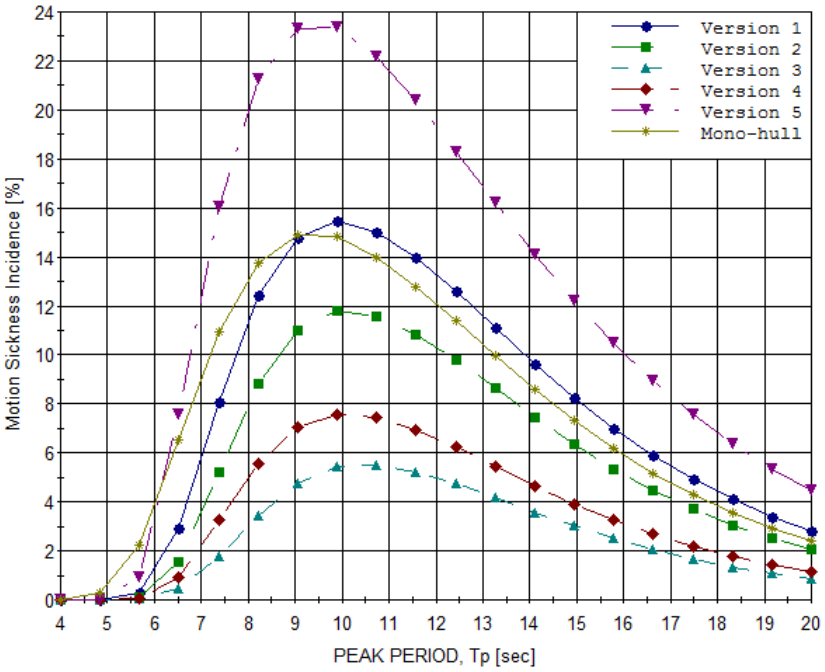

(a) 0 deg heading

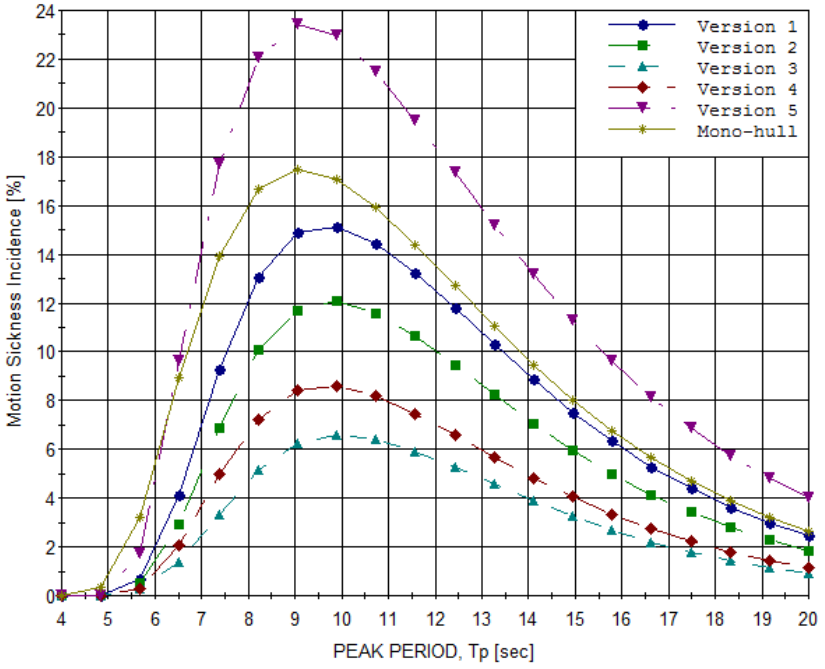

(b) 30 deg heading

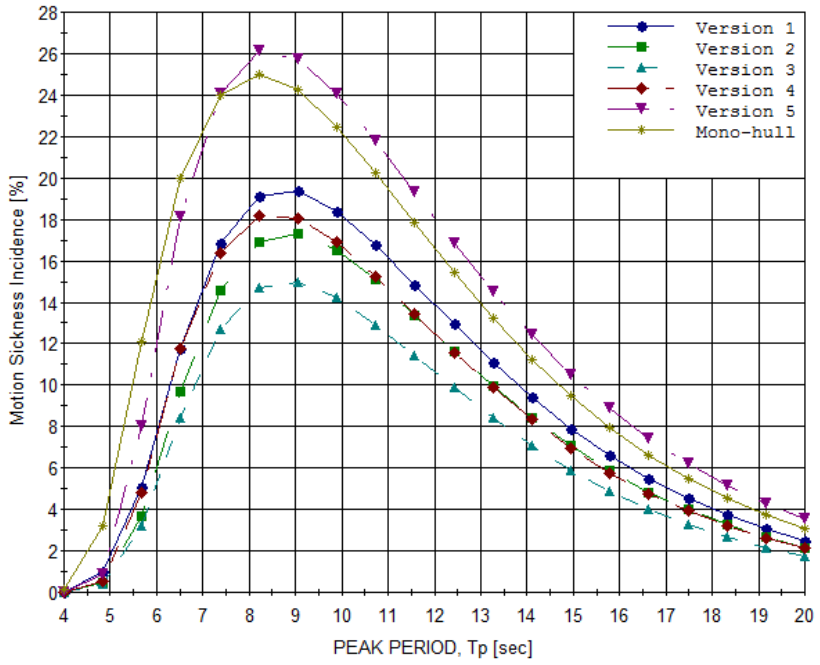

(c) 60 deg heading

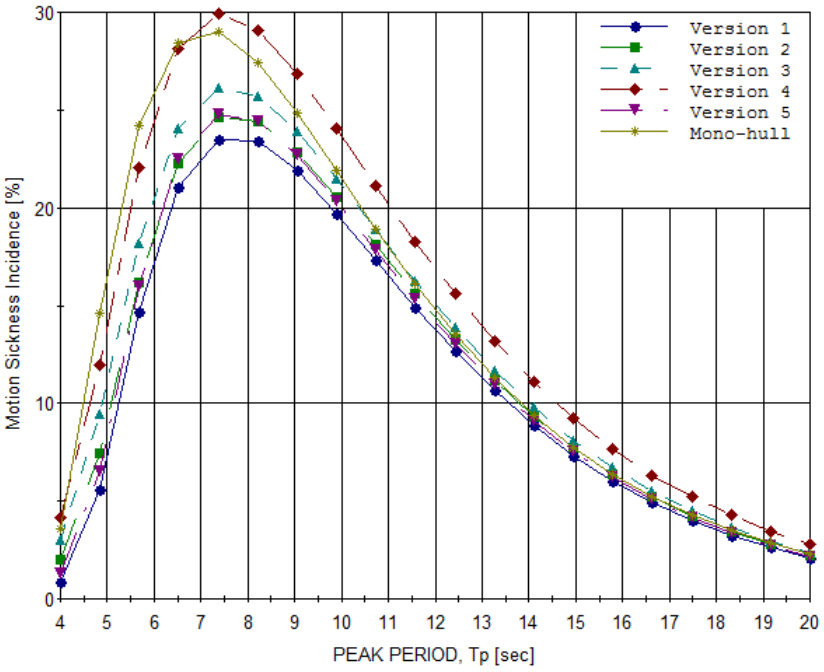

(d) MSI 90 deg

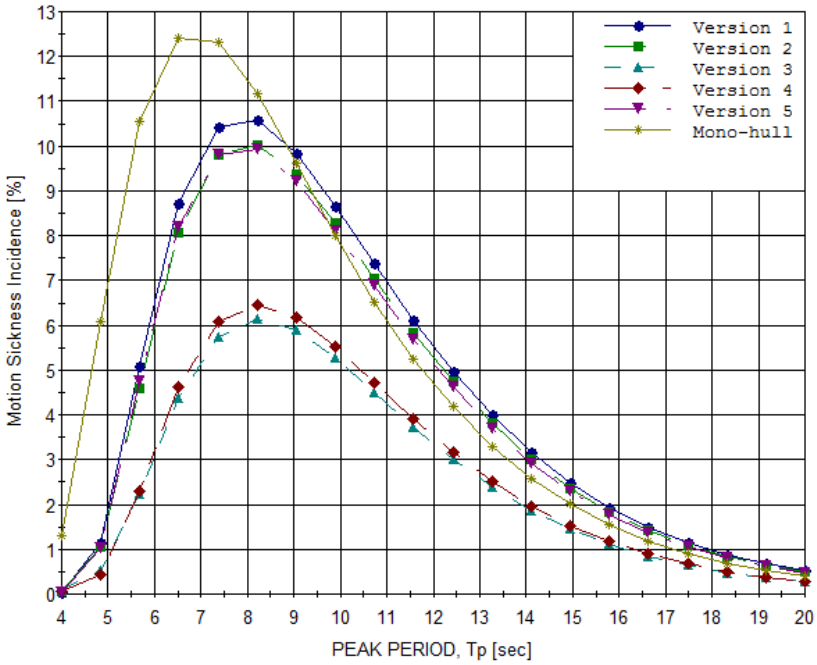

(e) 120 deg heading

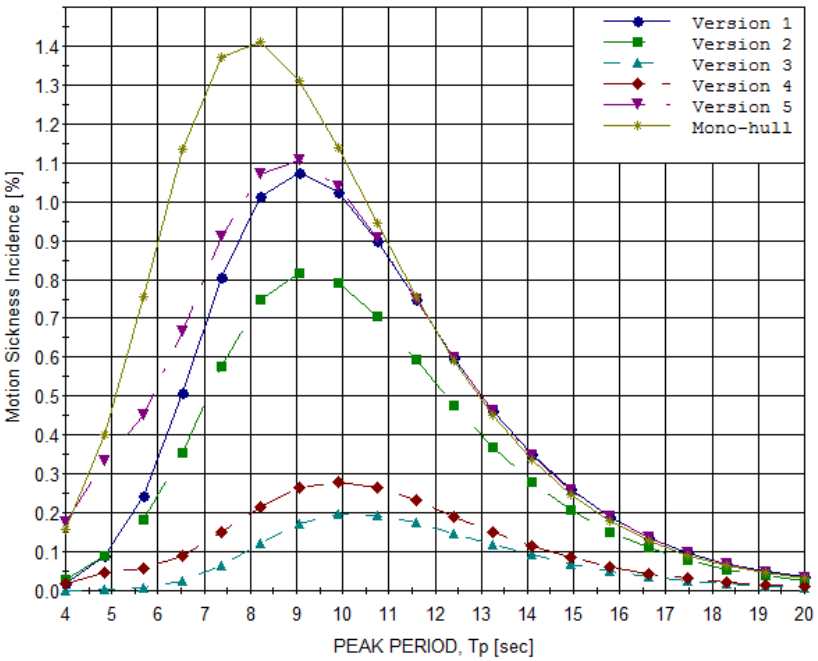

(f) 150 deg heading

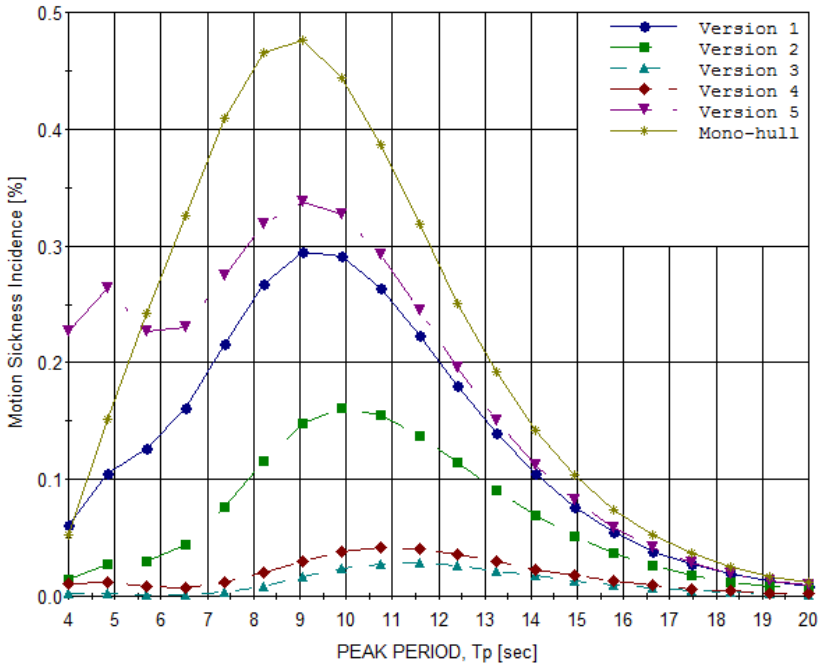

(g) 180 deg heading

Figure 8.2: The percentage occurrence of MSI against the peak period, T_p. $H_s = 4$ m. Each vessel has a forward speed of 5 knots. The position of the MSI is at the recording room.

The MSI occurrence at the recording rooms show many of the same tendencies as the MSI results at the bridge: Version 5 has the highest values in the case of wave directions of 0°, 30° and 90°. The occurrence of MSI is low in the case of following seas, and high in the case where the waves have a direction of 60°.

Version 3 and 4 show good results in all wave headings, except from the case of beam seas where the MSI is quite high compared to the other versions. As expected, the MSIs at the recording rooms are in general lower than the MSI at the bridge. This is because the recording room is located closer to the centre of gravity.

8.5 MSI at the bridge, 16 knot

The MSI at the bridge has been found in the case of a forward speed of 16 knot. The results are given in appendix A. The results correspond to the same significant wave height that was used in the case of 5 knots, i.e $H_s = 4$ m. It was found that the MSI values at 0°, 30° and 60° increase for all vessels. In these cases, version 3 reaches MSI values in the order of 30%, while the mono-hull has MSI values close to 45%. Version 5 has the largest values of MSI: The values reach 50% in the case of head sea waves. It was found that when the waves have directions of 90°, 120°, 150° and 180° the MSI values have significantly smaller values compared to the case of 5 knots.

8.6 MSI in the recording room, 16 knot

The MSI at the recording room was also found in the case of a forward speed of 16 knots. The results are given in appendix B. The results corresponds to the same significant wave height that was used in the case of 5 knots, i.e $H_s = 4$ m. The same trend that was seen at the bridge is seen in the recording rooms: The MSI values increase at 0°, 30° and 60°, while there is a reduction in the occurrence of MSI when the waves have a direction of 90°, 120°, 150° and 180°.

8.7 Relationship between pitch and roll natural period

As discussed in chapter 2, the relationship between the natural periods in roll and pitch should be compared to assess whether it is possible that the trimaran will show the characteristic cork-screw motion of a catamaran. The natural periods and the absolute value of the deviation for all headings are presented in table 8.1. The objective is to check if the deviation will be smaller or larger for certain headings. Hence, head sea and following sea are not included, as the roll motion will be minimal in these situations. As the cork-screw motion is not known to be a problem for mono-hull ships, the natural periods and deviation for the comparison ship are included to serve as reference values.

It is important to make clear that this comparison is not sufficient to prove or reject that the trimaran will exert cork-screw behaviour, as it is little information about this phenomenon in the literature. The comparison will only serve as an indicator of how the trimaran will behave.

Table 8.1: Roll and pitch natural periods for the comparison ship and the five versions of the Trimaran. The natural periods are given for five heading where roll and pitch motion occur simultaneously.

COMPARISON SHIP				VERSION 1			
0 knot	Roll Tn	Pitch Tn	Deviation	0 knot	Roll Tn	Pitch Tn	Deviation
30°	13	8	5	30°	7.5	8.5	1
60°	13	7	6	60°	7	8	1
90°	13	6.5	6.5	90°	7	7	0
120°	13	6.5	6.5	120°	7	7.5	0.5
180°	13	8.5	4.5	180°	7.5	9	1.5
5knot				5knot			
30°	14.5	8.5	6	30°	8	9	1
60°	14	6	8	60°	7.5	8.5	1
90°	13	7	6	90°	7	7	0
120°	12	6	6	120°	6.5	7	0.5
150°	11.5	8.5	3	150°	8	9	1
16 knot				16 knot			
30°	17	9	8	30°	9.5	11	1.5
60°	15.5	8	7.5	60°	8.5	8	0.5
90°	13	7	6	90°	7	7	0
120°	9.5	6.5	3	120°	7.5	7	0.5
150°	6	9	3	150°	9	10	1

VERSION 2

0 knot	Roll Tn	Pitch Tn	Deviation
30°	8	8.5	0.5
60°	7.5	8	0.5
90°	7	7	0
120°	7.5	8	0.5
180°	8	8.5	0.5
5knot			
30°	8.5	9.5	1
60°	8	8.5	0.5
90°	7.5	7	0.5
120°	7	7.5	0.5
150°	8	9.5	1.5
16 knot			
30°	9.5	10	0.5
60°	8.5	8	0.5
90°	7	7	0
120°	7.5	7	0.5
150°	9	9.5	0.5

VERSION 3

0 knot	Roll Tn	Pitch Tn	Deviation
30°	8	9	1
60°	7.5	8	0.5
90°	7	7	0
120°	7	8	1
180°	8.5	9.5	1
5knot			
30°	8.5	9.5	1
60°	8	8.5	0.5
90°	7.5	6	1.5
120°	7	7	0
150°	8.5	9.5	1
16 knot			
30°	8.5	10	1.5
60°	7.5	8	0.5
90°	6.5	7	0.5
120°	8	7	1
150°	9.5	10.5	1

VERSION 4

0 knot	Roll Tn	Pitch Tn	Deviation
30°	8	9	1
60°	7	7.5	0.5
90°	7	7.5	0.5
120°	7	7.5	0.5
180°	8.5	9	0.5
5knot			
30°	8	9	1
60°	8	8	0
90°	7.5	6.5	1
120°	7	7.5	0.5
150°	8.5	10	1.5
16 knot			
30°	9.5	10.5	1
60°	8.5	9.5	1
90°	7	7	0
120°	8	7	1
150°	9	10.5	1.5

VERSION 5

0 knot	Roll Tn	Pitch Tn	Deviation
30°	8	8.5	0.5
60°	7.5	7.5	0
90°	7.5	6.5	1
120°	7.5	7.5	0
180°	8.5	8.5	0
5knot			
30°	8	9	1
60°	8	8	0
90°	7.5	7	0.5
120°	7.5	7	0.5
150°	9	9	0
16 knot			
30°	9.5	11	1.5
60°	8.5	10	1.5
90°	7	7	0
120°	7.5	7.5	0
150°	9.5	10	0.5

From table 8.1 it can be seen that the deviation between the roll and pitch natural period is very small for all headings for the trimaran, compared to the mono-hull. One could expect that the different trimaran configurations would lead to varying correlation between roll and pitch motion. However, there are small differences between the different trimaran versions. Hence, it is not possible to state which version that is favorable regarding a possible cork-screw motion based on this comparison. Even though the different versions have varying displacement distribution and total displacement, all the versions have the same width. The length vary from 110 to 120 meters. This indicates that the strong correlation between roll and pitch is mainly influenced by the width-to-length ratio.

Based on the discussion above it can not be said that the trimaran concept has favourable characteristics with respect to cork-screw motion. In chapter 2 it was described that successful trimaran designs have the superior stability features of a catamaran and the favourable motion characteristics of a mono-hull. The trimarans that this statement refers to have a significantly smaller width and often small side hulls. Therefore, it can be concluded that the very large width of the OilCraft Trimaran will result in an unwanted correlation between pitch and roll motion. If the ship in question will exert the cork-screw motion is still uncertain, but the results above indicate this.

8.8 Motion induced interruption

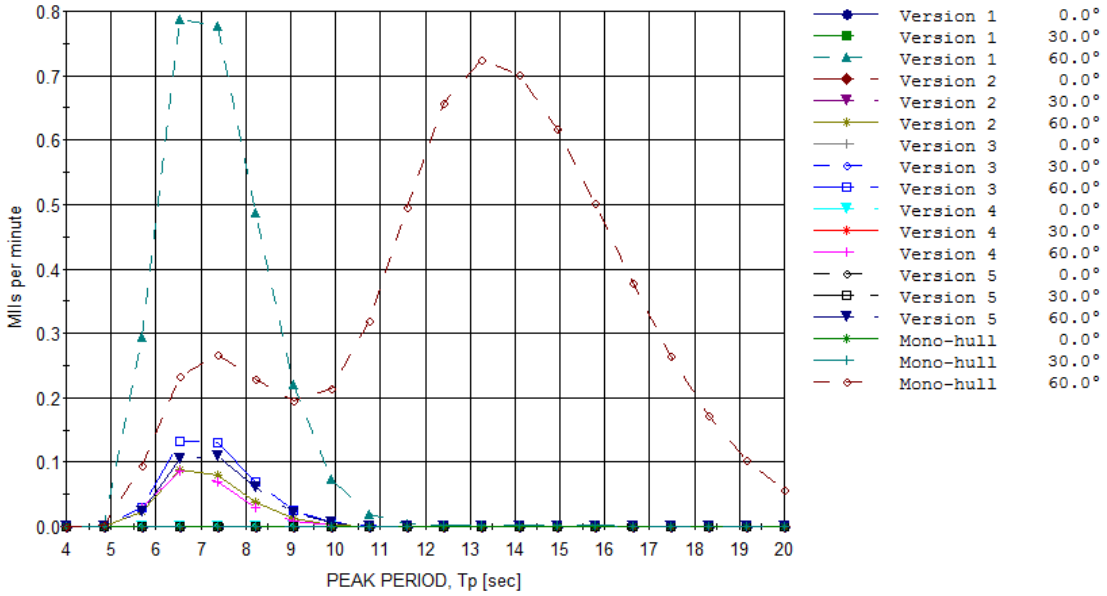

(a) Deck position 1, headings 0°, 30° and 60°

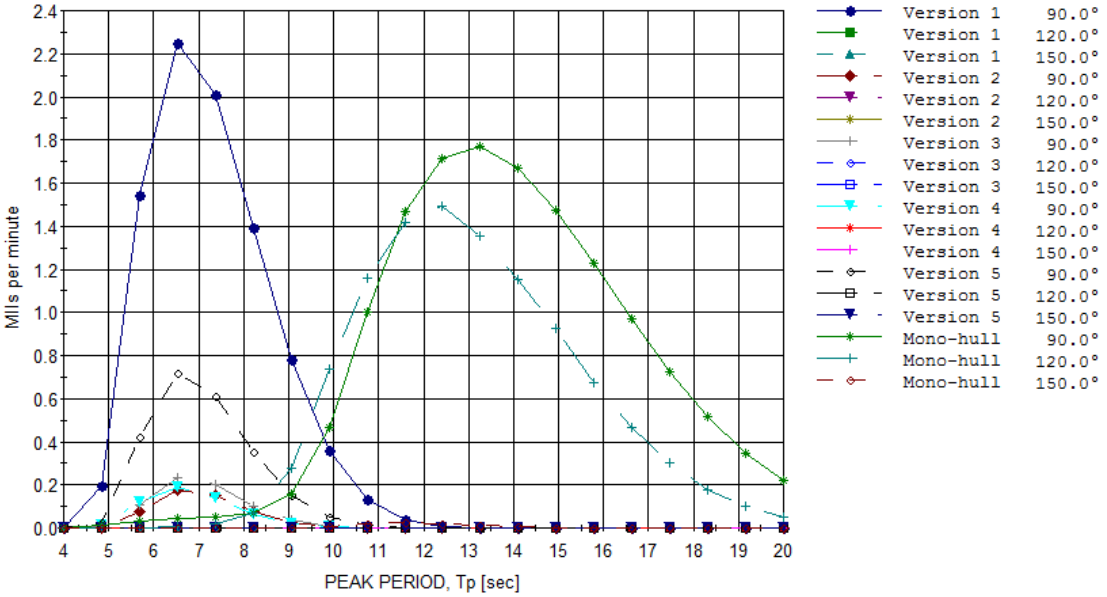

(b) Deck position 1, headings 90°, 120° and 150°

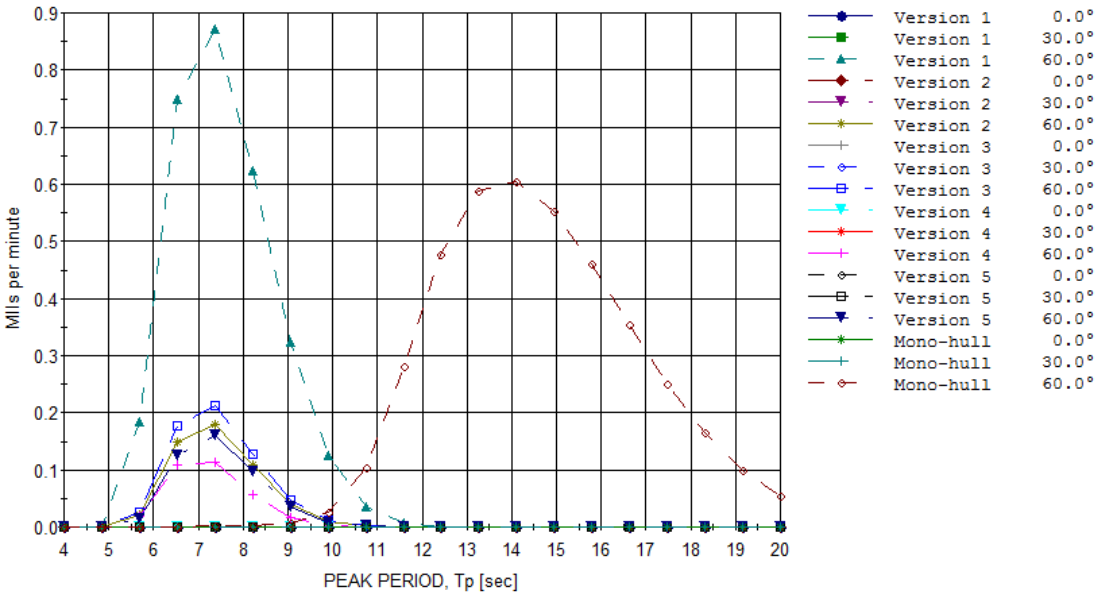

(c) Deck position 2, headings 0°, 30° and 60°

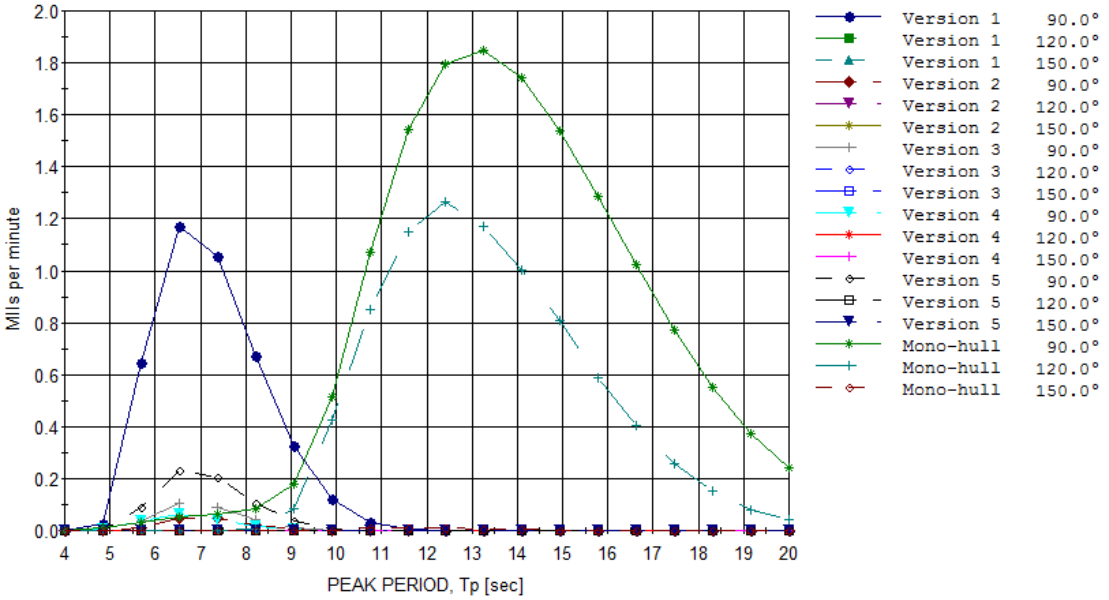

(d) Deck position 2, headings 90°, 120° and 150°

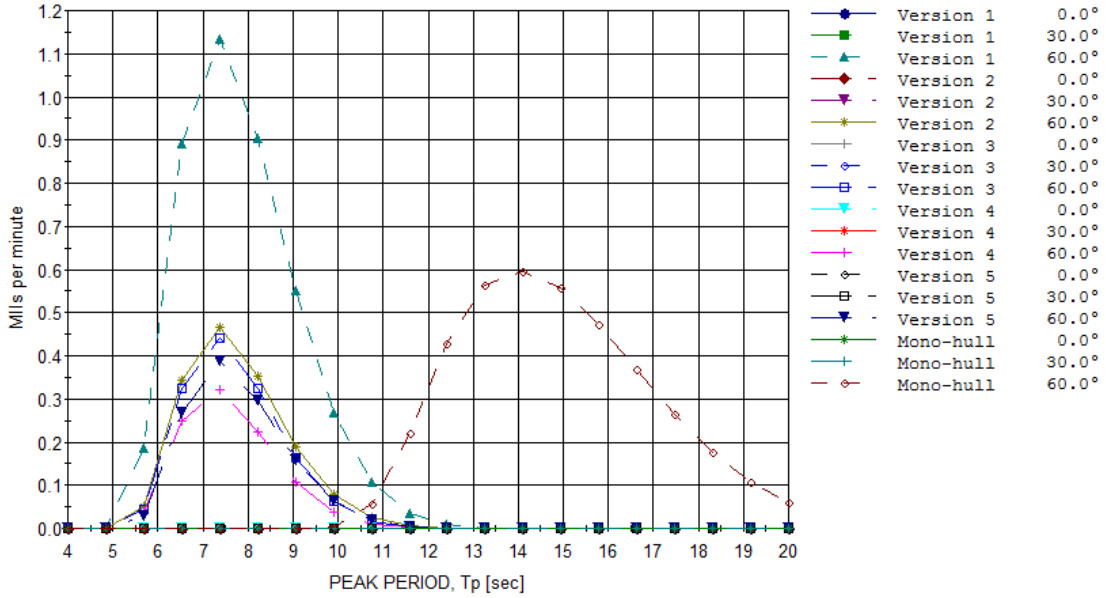

(e) Deck position 3, headings 0°, 30° and 60°

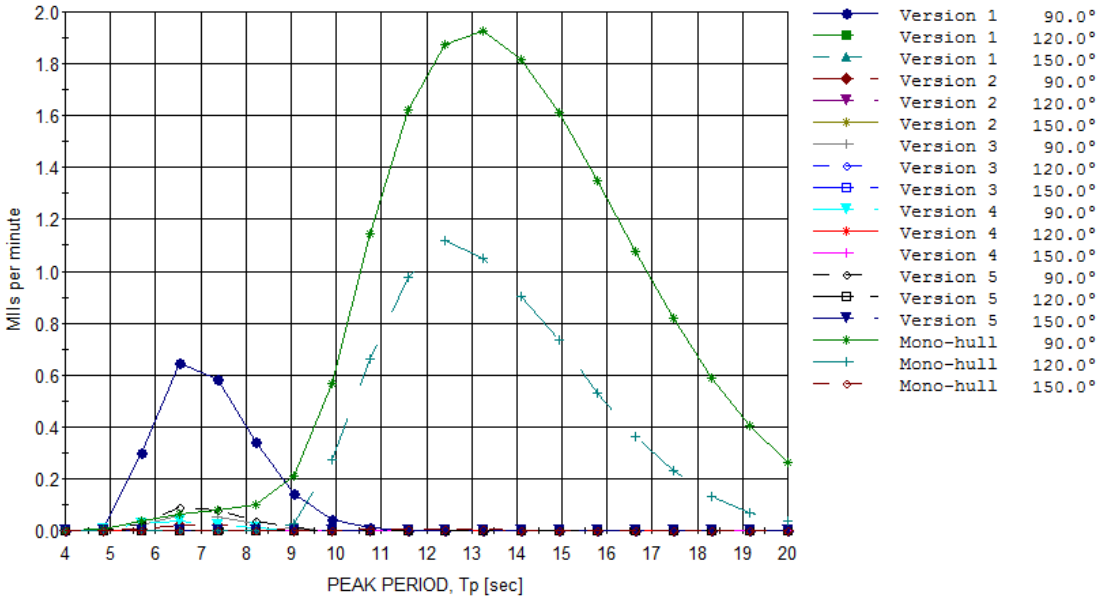

(f) Deck position 3, headings 90°, 120° and 150°

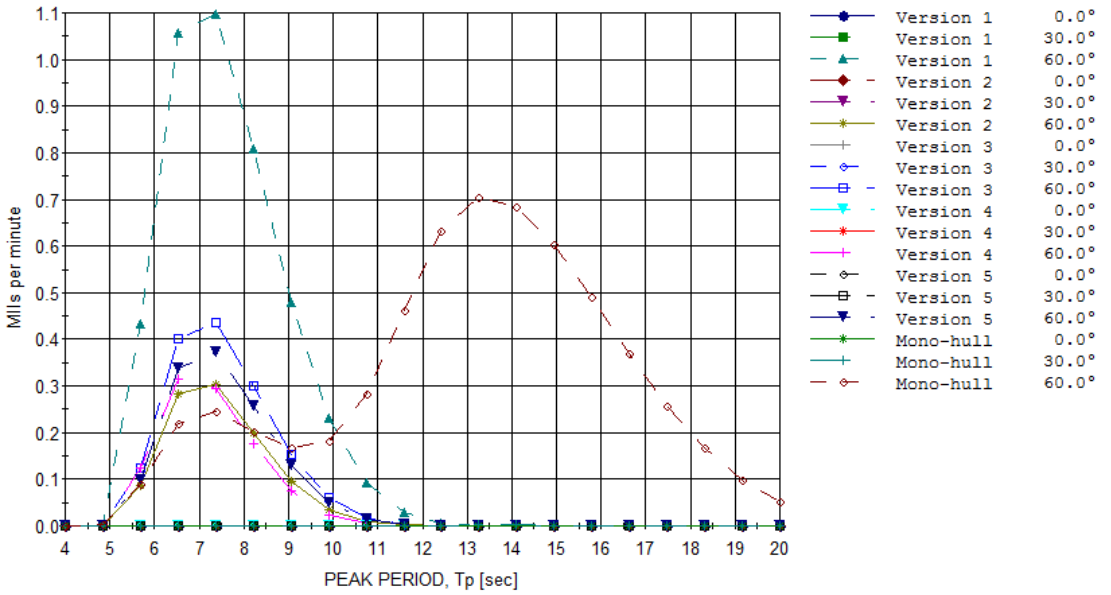

(g) Deck position 4, headings 0°, 30° and 60°

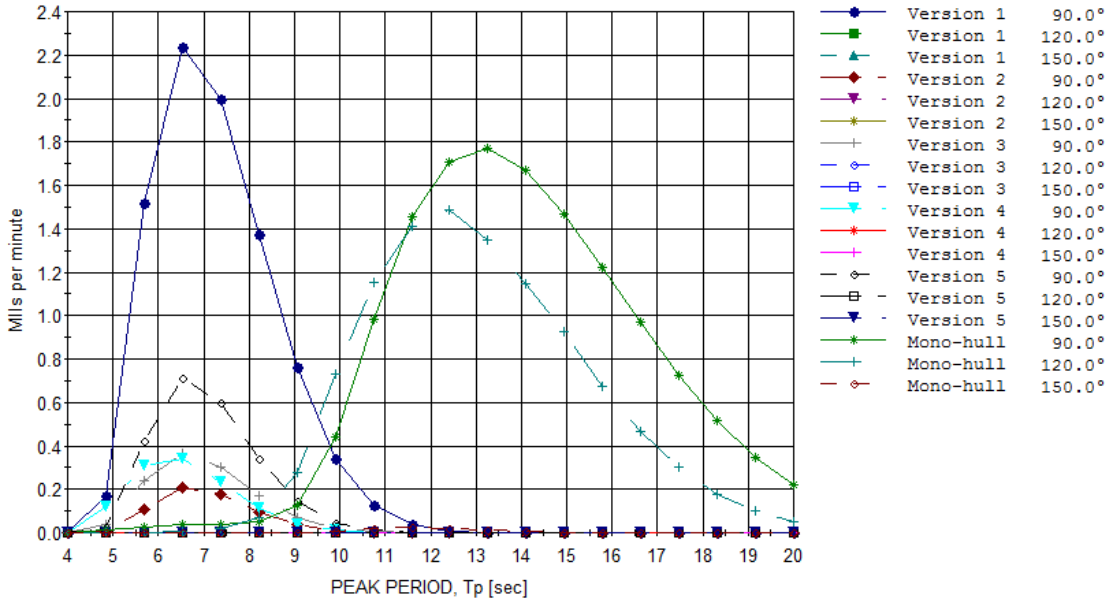

(h) Deck position 4, headings 90°, 120° and 150°

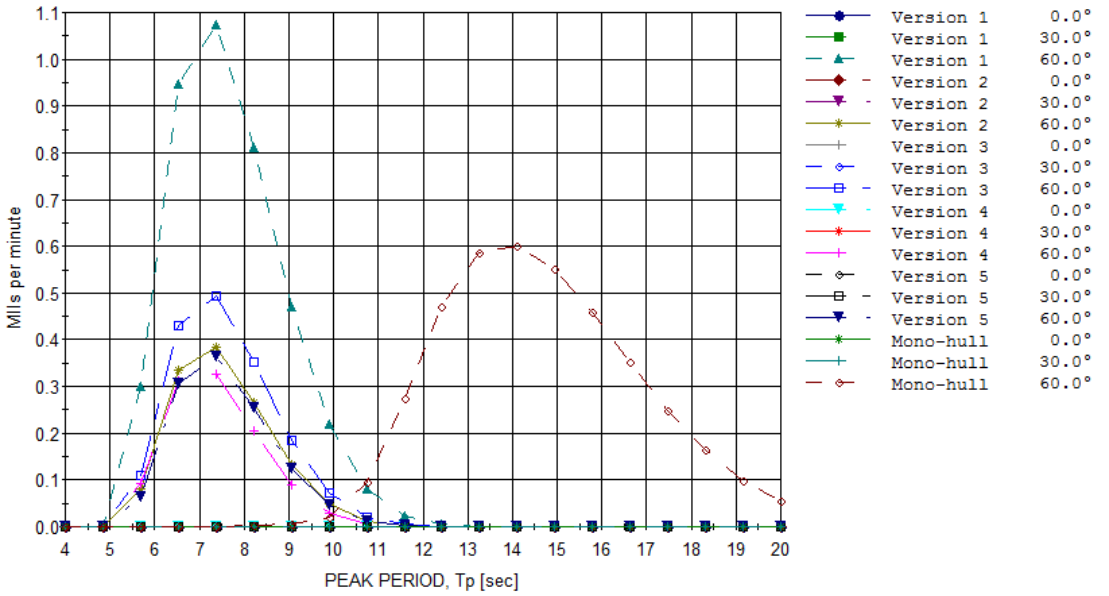

(i) Deck position 5, headings 0°, 30° and 60°

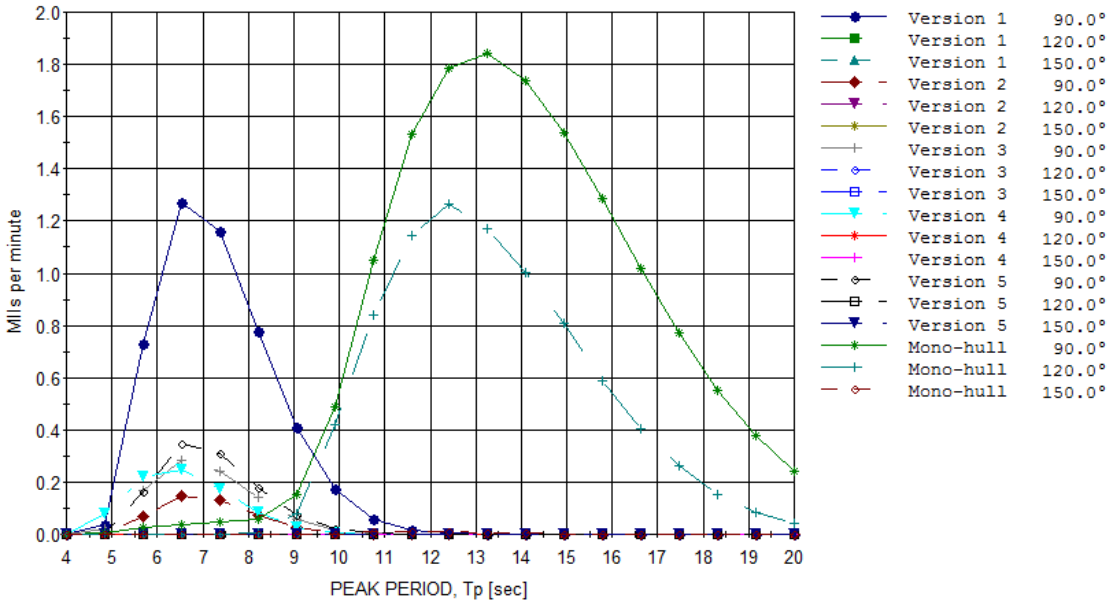

(j) Deck position 5, headings 90°, 120° and 150°

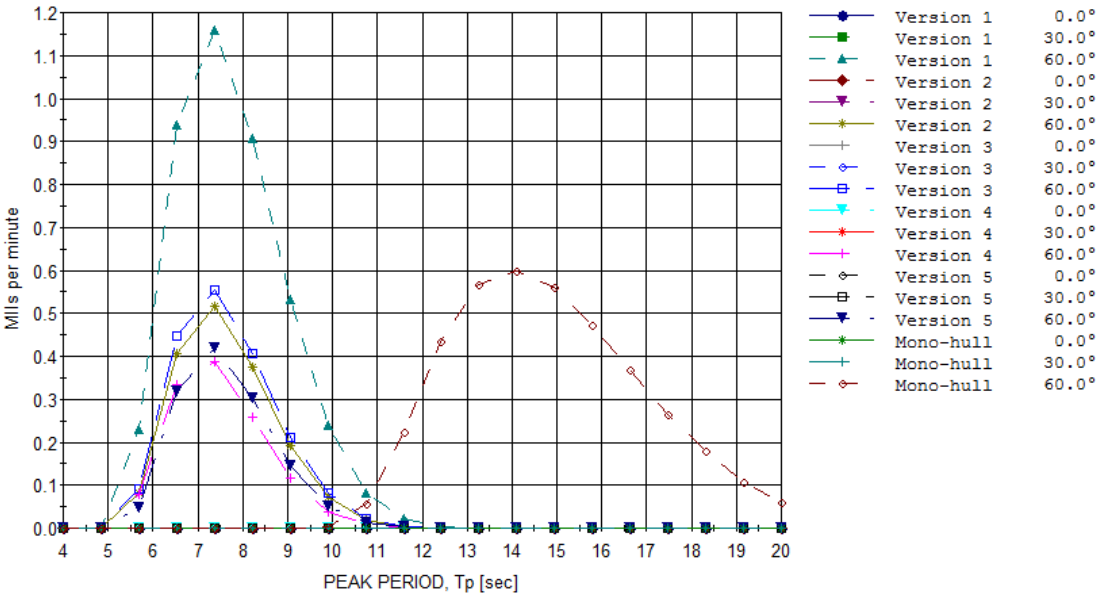

(k) Deck position 6, headings 0°, 30° and 60°

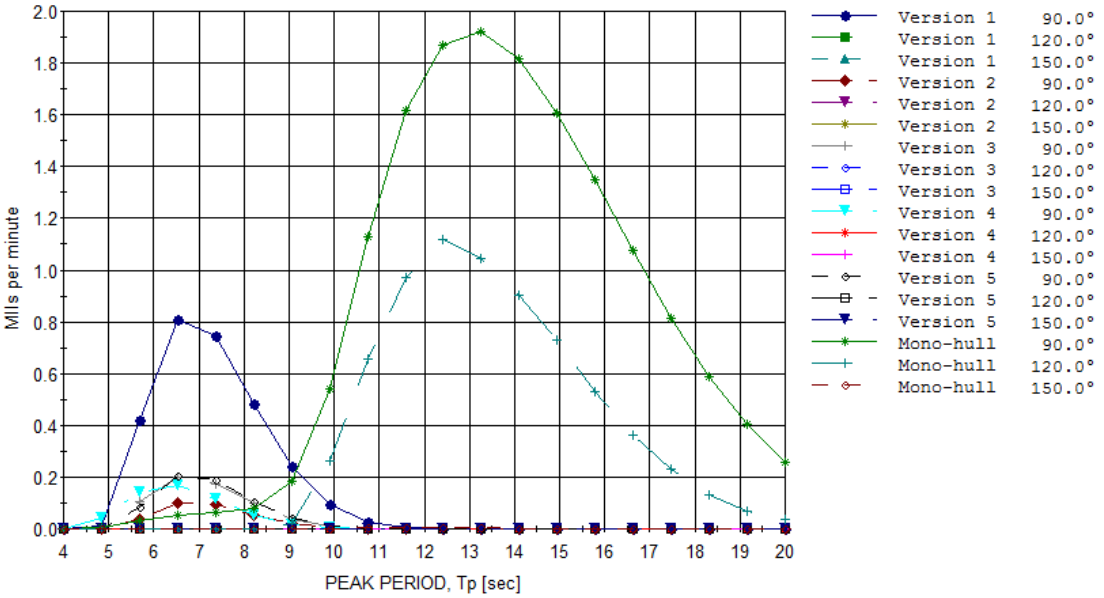

(l) Deck position 6 headings 90°, 120° and 150°

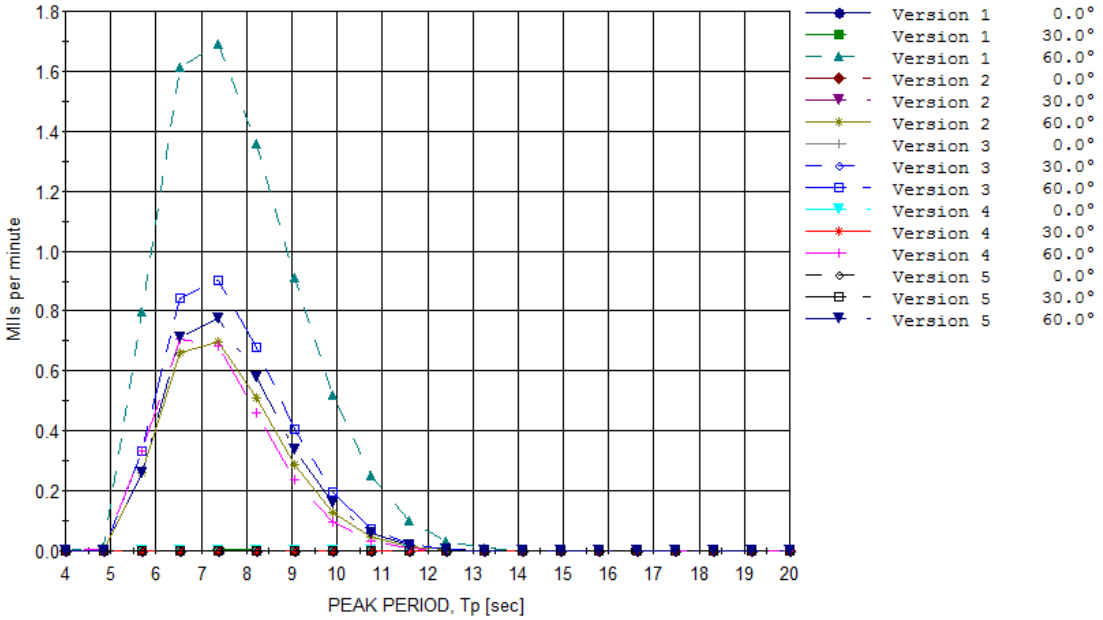

(m) Deck position 7, headings 0°, 30° and 60°

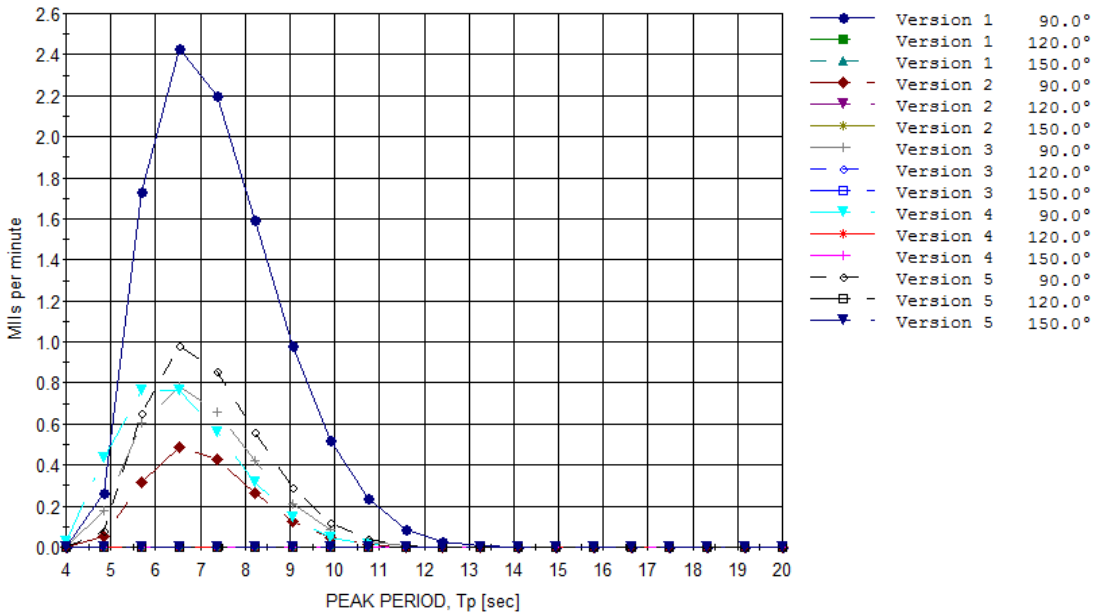

(n) Deck position 7 headings 90°, 120° and 150°

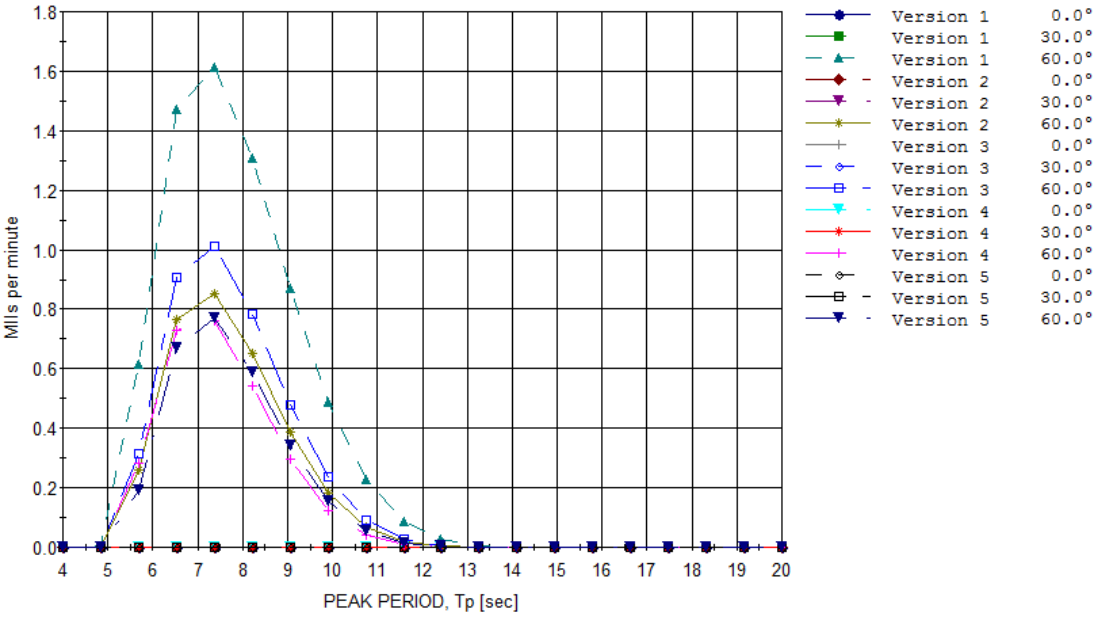

(o) Deck position 8, headings 0°, 30° and 60°

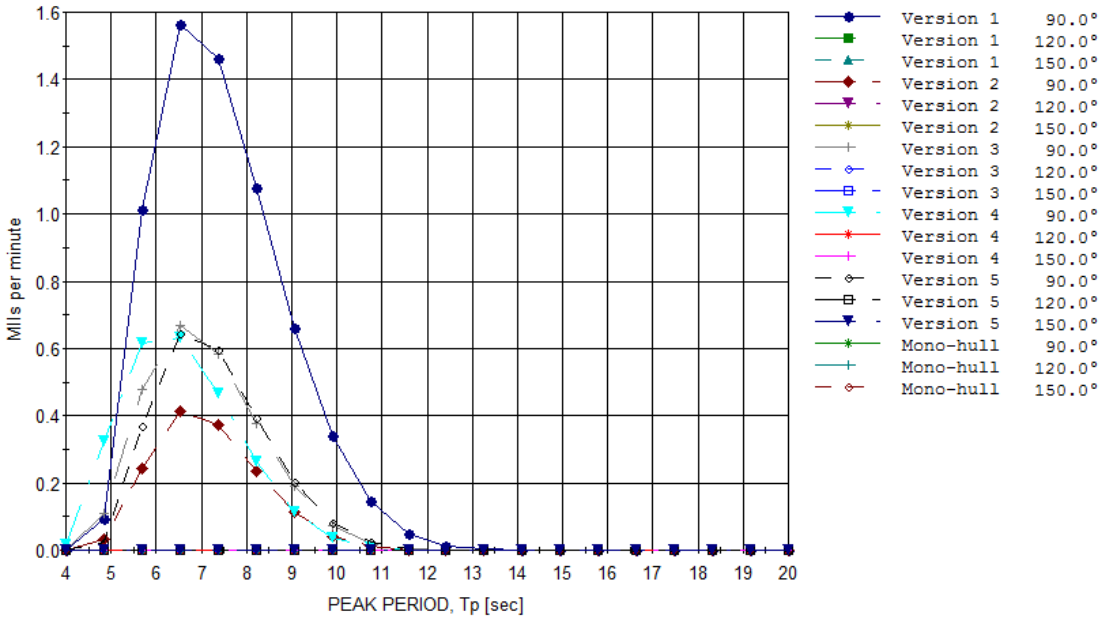

(p) Deck position 8 headings 90°, 120° and 150°

Figure 8.3: MIIs per minute at various deck positions against the peak period, T_p. $H_s = 4$ m. Each vessel has a constant forward speed of 5 knots. See figure 4.1 for a description of the positions.

By comparing the plots in figure 8.3 it is found that not all wave directions will result in significant values of motion induced interruptions. For the trimaran, only wave directions of 60° and 90° are of importance with respect to MII. For the mono-hull it was found that wave directions of 120° also are of importance. Wave directions of 180° were not included in the results as the occurrence of MIIs is minor in this case.

It is clear from the results above that version 1 comes out worst with respect to the deck operation criterion. The remaining versions have MIIs well below one per minute at almost all deck positions. As expected, the highest occurrence of MII is at position 7 and 8. These positions are located at the outer edge of the deck where the vertical acceleration caused by roll will be large due to the large beam. At deck position 7, the MIIs for version 1 reaches 2.4 per minute which is a serious- to severe risk level, see table 4.1. The MIIs for the remaining versions do not exceed 1 MII per minute, which is a possible but not severe risk level.

An important trend is that the MIIs occur at very different T_p values for the trimaran concept and the mono-hull. This was expected due to the special hull configuration of the trimaran. It can be understood from the results that motion induced interruptions will be a much larger issue in high sea states for the mono-hull. The trimaran hull will provide good working conditions in high sea states. This is a beneficial characteristic of a seismic ship, as the ship stays at site for long periods and may be exposed to rough weather. As discussed in chapter 3, it is difficult to retract seismic equipment during high sea states. It is very important to have safe working conditions when working at the deck in such cases. It was also discussed in chapter 3 that seismic ships operate mainly during low sea states. The downside of the trimaran behaviour is that the MIIs are significant in sea states of low T_p values. This is summarized in the operability diagram in figure 8.4.

The results above are corresponding to a significant wave height of $H_s = 4$ m, as this is the limiting wave height for seismic operations, see chapter 3. It should be noted that the MII peak values are corresponding to T_p values close to $T_p = 7$ s. The probability of a peak period smaller than $T_p = 7$ s in combination with a significant wave height larger than $H_s = 4$ m is rather small in a long term point of view, see table H.1. In other words, it is not likely that the MIIs will exceed the results above.

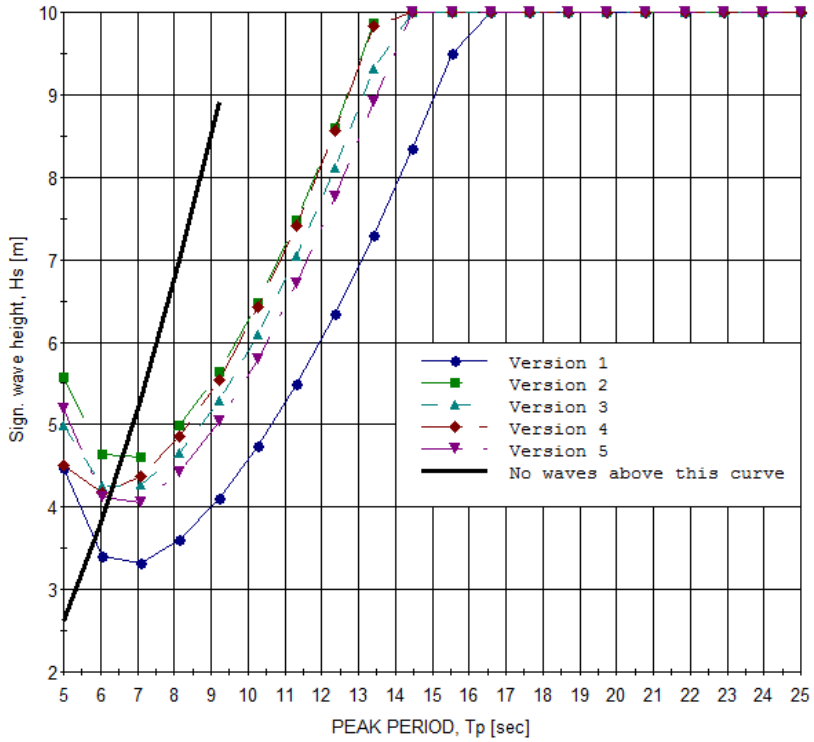

Figure 8.4: Operability diagram for the MII criteria. The results presented corresponds to a wave direction of 90° and are found at position 7, where the MIIs are at a maximum. The limiting criteria is set to one MII per minute.

The operability diagram shows the significant wave height where the MII criterion is violated. The wave breaking limit is plotted together with the results. It can be seen from the operability diagram that the limiting significant wave height increases as the peak period increases. It means that the trimaran concept is stable in higher sea states. The limiting wave height at low peak periods is quite small, meaning that the occurrence of MII will be significant in low sea states. Version 1 violates the criterion first.

8.9 Helicopter operation

Pitch criteria

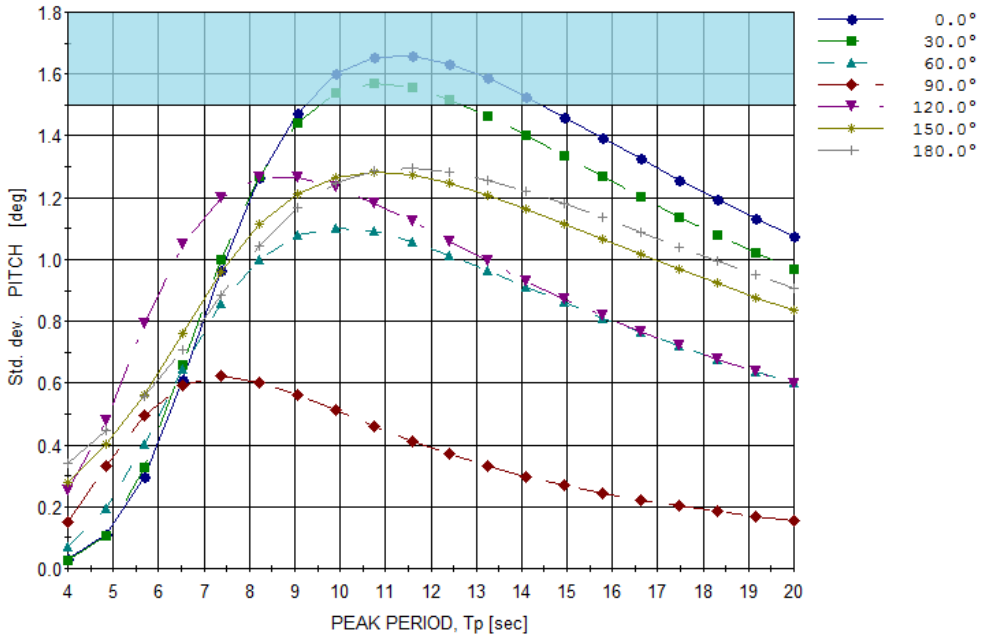

(a) Version 1

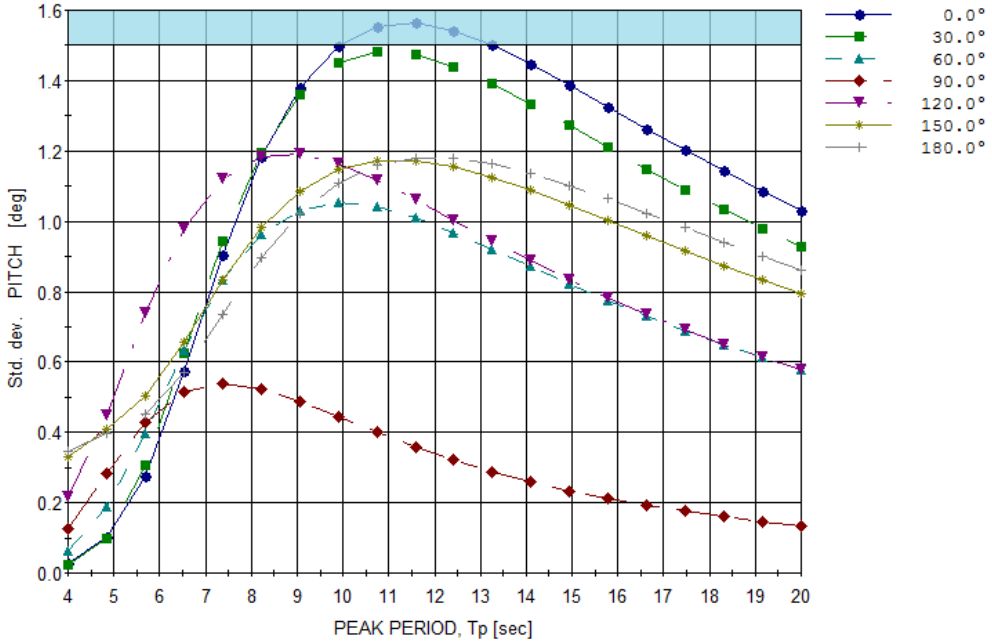

(b) Version 2

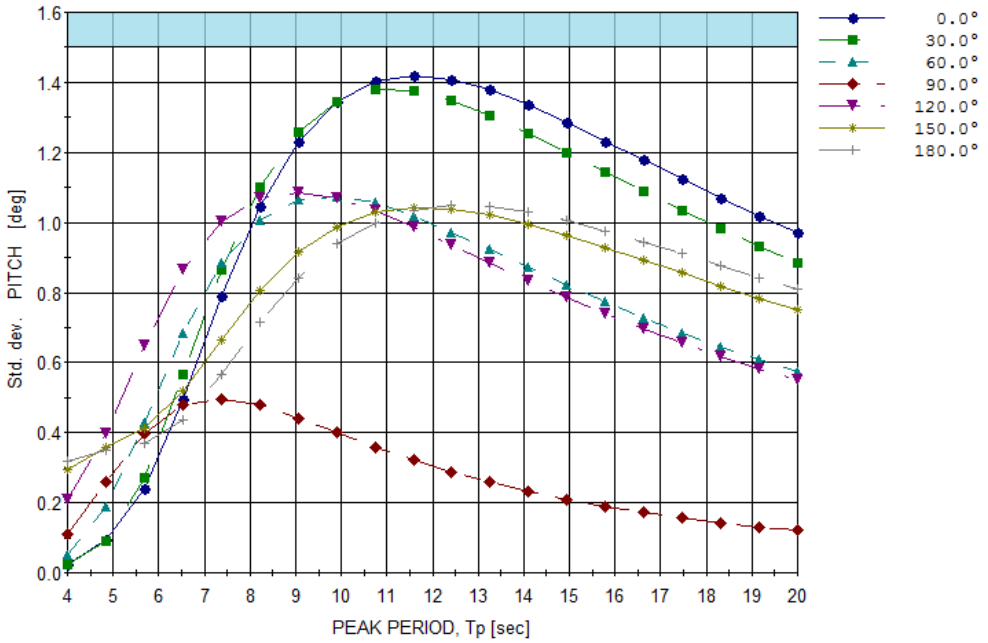

(c) Version 3

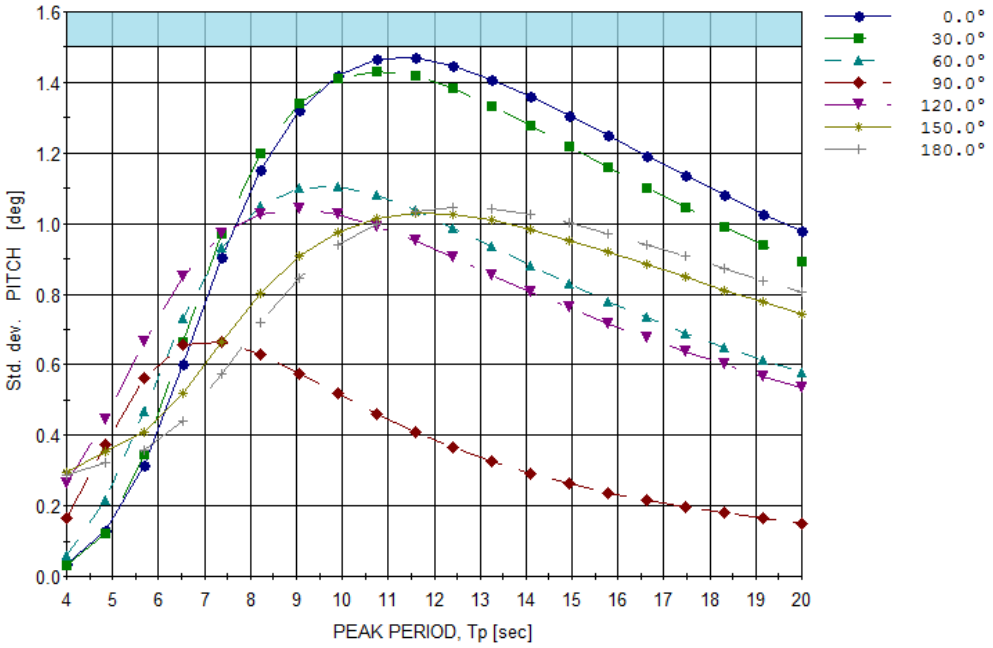

(d) Version 4

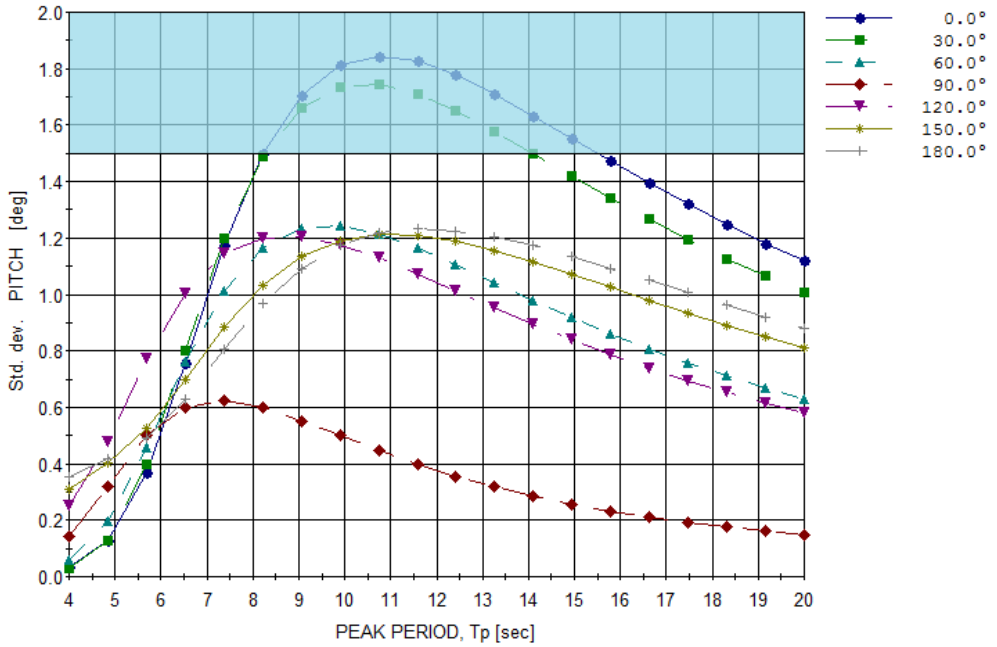

(e) Version 5

Figure 8.5: Pitch RMS against wave peak period at a forward speed of 5 knots. $H_s = 4$ m. The helicopter operation criteria is represented by the shaded region.

The pitch criterion is violated by version 1, 2 and 5, when the waves have directions of 0° and 30°. All these versions have a total length of $L_{oa} = 110$ m. Version 3 and 4 have a total length of 120 m and will therefore have a different pitch natural period. Version 5 has the largest violation of the criterion, followed by version 1 and version 2. Version 5 is a much more slender hull configuration than version 1 and 2, meaning that the hulls will generate less waves when pitching. Because potential damping is related to wave generation, the larger pitch amplitudes of version 5 can be explained by this.

Version 1 and 2 have the same main hull width and loading condition. However, version 1 has a smaller main hull block coefficient, C_b, than version 2, see table 2.1. The side hulls will also contribute to the pitch damping. Version 1 and 2 have the same length, width and block coefficient of the side hulls. However, since the side hulls of version 2 have a larger B/D-ratio than version 2 they will probably be better wave generators. It is believed that this explains why version 1 has a stronger violation of the criteria.

Roll criteria

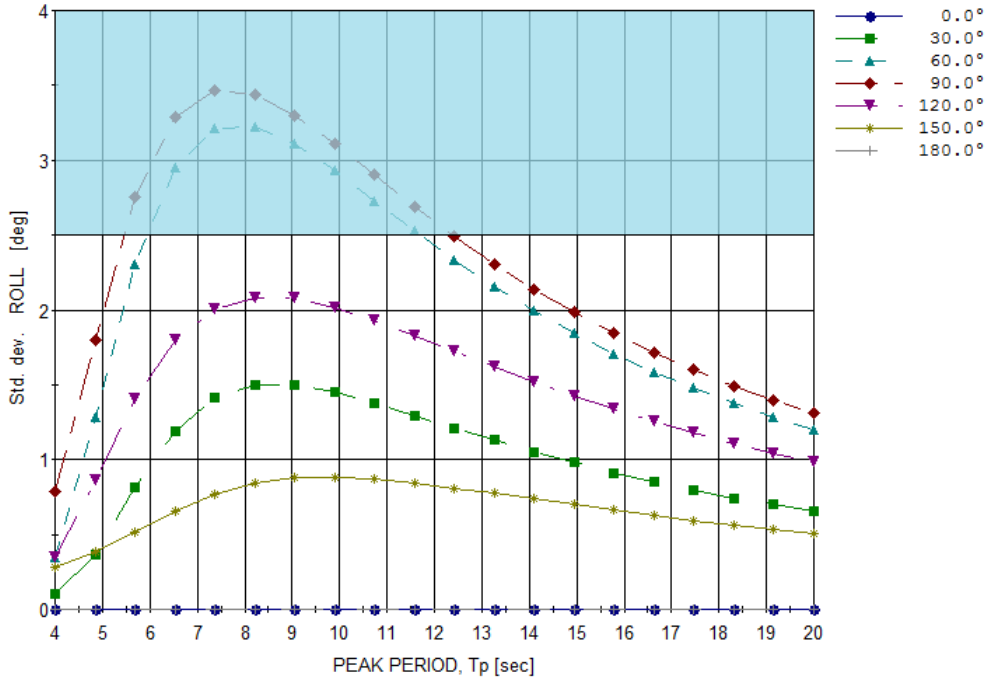

(a) Version 1

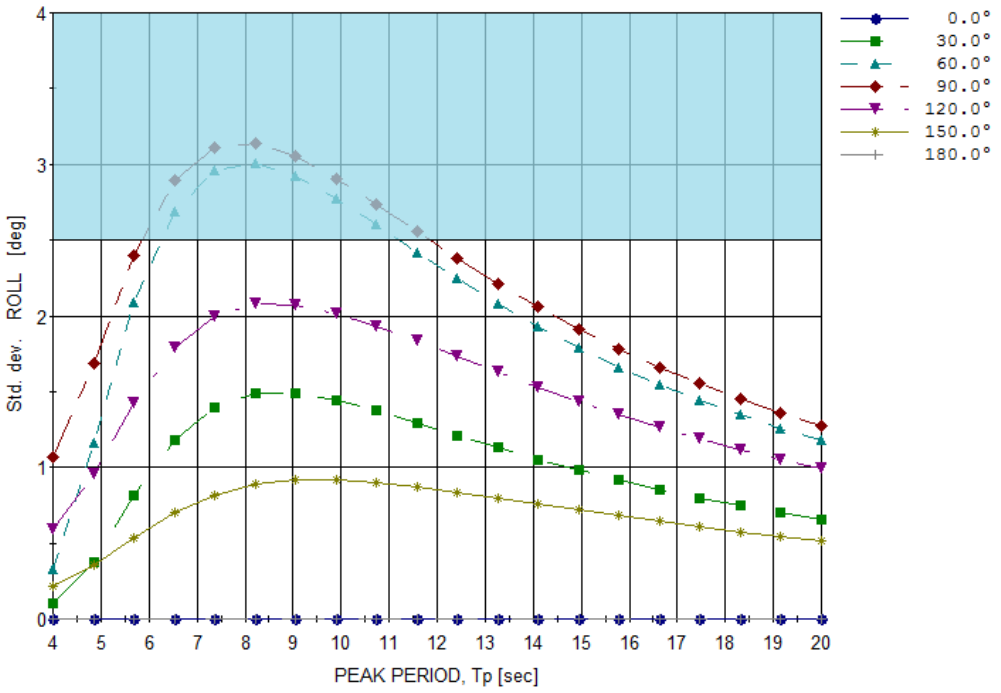

(b) Version 2

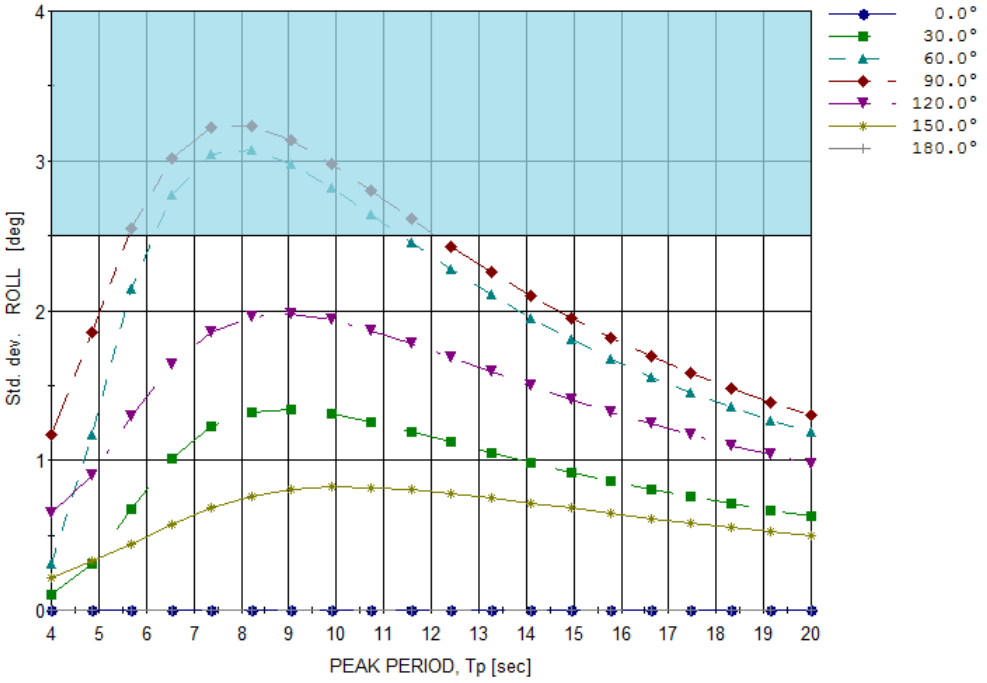

(c) Version 3

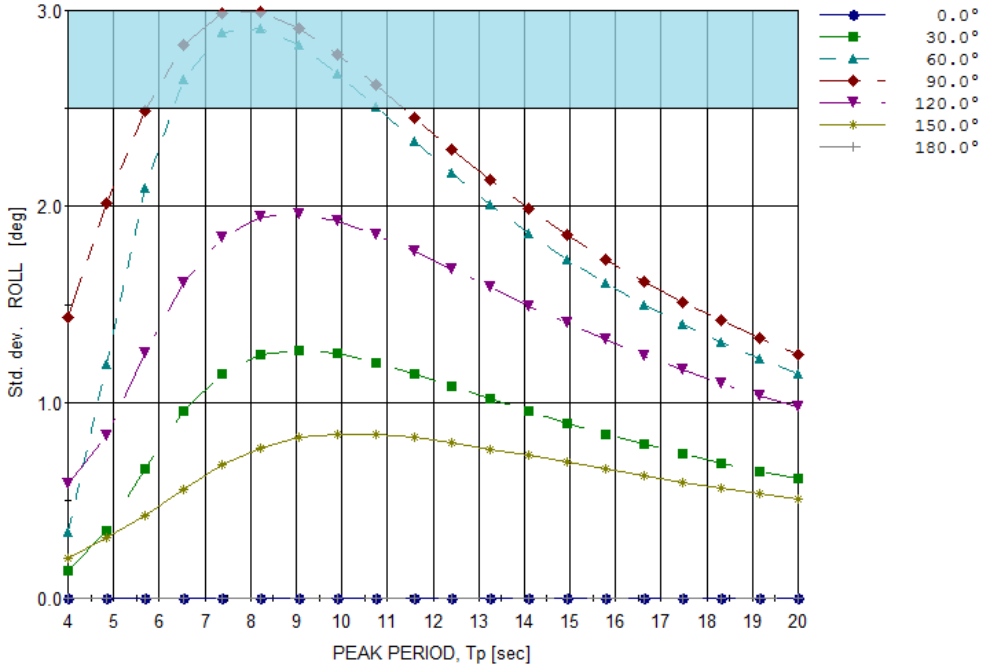

(d) Version 4

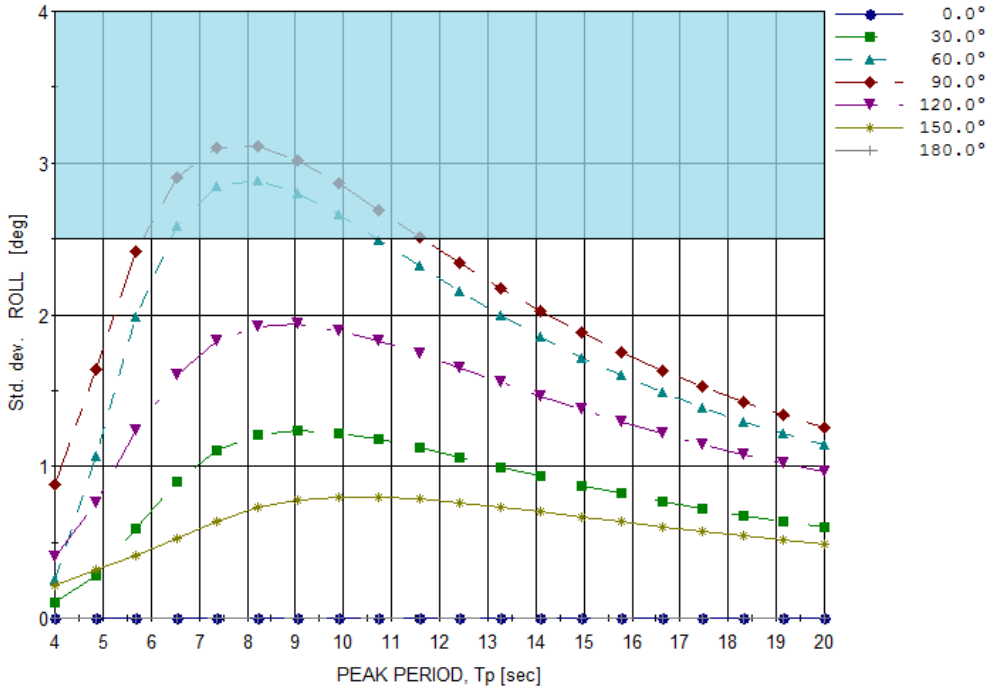

(e) Version 5

Figure 8.6: Roll RMS against wave peak period at a forward speed of 5 knots. $H_s = 4$ m. The helicopter operation criteria is represented by the shaded region.

From potential theory it is a known fact that mono-hulls are poor wave generators in roll. As mentioned in section 7.2.1, Veres has the option to approximate the viscous roll damping. A shared characteristic of all the trimaran versions is that the side hulls are located far away from the roll centre due to the large width. This means that in roll mode, the side hull will feel a large vertical motion. In other words, it will appear as if the side hulls are heaving when the ship is set in roll motion. Therefore, it is understood that there will be a significant amount of potential damping due to the vertical motion of the side hulls. To investigate this hypothesis, a Veres run without adding viscous damping was initiated. It was found that the roll RAOs were almost identical, which implies that the roll damping is actually dominated by potential damping, see appendix C. The same was done for the comparison ship, which is a mono-hull. As expected, the viscous damping has a significant importance in this case.

According to figure 7.14 in Faltinsen (2010), the two-dimensional damping coefficient in heave will increase as the B/D-ratio increases. The damping coefficient is found by integrating over the length of the hull, which means that a longer side hull will provide a larger roll-damping coefficient. A fuller side hull will generate more waves than a slender side hull. It is also important to note that the damping coefficient is frequency dependent, meaning that the restoring moment will have an effect. A large restoring

moment will lead to a stiff roll motion and a large vertical acceleration of the side hulls and vice versa. In other words, there are many parameters that influence the roll motion and it is therefore difficult to point out which hull configuration that is beneficial in terms of roll damping.

By looking at the results in figure 8.6 it is seen that all versions violate the criteria in the cases where the wave direction is 90° and 60°. In the case of beam seas, version 4, 5, 2, 3 and 1 have a maximum RMS roll amplitude of 2.99°, 3.11°, 3.13°, 3.23° and 3.47°, respectively. I.e, the differences between the versions are relatively small. The parameters that influence the roll damping are changing simultaneously between the versions. It is therefore difficult to point out a reason for the differences, and will therefore not be attempted. However, it could be a topic for another study to investigate this in detail. In that case, all parameters, except one, should be kept constant to see how this parameter affects the roll damping coefficient.

Vertical velocity criteria

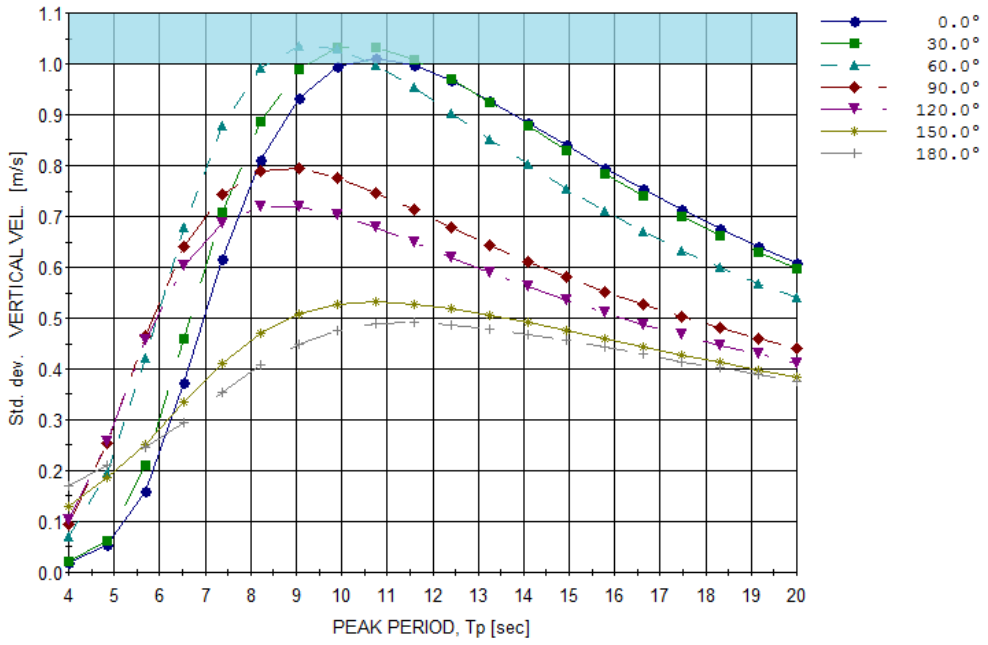

(a) Version 1

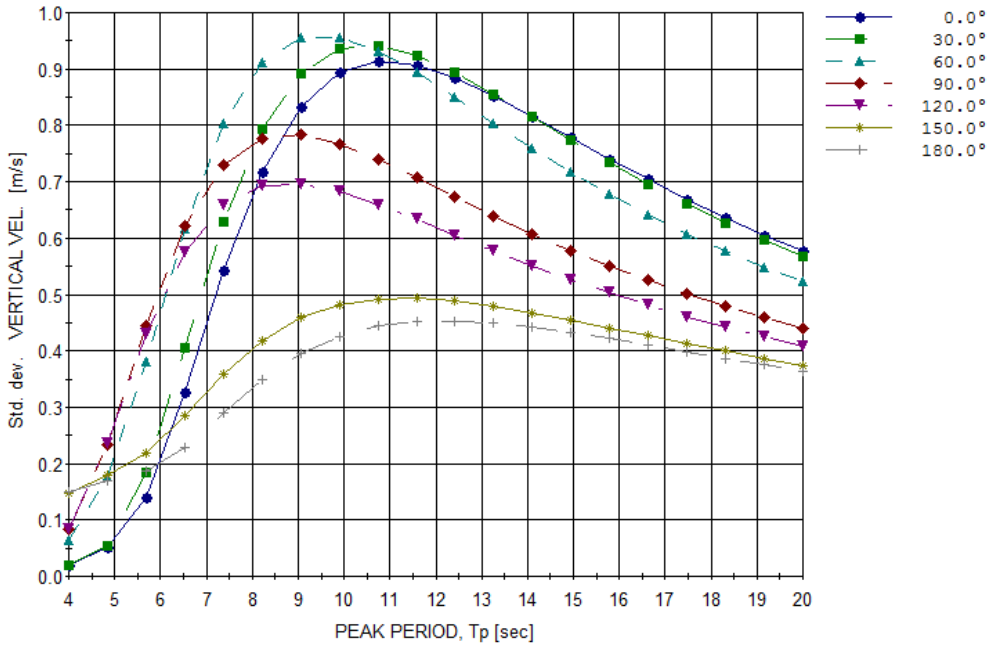

(b) Version 2

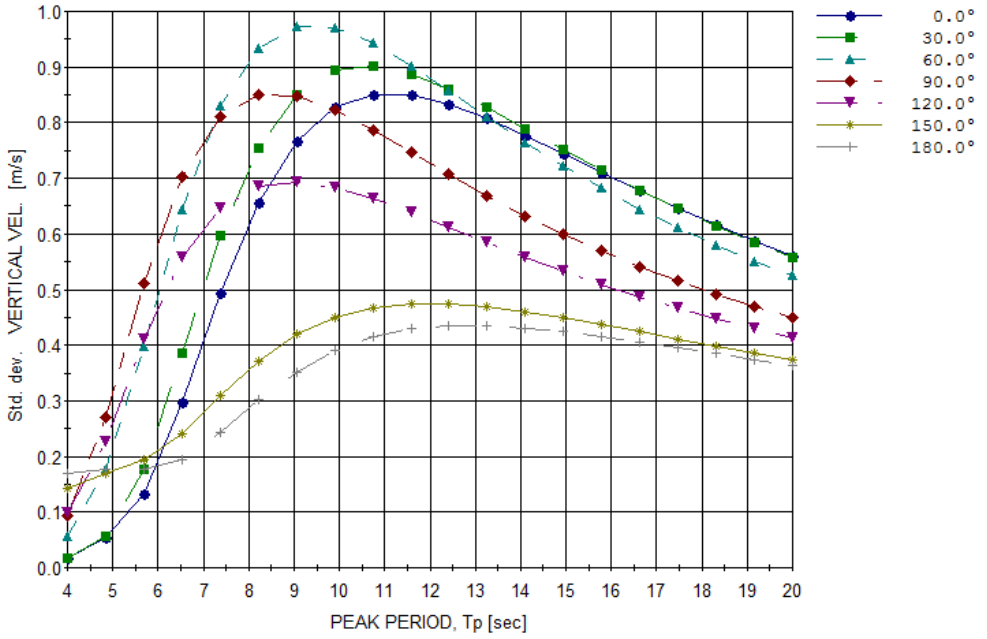

(c) Version 3

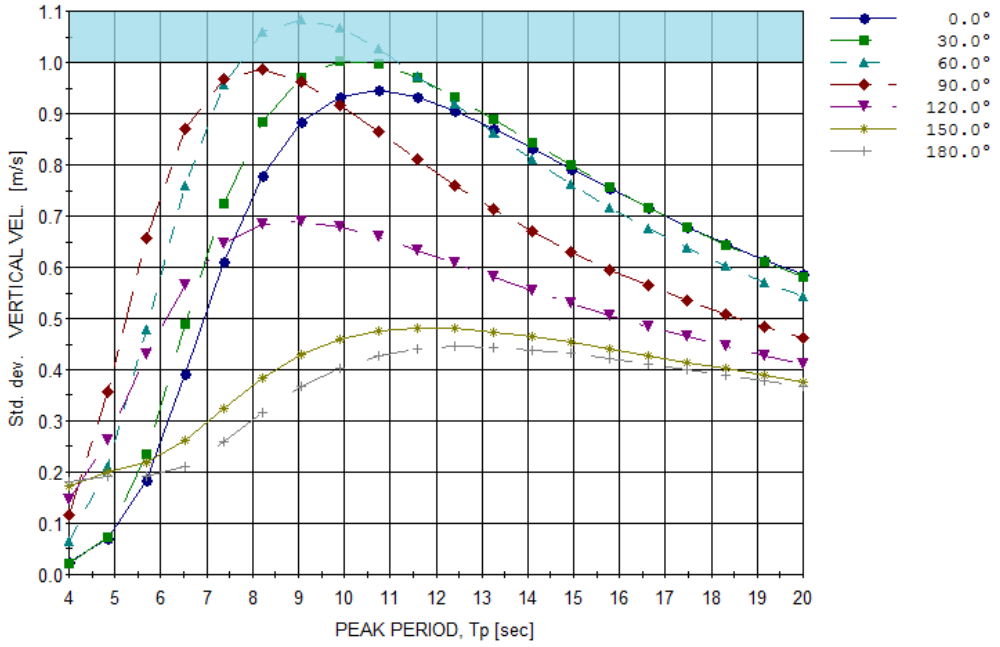

(d) Version 4

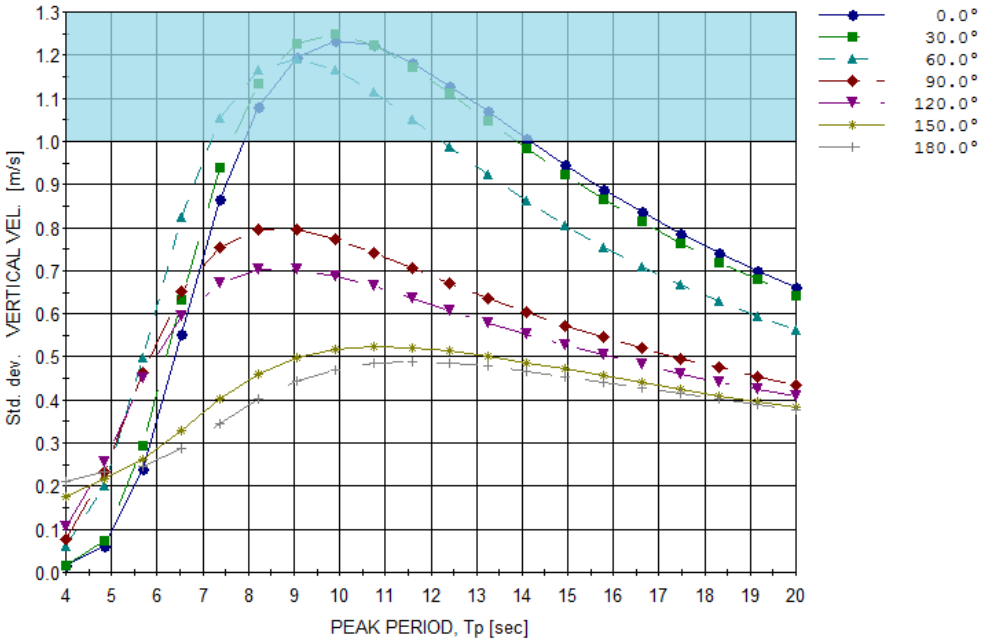

(e) Version 5

Figure 8.7: Vertical velocity RMS against wave peak period at a forward speed of 5 knots. H_s = 4 m. The helicopter operation criteria is represented by the shaded region.

The vertical velocity at the helicopter deck is influenced by both the pitch and heave response. By separating the vertical velocity, it can be seen that the largest contribution comes from the pitch motion, see appendix E.[2] A large pitch amplitude combined with a small pitch natural period will lead to a large vertical velocity component. It can be seen from the results above that the sequence of how version 1 and 5 violate the criteria is corresponding to the pitch RAOs, see appendix D. It is important to have in mind that the pitch and heave motion will cancel each other if they are in counter phase. It is believed that this is the explanation of why version 4 violates the criteria before version 2 and 3.

The criterion is evaluated amidships, meaning that the roll motion will not influence the vertical velocity. This is found reasonable as the helicopter will land close to the centre of the helicopter deck.

[2]Appendix E gives a representation of the short term statistics of the heave velocity

8.10 Short term response of relative Motion

Wasim Postresp provides the option of obtaining the short term response of the relative vertical motion at a pre-described position. When this option is chosen the user must specify the wave spectrum and provide the transfer function for relative motion. Further, the short term response can be found from the response spectrum. It is defined as a function of T_z values calculated from the full range wave spectrum. For a given T_z the response is given as in the following:

$$\eta_s = \frac{4 \cdot \sqrt{m_0}}{H_s} \tag{8.1}$$

This means that the short term response is defined as the mean of one third of the largest responses and is given as the double amplitude response per significant wave height. As a consequence of linear theory, the single amplitude response is simply half of this value. Now the expected maximum can be found for a sea state with significant wave height of $H_s = 4$ m and a duration of three hours, ref. section 5.4.3 eq. 5.33.

The short term response is found for combinations of the RAOs and wave spectrums with T_z values ranging from 4-12 s. The expected maximum can now be plotted as a function of T_z. One should have in mind that some combinations of H_s and T_z will not occur in reality, because the wave will be too steep and therefore unstable. The breaking wave height, H_s^{br}, can be found as a function of the spectral peak period, T_p, (Myrhaug and Dahle, 1994):

$$H_s^{br} = 0.105 \cdot T_p^2 \tag{8.2}$$

This means that for a significant wave height of 4 m the waves will start to break at a peak period of approximately $T_p = 6.2$ s. The relationship between the peak period, T_p and the zero up-crossing period, T_z, for the Pierson-Moskowitz spectrum can be approximated by the following equation, (CodeGogs®, nd):

$$5\pi^4 \frac{H_s^2}{T_p^4} = 4\pi^3 \frac{H_s^2}{T_z^4} \Rightarrow T_p^4 = \frac{5\pi}{4} T_z^4 \tag{8.3}$$

The corresponding T_z for breaking waves will therefore be approximately $T_z = 4.4s$. This implies that almost the entire range of combinations of T_z and H_s represents physical waves. However, in a long term point of view it is not very likely that a combination of peak periods below 7 s and a significant wave height of 4 meters will occur, ref. (Faltinsen, 1990). This can be seen from a table of joint frequency of significant wave height and spectral peak period. This table is attached in appendix H.

The relative motion is found at various positions along the side-hull. It was found sufficient to represent a selection of positions: One position at the front, middle and aft on port- and starboard side. The positions on the port side will be on the lee side, ref section 6.2.2. The positions that are evaluated are presented in figure 8.8.

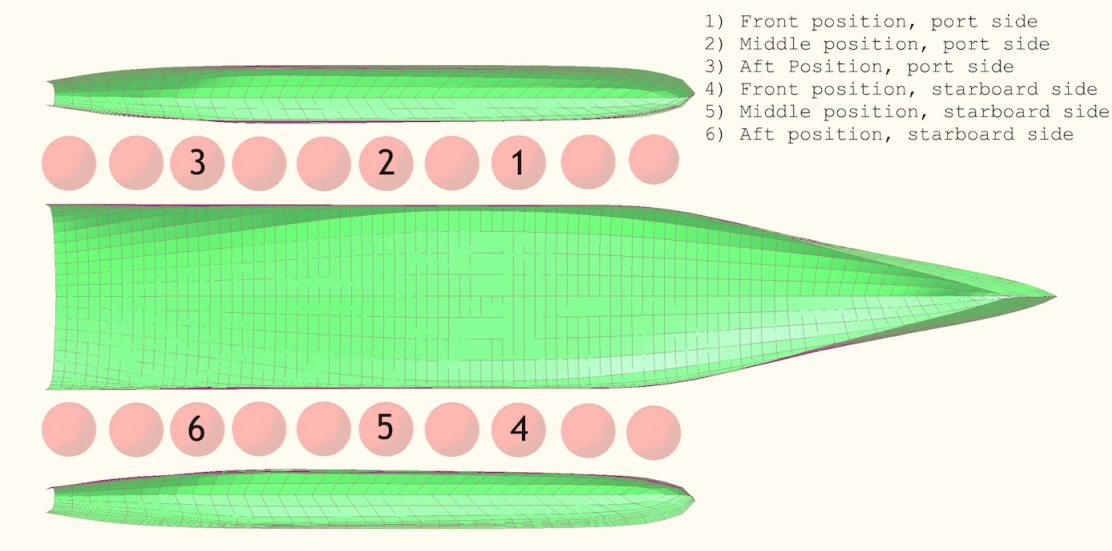

Figure 8.8: Positions for evaluation of relative motion

The results presented in the following are corresponding to zero forward speed. Due to the problems related to unphysical values of a trapped wave between the hulls, results for the operating speed of 5 knots and transit speed of 16 knots were not obtained for all the versions, ref. chapter 7. Therefore, it was not possible to give a complete presentation of relative motion for 5 and 16 knots similarly to the results of 0 knot. As a substitute, some result of the successful analyses will be given in section 8.11. In addition, the relative motion were also found by utilizing Veres results. The relative motion at port- and starboard middle position for vessel speeds of 0, 5 and 16 knots are included in appendix G.

8.10.1 Relative motion at zero forward speed

As discussed in section 5.3, the wave interaction will decrease as the forward speed increases. Therefore, the most critical case concerning hull interaction is the case of zero forward speed. Although a seismic ship will rarely operate at such low speeds in sea states with a significant wave height of 4 meters, this case will give an idea of the influence of hull interaction and a foundation for comparison between the five trimaran versions. The results of the analysis is presented in figure 8.9 through 8.13. The response presented is the single amplitude of the expected maximum value. Recall that 180° corresponds to head sea waves and 0° corresponds to following sea as the results originate from Wasim.

Version 1

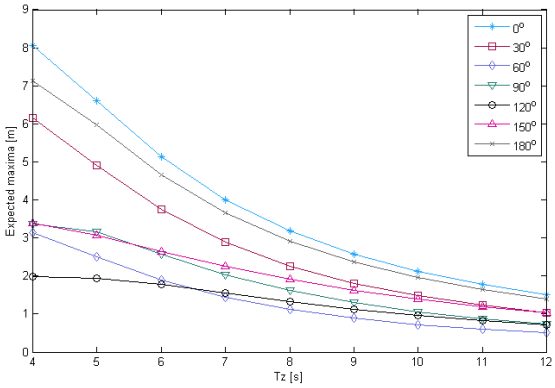

(a) Front position, port side

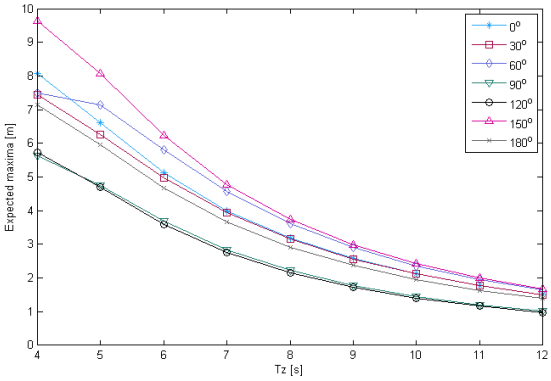

(b) Front position, starboard side

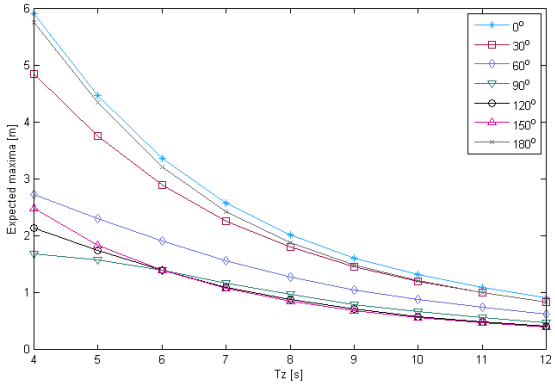

(c) Middle position, port side

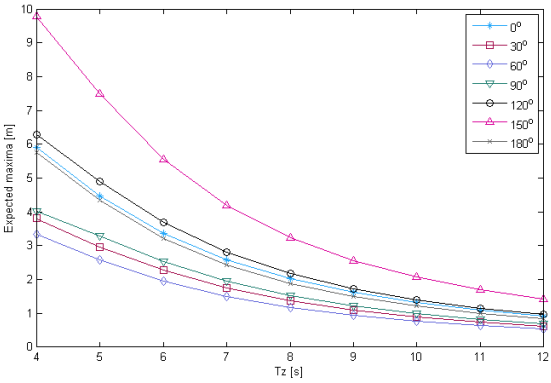

(d) Middle position, starboard side

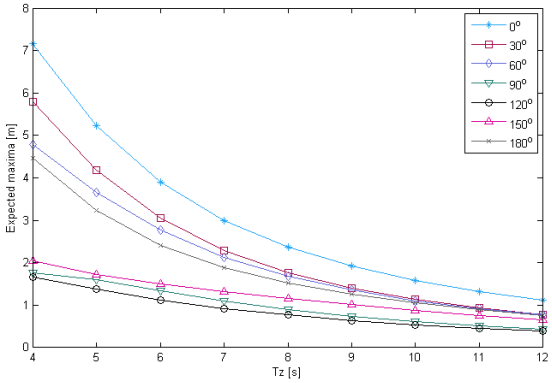

(e) Aft position, port side

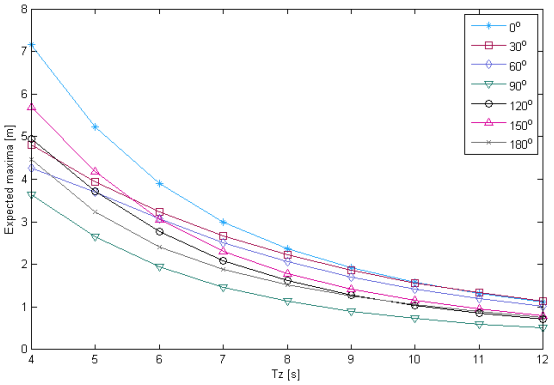

(f) Aft position, starboard side

Figure 8.9: Expected maxima of relative motion against the zero up-crossing period, T_z. The duration of the sea state is 3 hours. The vessel has zero forward speed. $H_s = 4$ m. Version 1.

Version 2

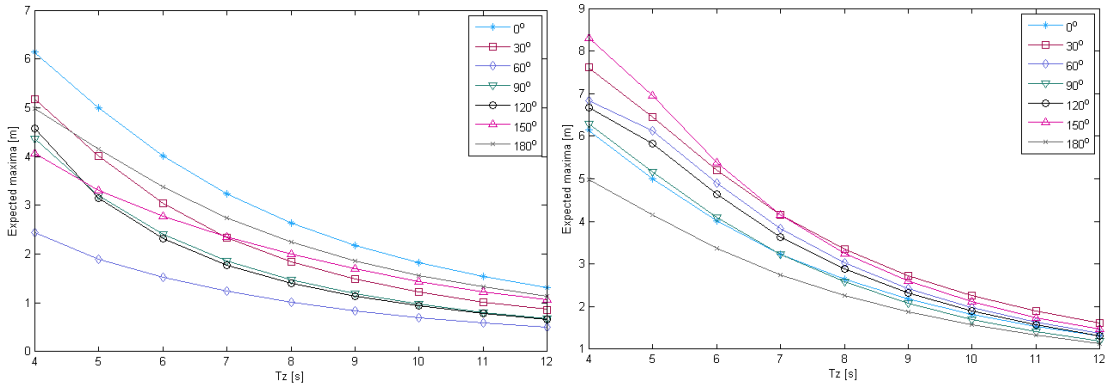

(a) Front position, port side

(b) Front position, starboard side

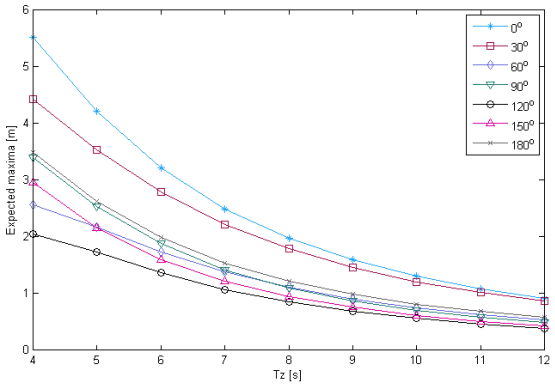

(c) Middle position, port side

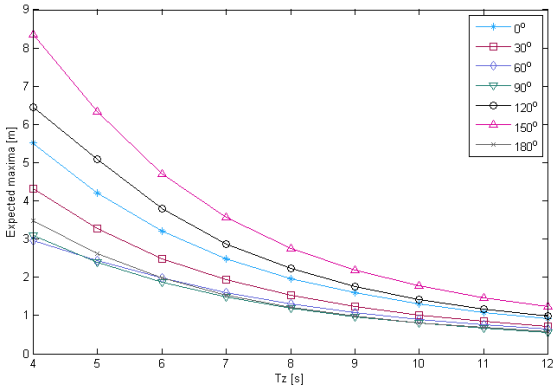

(d) Middle position, starboard side

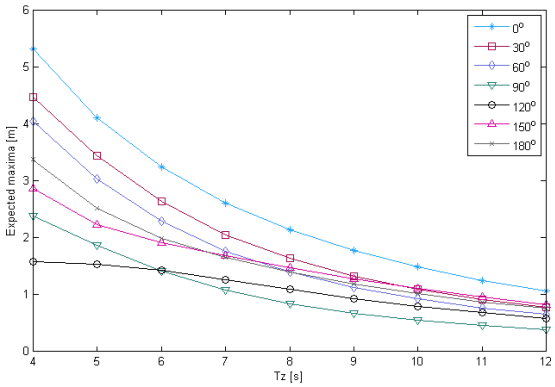

(e) Aft position, port side

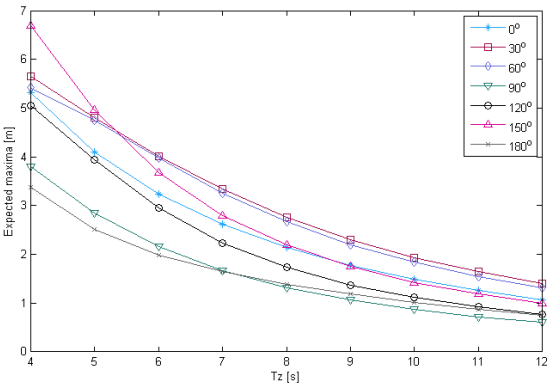

(f) Aft position, starboard side

Figure 8.10: Expected maxima of relative motion against the zero up-crossing period, T_z. The duration of the sea state is 3 hours. The vessel has zero forward speed. $H_s = 4$ m. Version 2.

Version 3

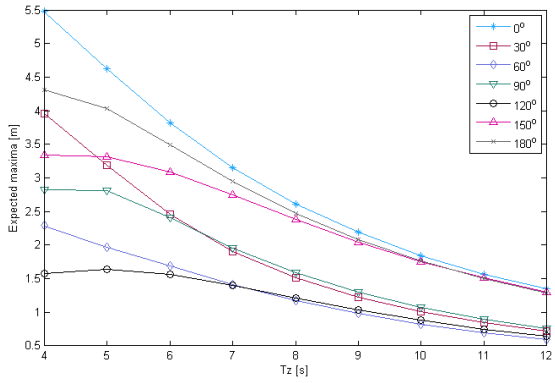

(a) Front position, port side

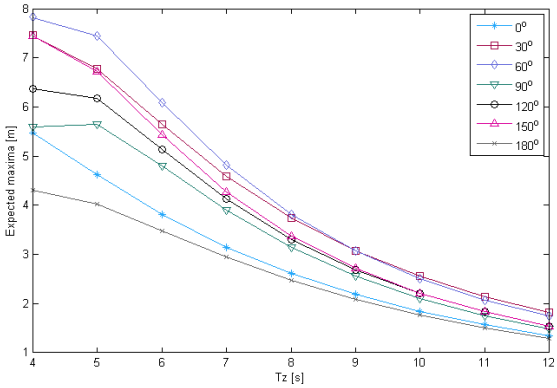

(b) Front position, starboard side

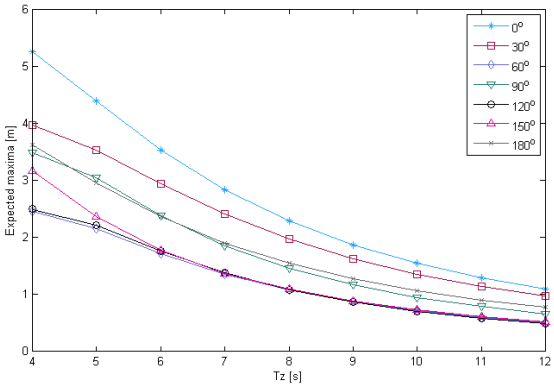

(c) Middle position, port side

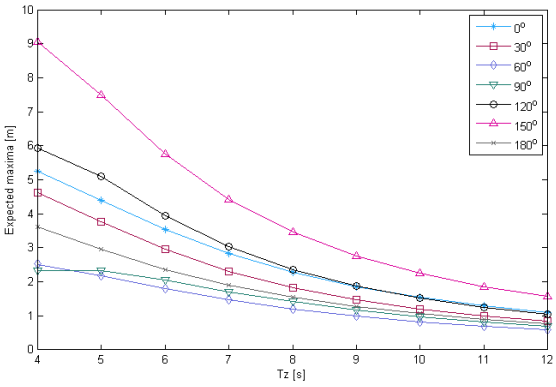

(d) Middle position, starboard side

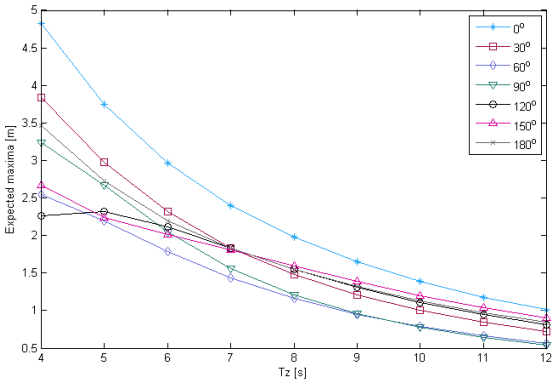

(e) Aft position, port side

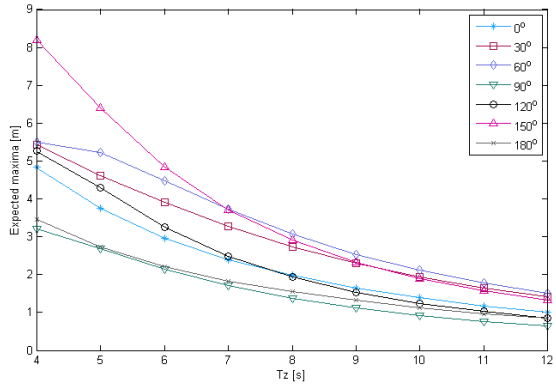

(f) Aft position, starboard side

Figure 8.11: Expected maxima of relative motion against the zero up-crossing period, T_z. The duration of the sea state is 3 hours. The vessel has zero forward speed. $H_s = 4$ m. Version 3.

Version 4

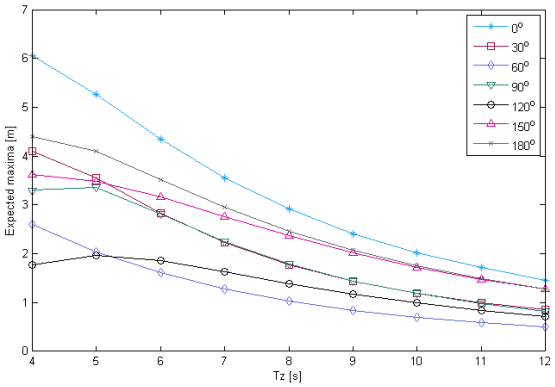

(a) Front position, port side

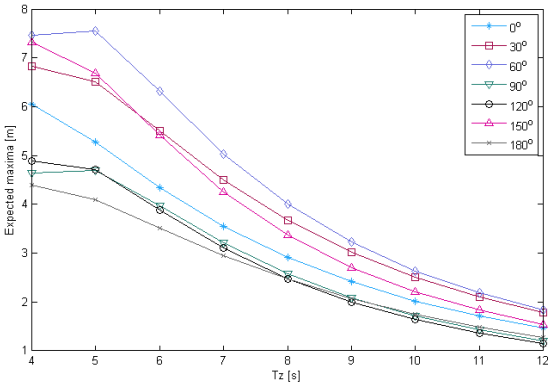

(b) Front position, starboard side

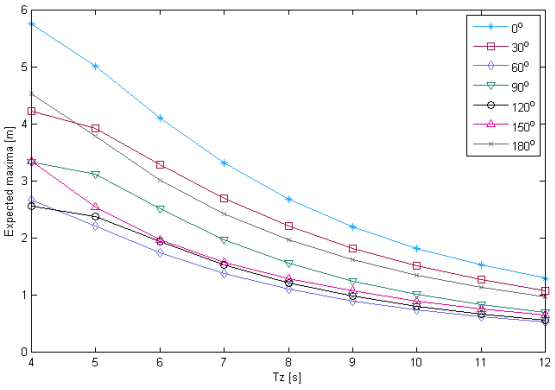

(c) Middle position, port side

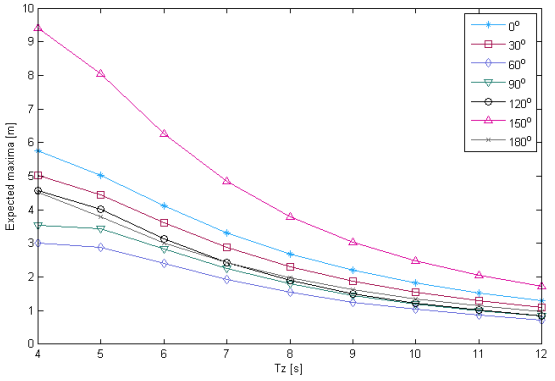

(d) Middle position, starboard side

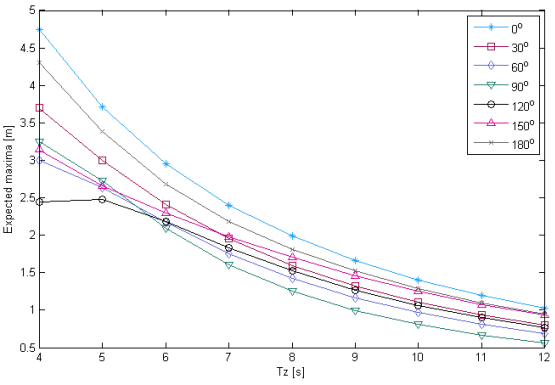

(e) Aft position, port side

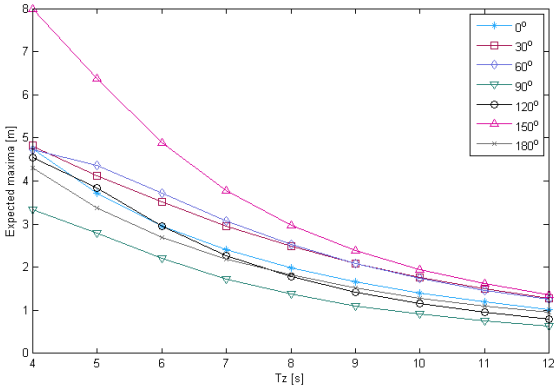

(f) Aft position, starboard side

Figure 8.12: Expected maxima of relative motion against the zero up-crossing period, T_z. The duration of the sea state is 3 hours. The vessel has zero forward speed. $H_s = 4$ m. Version 4.

Version 5

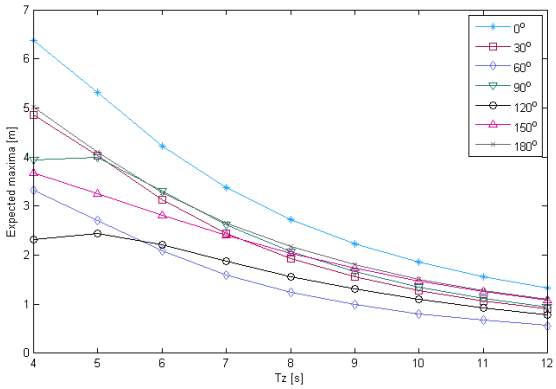

(a) Front position, port side

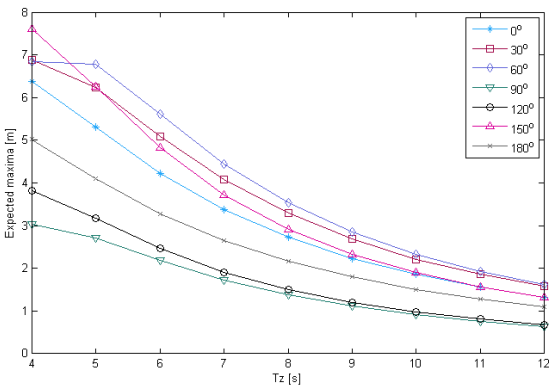

(b) Front position, starboard side

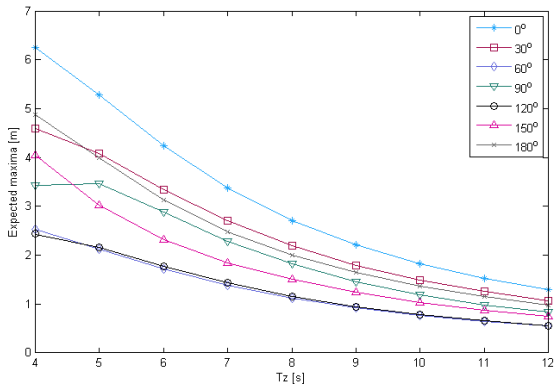

(c) Middle position, port side

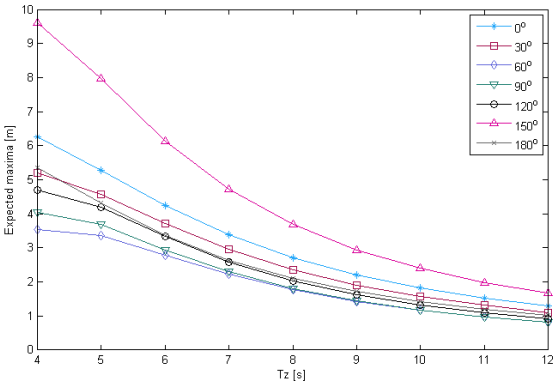

(d) Middle position, starboard side

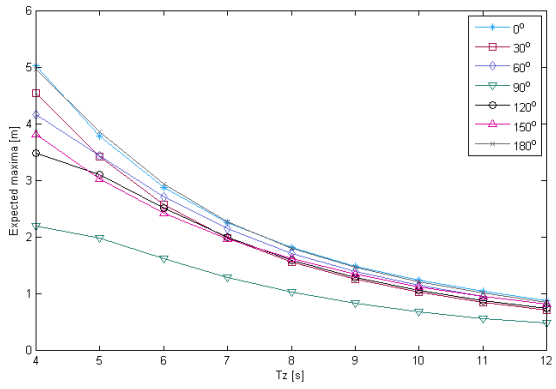

(e) Aft position, port side

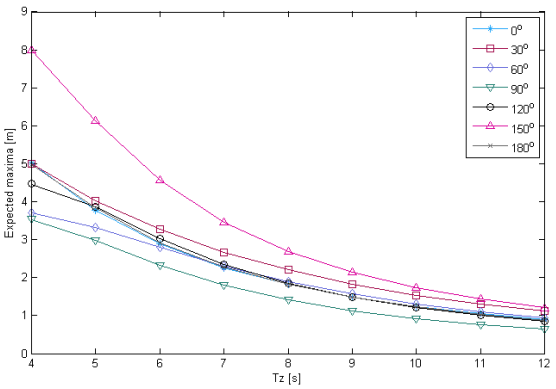

(f) Aft position, starboard side

Figure 8.13: Expected maxima of relative motion against the zero up-crossing period, T_z. The duration of the sea state is 3 hours. The vessel has zero forward speed. $H_s = 4$ m. Version 5.

Comparison

To compare the five versions the results corresponding to the direction that gives the largest response are presented in the same plot.

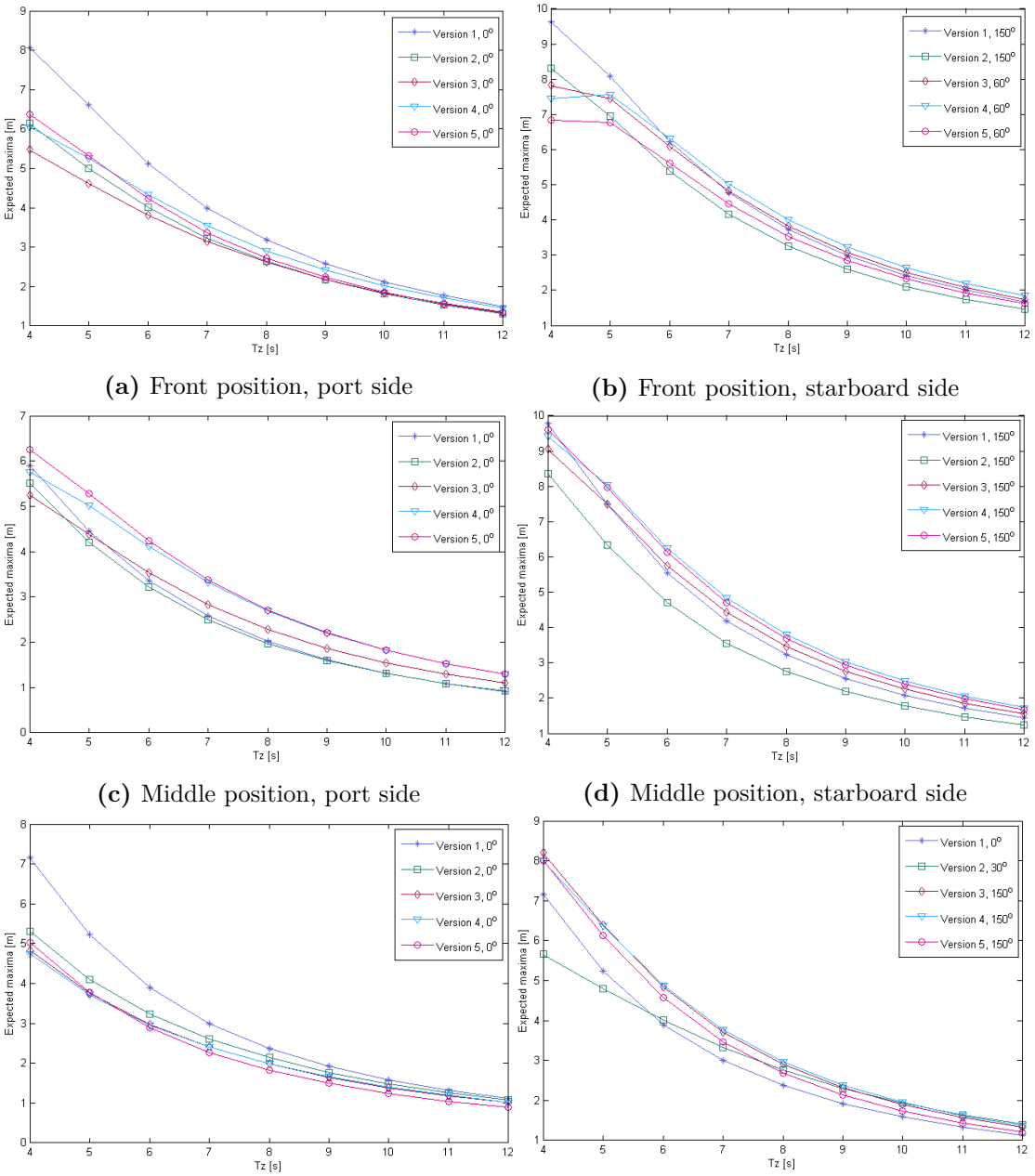

(a) Front position, port side

(b) Front position, starboard side

(c) Middle position, port side

(d) Middle position, starboard side

(e) Aft position, port side

(f) Aft position, starboard side

Figure 8.14: Expected maxima of relative motion against T_z, during a 3 hour sea state, at zero forward speed. $H_s = 4$ m. The plots gives a presentation of the largest response for all versions.

The first trend that should be noted in all the plots is that the amplitude values at low T_z values are very large. In the worst cases the amplitude values are close to 10 meters. When compared to the significant wave height of the incoming waves it is clear that this must be a severe overestimation of the reality. It can be seen from the plots that the maxima values occur at the lowest T_z value, $T_z = 4$ s. The lowest T_z value corresponds to a peak period of approximately $T_s = 5.6$ s, ref. eq. 8.3. This peak period is very close to the natural period of the relative response RAO, meaning that the response values are expected to be high in this case, see figure F.1. Still, amplitudes of this magnitude is too large to be related to physical values. If we recall the discussion in section 5.3, it was referred to the study of Lu et al. (2010) on fluid resonance in narrow gaps. This study concluded that potential theory highly overestimates the wave elevation amplitude close to the resonance frequency. This explains the response behaviour that is seen in relation with low T_z values. It should also be noted that the response amplitudes drop down to more physical values as the T_z value increase. The results related to T_z values far away from the natural period of the response RAO are more reliable, ref. Lu et al. (2010).

The other trend that can be noted is that the response amplitude at the positions located at the starboard side is in general larger compared to the response on the port side. This is expected as the port side is the lee side of the vessel, meaning that the response will be influenced by sheltering effects. By looking at the positions at port side, it can be seen that the largest responses are caused by waves with a direction of 0°. This corresponds to following seas. At the front positions, the second largest response corresponds to head sea waves. This trend is also expected since the sheltering effect from the opposite hulls are at a minimum in these cases.

By looking at the positions at starboard side, it can be seen that the largest response is caused by waves with a direction of 150° in most cases, i.e waves approaching the bow with an angle of 30°. Other problematic wave directions are 60° and 30°. From this the following can be understood: When the waves are either approaching the bow or coming from behind the vessel with a relatively small angle, the waves are allowed into the gap between the hulls without being reflected away by the outer side hull. Due to the oblique sea, the waves will be transmitted by the main hull to the side hull, and vice verca. This allows the waves inside the gap to build up. It seems that when the wave direction approach 90°, more waves will be reflected away by the outer side hull. When the waves have no angle, more waves will pass through the gap without being transmitted back and forth. In one case, i.e at the starboard aft position for trimaran version 1, following sea waves give the largest response, ref 8.9f. It is not easy to comment on this exception. It may have to do with the fact that the side hulls of version 1 have a very large draft compared to the remaining versions. It is believed that a large draft and small gap will reflect more waves from entering the gap in the case of oblique seas. This sheltering effect may be the explanation of why following seas results in the largest relative response in this particular case.

The motivation of the comparison in figure 8.14 is to determine if there is any consistent trend that indicates a beneficial hull configuration with respect to hull interaction. By comparing the plots in figure 8.14, it can be seen that there are no consistent trends to rate the vessels on. However, version 2 often shows good result compared to the remaining versions. Otherwise it is seen that the results varies frequently regarding to which hull configuration that shows the largest response. It was somewhat surprising that version 2 seems to have a beneficial hull configuration compared to the remaining versions, because of the relative small gap between the hulls. The gap size is 6.5 meters, found by utilizing the information in table 2.1. Version 3, 4 and 5 have a gap size of 9.5, 11 and 9 meters respectively. In theory, the amplitude of the gap wave should be decreasing with increasing gap size due to free surface damping. This implies that other main particulars have a considerable effect on the result. By comparing the main particulars of version 2 through 5 it is noted that version 2 has a side hull that is 10 meters shorter than the remaining versions. An explanation could be that a longer extent of the side hulls will give a longer stretch for the waves to be transmitted back and forth, leading to a larger amplitude up stream. This would mean that in the case of following waves, this trend should be visible at the front positions. In the case of head sea waves this trend should be visible at the aft position. If the aft positions at starboard side is considered, it can be seen that waves with a heading of 150° are dominating for version 3, 4 and 5, ref. figure 8.13. If the front starboard positions are assessed, it can be seen that wave directions of 30° and 60° are dominating. Both cases therefore supports the argumentation about the importance of side hull length. However, one should be careful with making any definitive conclusions when comparing the versions, because multiple main particulars have different values. In another context, where the influence of the side hull length is the main interest, it would be better to compare a number of trimarans with identical shapes and vary only one parameter, i.e the side hull length.

Despite the results of relative motion for version 2 it is not going to be concluded that this is the preferred hull configuration with respect to hull interaction. It is suspected that the results from potential theory leave out important information concerning the influence of gap size. In theory, a larger gap size will prevent more waves from reaching the adjacent hull before they are damped out by viscous and 3D effects. As potential theory neglects viscous damping, only 3D effects are left as a source to surface damping. It is suspected that model trials or a numerical method that predicts viscous effects will show a more prominent dependence on gap size.

As mentioned in the beginning of this section, the most relevant information is represented by the results corresponding to spectral peak periods larger than $T_z = 6$ s, ref. appendix H. This corresponds to a zero up-crossing period of approximately $T_z = 8$ s, ref. eq. 8.3. This gives a surface elevation of 4 meters relative to the vessel motion, ref. figure 8.14b, version 4. It means that the tunnel height should be more than 4 meters to avoid cross-structure slamming. This holds for a sea state with a significant wave height up to $H_s = 4$ m. When considering a sea state with a significant wave height of $H_s = 6$ m, it can be seen from table H.1 that it is not very likely that the waves will reach

this height in combination with T_p values lower than $T_p = 9$ s. This corresponds to a zero up-crossing period of approximately $T_z = 12.5$ s. As a consequence of the linear relationship, it can be found that the relative response for the case of a significant wave height of $H_s = 6$ m and $T_z = 12$ s will give a surface elevation of 2.75 m, ref. eq. 8.1 (same case as presented in figure 8.14b). This means that a tunnel height which is higher than 4 meters will also be sufficient in higher sea states, taking the long term long-term sea state probabilities into account.

8.11 Relative motion at 5 knop

Section 7 described the problems related to obtain reasonable result once a forward speed is introduced. However, it was achieved for some of the versions, more precisely version 3 and 4. To review the influence of forward speed, the results of version 4 are included. The results are presented in the same manner as it was done for the case of zero forward speed. The results are given in figure 8.15.

Version 4

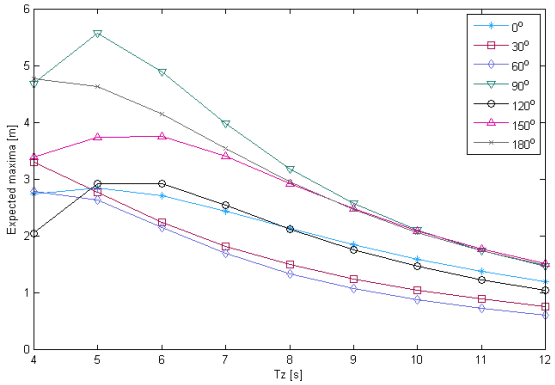

(a) Front position, port side

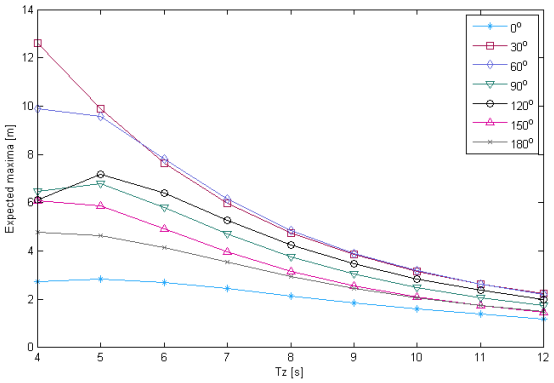

(b) Front position, starboard side

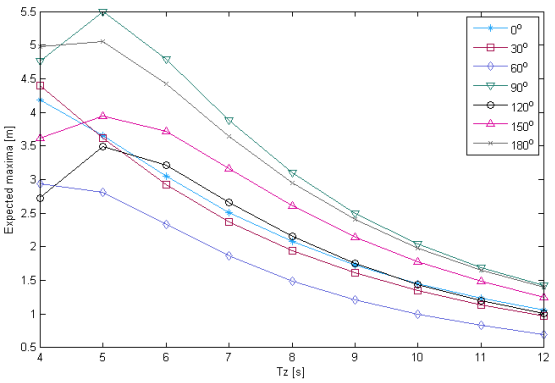

(c) Middle position, port side

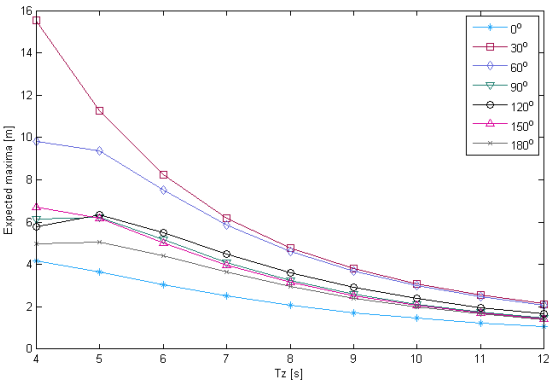

(d) Middle position, starboard side

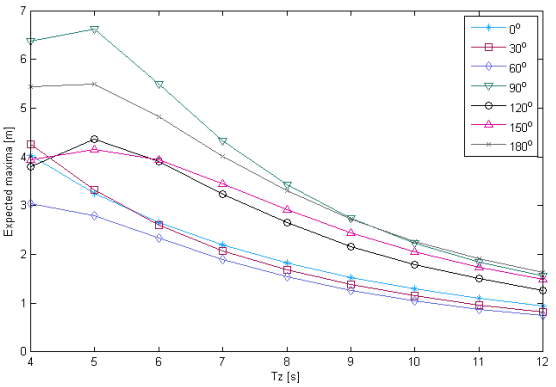

(e) Aft position, port side

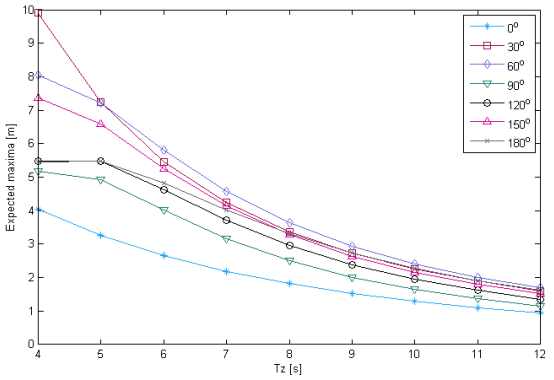

(f) Aft position, starboard side

Figure 8.15: Expected maxima of relative motion at a forward speed of 5 knots during a 3 hour sea state, Version 4

By considering the port side positions it is noticed that the expected maxima reaches a peak value inside the plot area. This is due to the effect of encounter frequency:

$$\omega_e = \omega + \frac{\omega^2}{g} U \cos\beta \Leftrightarrow T_e = \frac{\lambda}{c + U\cos\beta} \tag{8.4}$$

where c is the phase velocity:

$$c = \frac{\lambda}{T} = \frac{\omega}{k} \tag{8.5}$$

Due to this effect, the vessel will feel a period that is larger than the period of the incident wave in the case where the waves are travelling in the same direction as the vessel. I.e when β is in the range 0° - 60°. When the waves are travelling in the opposite direction of the vessel, the vessel will feel a period that is smaller than the period of the incident waves. I.e when β is in the range 120° - 180°. In the case of beam sea waves, the encounter period is equal to the incident wave period. By comparing the RAOs in figure F.1d and F.1f it is clear that the response peaks are shifted to a higher period for 120°-180°. This is corresponding to the discussion above. In the case of beam seas the natural periods are approximately the same. This was also seen in the case of a wave direction of 60°. As expected, the response peak at a wave direction of 30° is shifted to a smaller period. It is not easy to interpret the case where the wave direction is 0°, as the smallest period included in the result is 2 s. It can be seen that the RAO is increasing towards $T = 2$ s in the case of a forward speed of 5 knots. This implies that there is a response peak outside the frequency range.

It was expected that the relative response would be smaller in the case of forward speed, according to the discussion in section 5.3. This was seen in the case of a wave heading of 0° and 150°. However, all other cases showed a significant increase of the RAOs. Due to the analysis problems connected to forward speed that was discussed in section 7 and the unexpected increase in the RAOs, the credibility of these results are poor. As a consequence, a detailed discussion of the result will not be valid and is therefore omitted.

8.11.1 Relative motion: Veres results

The Veres results for relative motion were included in this study for the purpose of comparison, see appendix G. As mentioned, 2D strip theory methods does not take any longitudinal interaction into account. Veres solves the wave-vessel interaction problem separately for each hull and utilizes the superposition principle to obtain the global motions. I.e no interaction between the hulls is accounted for. The objective of including the results is to check if Veres over- or under predicts the relative motion.

As expected, the Veres results are quite different from the Wasim results: By looking at the results corresponding to a spectral peak period of $T_z = 6$ s, it can be found from the results that the surface elevation relative to the vessel motion is close to 5 meters for version 1, in the case of zero forward speed. The port side is considered, as starboard side is the lee side. For version 2, 3 and 4 the relative surface elevation is close to 4.5 meters, while version 5 has the smallest relative motion. For version 1, the worst wave heading is 90° at port side. At the lee side, the worst heading is head sea waves. For the remaining versions, head sea waves are corresponding to the largest response, both at port- and starboard side. Although the results from Wasim and Veres shows different trends, the expected maximum values are in the same order. Veres shows a slight over-prediction of the relative motion compared to Wasim. The Veres results cannot be commented on, as there are no Wasim results to compare with. Based on the comparison between Veres and Wasim results corresponding to zero forward speed, the following can be assumed: If Veres are utilized to calculate relative motion, the results will be slightly over-predicted in the case of zero forward speed. This implies that the results corresponding to forward speed will also be over-predicted.

By looking at the results for zero forward speed, it can be argued that a tunnel height of 5 meters will be sufficient. This tunnel height will also respect the findings from the Wasim results with a margin. In the case of a forward speed of 16 knots, the relative motion exceeds 6 meters. Hence, if the designer suggests that a tunnel height lower than 6 meters, it is advised to further investigate the challenges related to cross-structure slamming by more reliable methods.

CHAPTER 9

Conclusion and Further Work

A new trimaran concept intended for the seismic industry has been evaluated with respect to a set of seakeeping criteria. The analyzes have been done by the use of two commercial softwares: Wasim (by DNV) and Veres (by MARINTEK). Wasim uses a 3D potential Rankine panel method, while Veres is based on a 2D strip theory. Due to analysis problems related to resonant gap waves, the initial plan to do the complete seakeeping analysis in Wasim has been altered. Therefore, a large part of the analyzes have been done in Veres. Veres does not include any interaction effects, meaning that diffraction loads due to the hull interaction are excluded in the calculation of global motions. Results from Wasim have been used to evaluate the relative motion, where diffraction is essential. However, these results only include the case of zero forward speed, as valid result were not obtained when the vessel has forward speed. A total of five different hull configurations have been investigated. A mono-hull that is known to operate as a seismic vessel has been included for comparison. The seakeeping criteria that were used in the verification study deals with comfort, safety and helicopter operations. The relative motion between the wave elevation and the vessel has been investigated to assess the hydrodynamic hull interaction.

This research has been conducted in collaboration with LMG Marin, who has provided the hull line drawings. The different hull configurations that have been investigated are referred to as version 1, 2, 3, 4 and 5. Version 1, 2 and 5 have a main hull length of 110 meters, while version 3 and 4 have a main hull length of 120 meters. Version 1 and 2 have a full main hull, while version 4 and 5 have a slender main hull. The side hulls of version 1 contribute to a large part of the total displacement by having a large draft and side hull width. Version 5 shares this characteristic. Version 2, 3 and 4 have side hull dimensions that are more similar to other trimaran designs. The conclusions are given in the following.

It was found that trimaran version 5 has the highest occurrence of motion sickness incidence. In the worst cases it was found that the MSI values exceeded the MSI values of the comparison ship. Version 1 also showed relatively high MSI values, compared to version 3 and 4. This implies that it is beneficial to choose a hull configuration where the main hull is long and slender in combination with side hulls that have a small contribution to the total displacement.

A common characteristic of all the trimaran versions is that, compared to the monohull, the natural roll and pitch periods are quite similar. This suggests that the trimaran concept will exert a cork-screw motion. A possible approach to reduce the correlation between pitch and roll natural period is to decrease the total beam of the vessel. It can also be effective to decrease the side hull displacement by making them shorter and half planing.

From the evaluation of the deck operation criterion, it was found that version 1 has the least beneficial hull configuration. The remaining versions do not exceed the criterion of 1 MII per minute in any sea states. It was also found that all the trimaran versions have the benefit of providing a stable work platform in high sea states, compared to the mono-hull.

Regarding the helicopter operation criteria it was found that version 3 and 4 have pitch amplitudes within the recommended values. The roll criterion is exceeded by all versions when the waves have a direction of 60° or 90°. The vertical velocity criterion was exceeded by version 5 when the waves have a direction of 0°, 30° and 60°. Version 1 and 4 have a slight violation of the criteria. Overall, version 3 has the most beneficial hull configuration with respect to helicopter operations, followed by version 2 and 4. It was also found that the large beam of the trimaran concept will introduce a significant amount of potential roll damping by the side hulls.

Version 2 came out best from the evaluation of the vertical motion between the wave and vessel. This implies that it is beneficial to have shorter side hulls with a small draft. However, it is suspected that the importance of viscous wave damping will have an important influence on the outcome of this evaluation. As viscous effects are not included in potential theory methods, the credibility of the results is weakened. Therefore, a definite conclusion can not be drawn. The results showed that the natural period of the resonant gap wave is close to 4 seconds. Therefore, the results can not be used to evaluate the required tunnel height in low sea states where the spectral peak period is close to 4 seconds. In such cases the gap wave amplitude is highly overestimated. In higher sea states, where the significant wave height is larger than 4 m and the spectral peak period is much larger than the gap wave natural period, the results are more reliable. In this case, the results imply that the tunnel height should be at least 4 m to avoid cross-structure slamming. However, the results indicate that viscous effects will affect the results and should be taken into account to obtain better results. It is therefore recommended to perform model tests to investigate the relative motion. The alternative is to perform an URANS-VOF simulation to include both viscous and rotational effects in the flow and free surface waves.

The latest versions of Wasim have the option of adding an artificial free surface damping on the surface between the hulls. This is a convenient, but controversial, method to avoid the problems related to the resonant gap wave. The reason is that the application of such damping can not be supported by any physical arguments. Therefore, a topic for another study could be to investigate the viscous wave damping between adjacent floaters. A range of floaters with different gap, draft and width should be included in the study to obtain a range of empirical damping values. Such empirical values could be useful when using potential theory to evaluate multi-bodied floaters and side-by-side operations.

Overall, version 3 has the most beneficial hull configuration with respect to the criteria

that were included in the verification. In the continuation of this project, it is recommended to make the side hulls shorter and keeping a small draft. This will be beneficial both in terms of correlation between pitch and roll motion and hydrodynamic hull interaction.

The trimaran concept shows promising results that are significantly better than the attributes of the mono-hull comparison ship. However, there are still important aspects that need to be investigated, such as an assessment of building costs and fuel consumption. The trimaran vessel has a potential of cost savings due to the increased towing capacity. If the additional building costs of this ship concept does not exceeds the potential savings, it will indeed create an interest in the seismic market.

References

Amundsen, L. and Landrø, M. (2008). Seismic Imaging Technology Part IV. *GEO ExPro - Geoscience & technology explained*, 5(5).

Baitis, A. E., Applebee, T. R., and McNamara, T. M. (1984). Human factors considerations applied to operations of the FFG-8 and LAMPS MK III. *Naval Engineers Journal*, 96(3):191–199.

Beckett, C., Brooks, T., Parker, G., Bjoroy, R., Pajot, D., Taylor, P., Deitz, D., Flaten, T., Jaarvik, L. J., Jack, I., Nunn, K., Strudley, A., and Walker, R. (1995). Reducing 3D Seismic Turnaround. *Oilfield Review*, 7(1):23–37.

Berchiche, N. (2014). Calm water resistance evaluation for OilCraft's trimaran. Report, Norwegian Marine Technology Reserach Institute.

Blanchard, T. and Ge, C. (2007). Rules for the Classification of Trimarans. *Journal of Naval Engineering*, 44(1).

Boreham, D., Kingston, J., Shaw, P., and Zeelst, J. v. (1991). 3D Marine Seismic Data Processing. *Oilfield Review*, 3(1):41–55.

CGG (nd). *Geoscience Overview*. available from: `http://www.cgg.com/en/Who-We-Are/Geoscience-Overview`. [15. November 2015].

Chen, G.-R. and Fang, M.-C. (2001). Hydrodynamic interactions between two ships advancing in waves. *Ocean Engineering*, 28(8):1053–1078.

CodeGogs®, t. . *Pierson Moskowitz*. available from: `http://www.codecogs.com/library/engineering/fluid_mechanics/waves/spectra/pierson_moskowitz.php`. [20. December 2015].. (nd).

Comstock, E. N., Bales, S. L., and Gentile, D. M. (1982). Seakeeping Performance Comparison of Air Capable Ships. *Naval Engineers Journal*, 94(2):101–117.

DNV (2011). *SESAM User Manual Wasim, Wave Loads on Vessels With Forward Speed*.

DNV (2014). Modelling and Analysis of Marine Operations, DNV-RP-H103. Recommended practice.

Elboth, T. and Andreassen, O. (2009). Flow and swell noise in marine seismic. *Geophysics*, 74:17–25.

Faltinsen, O. (1990). *Sea loads on ships and offshore structures*. Cambridge university press.

Faltinsen, O. (2010). *Hydrodynamics of High-Speed Marine Vehicles*. Cambridge university press.

Fang, M.-C. and Too, G.-Y. (2006). The Effect of Side Hull Arrangements on the Motions of the Trimaran Ship in Waves . *Naval Engineers Journal*, 118(1):27–37.

Fathi, D. (2004). ShipX Vessel Responses (VERES) Ship Motions and Global Loads User's Manual. User manual, Norwegian Marine Technology Research Institute.

Graham, R. (1990). Motion-Induced Interruptions as Ship Operability Criteria . *Naval Engineers Journal*, 102(2):65–71.

Greco, M. (2012). *TMR 4215: Sea Loads*.

Kearey, P., Brooks, M., and Hill, I. (2002). *An Introduction to Geophysical Exploration*. Blackwell Science Ltd.

Kim, Y., Kim, K.-H., Song, M.-J., Kim, M.-S., Sun, J., Song, K.-H., Shin, K.-S., and Yang, J.-H. (2008). Comparative Study on Time-Domain Analysis of Ship Motions and Structural Loads in Waves.

Kring, D. C. (1994). *Time Domain Ship Motions by a Three-dimensional Rankine Panel Method*. Phd. thesis.

Lawhter, A. and Griffin, M. J. (1987). Prediction of the incidence of motion sickess from the magnitude, frequency, and duration of vertical oscillation. *Journal of Acoustical society of America*, 82:957–966.

Lu, L., Cheng, L., Teng, B., and Sun, L. (2010). Comparison of Potential Flow and Viscous Fluid Models in Gap Resonance. *25th International Workshop on Water Waves and Floating Bodies*, 2010/05/09 - 2010/05/12.

Luo, Y. (2013). *Numerical Investigation of Wave-Body Interactions in Shallow Water*. Msc thesis.

McCauley, M. E., Royal, J. W., Wylie, C. D., O'Hanlon, J. F., and Mackie, R. R. (1976). Motion sickness incidence: exploratory studies of habituation, pitch and roll, and the refinement of a mathematical model. Report, Office of naval research Department of the Navy.

Myrhaug, D. and Dahle, E. (1994). *Ship capsize in breaking waves*. Computational Mechanics Publications.

Naess, A. and Moan, T. (2012). *Stochastic Dynamics of Marine Structures*. Cambridge University Press.

NATO (2000). Standardization agreement, STANAG No. 4154 (Edition3), 'Common procedures for seakeeping in the ship design process'.

O'Dea, J. F. (2005). Correlation of VERES Prediction for Multihull Ship Motions. Report, Naval Surface Warfare Center, Hydromechanics Department.

O'Hanlon, J. F. and McCauley, M. E. (1973). Motion sickness incidence as a function of the frequency and acceleration of vertical sinusoidal motion. Report, Office of Naval Research.

Oljedirektoratet (2013). *Gjennomføring av seismiske undersøkelser på norsk kontinentalsokkel* avalable from: `http://npd.no/no/Rapportering/Seismikk/` [17 October 2015].

OPG (2011). An overview of marine seismic operations. Report, International Association of Oil & Gas Producers.

Pedersen, L., Ryan, S., Sayers, C., Sonnerland, L., and Veire, H. H. (1996). Seismic Snapshots for Reservoir Monitoring. *Oilfield Review*, 8:32–43.

PGS (nd). *Field Crew*. available from: `http://www.pgs.com/Careers/Job-Descriptions/Field-Crew---Marine/`. [7. October 2015].

Salvesen, N., Tuck, E., and Faltinsen, O. (1970). Ship Motions and Sea Loads. *Transactions of the Society of Naval Architects and Marine Engineers*, 78:250–287.

Steen, S. (2011). *TMR4247 Marin teknikk 3 - Hydrodynamikk: Motstand og propulsjon, propell og foilteori*, volume UK-2011-99. Department of marine technology, Trondheim.

Xiang, X. and Faltinsen, O. M. (2011). Time domain simulation of two interacting ships advancing parallel in waves . *Ocean Engineering*, 6:357:369.

Yun, L. and Bliault, A. (2012). *High Performance Marine Vessels*. Springer.

Zhang, J. (1997). *Design and hydrodynamic performance of trimaran displacement ships*. Phd. thesis.

Appendices

A MSI at the bridge, 16 knop

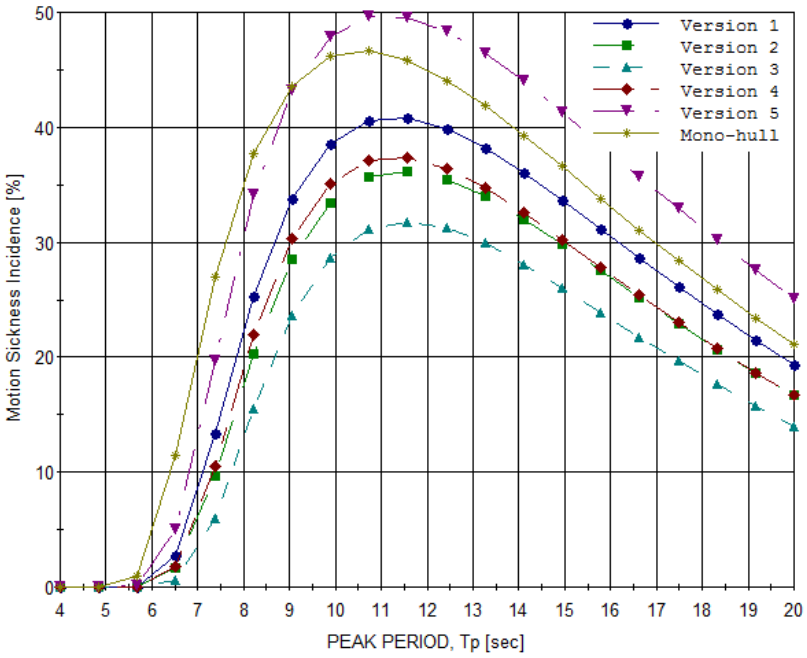

(a) 0 deg heading

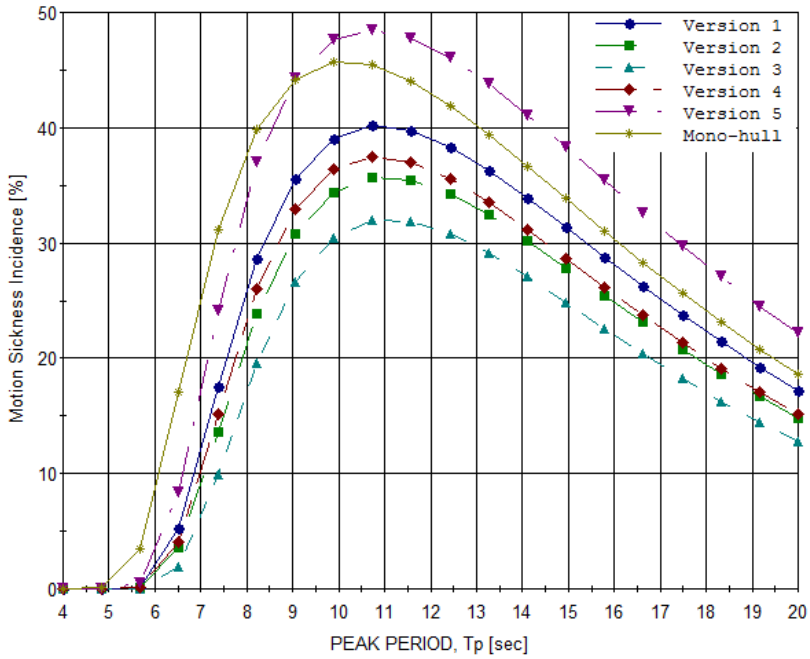

(b) 30 deg heading

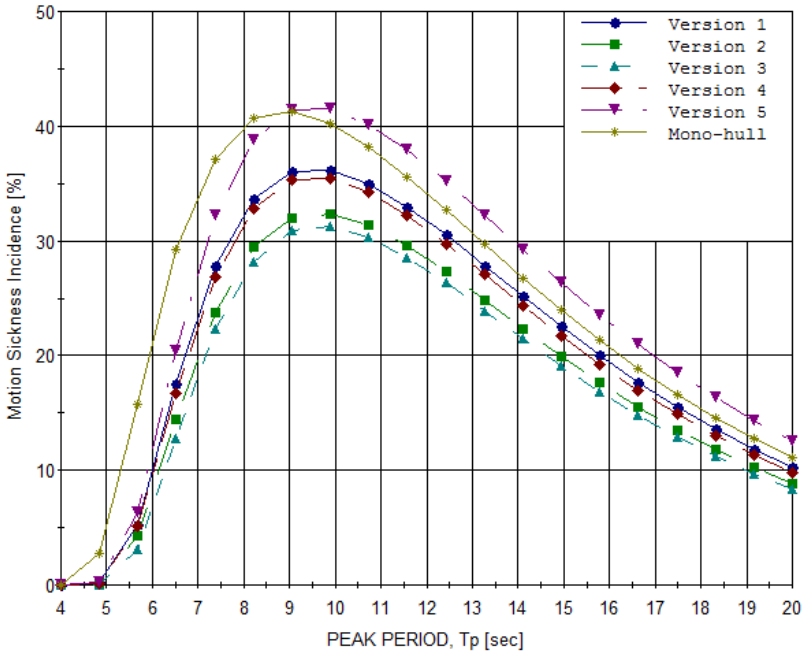

(c) 60 deg heading

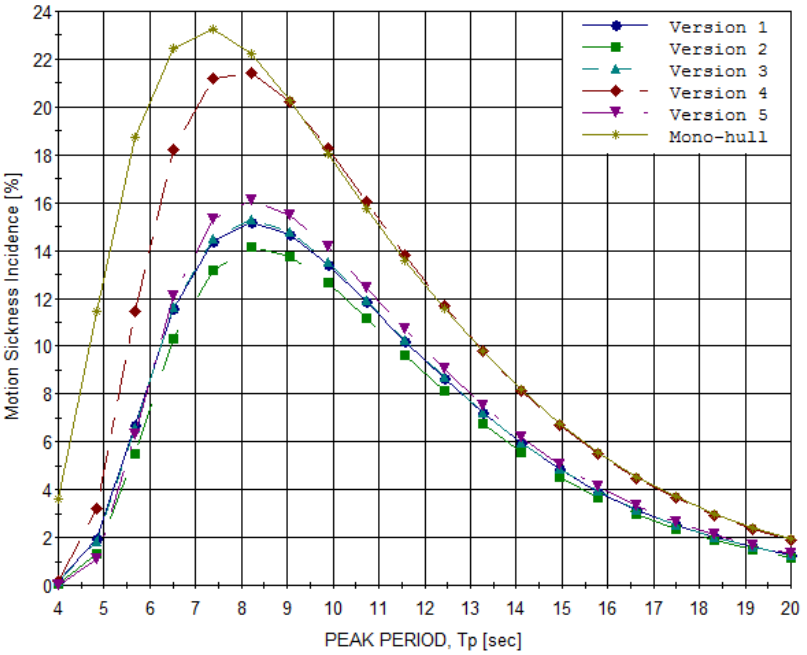

(d) MSI 90 deg

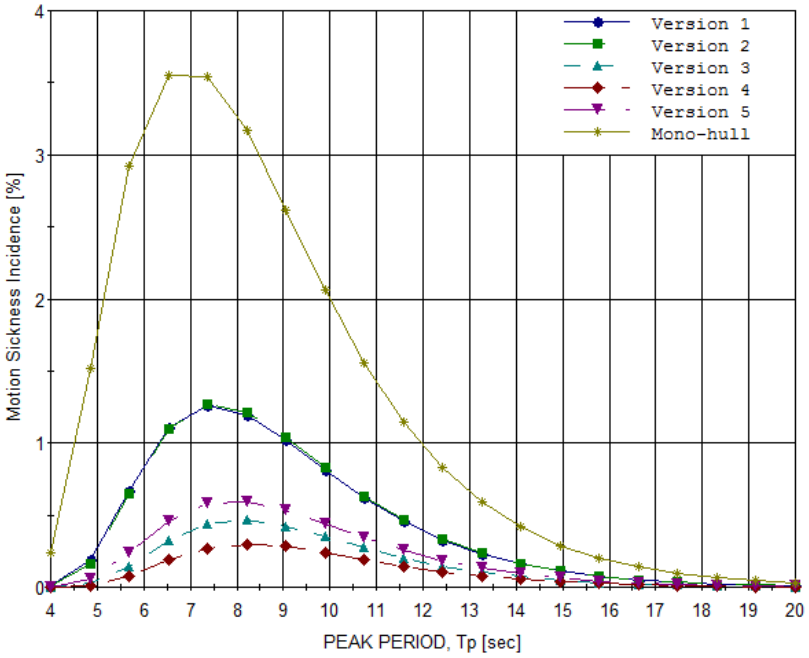

(e) 120 deg heading

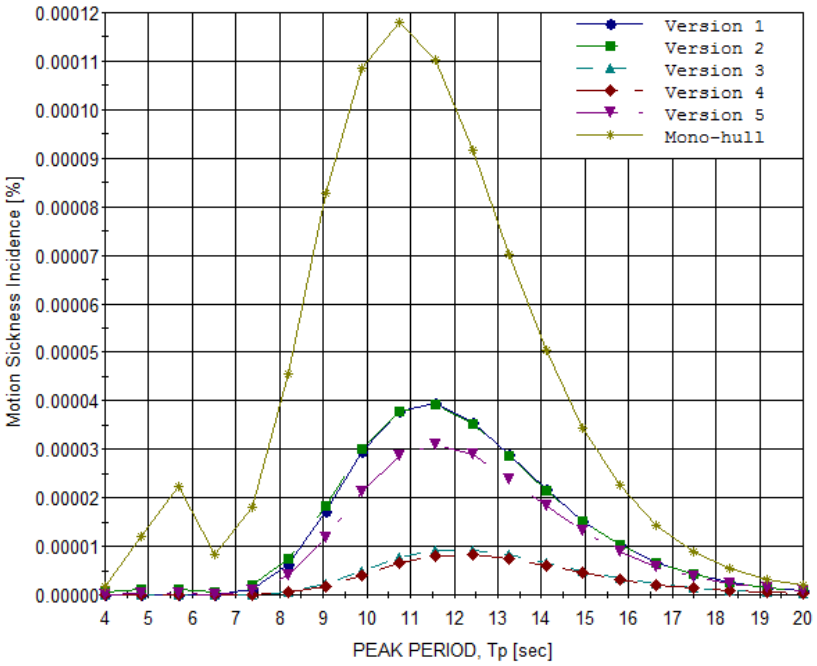

(f) 150 deg heading

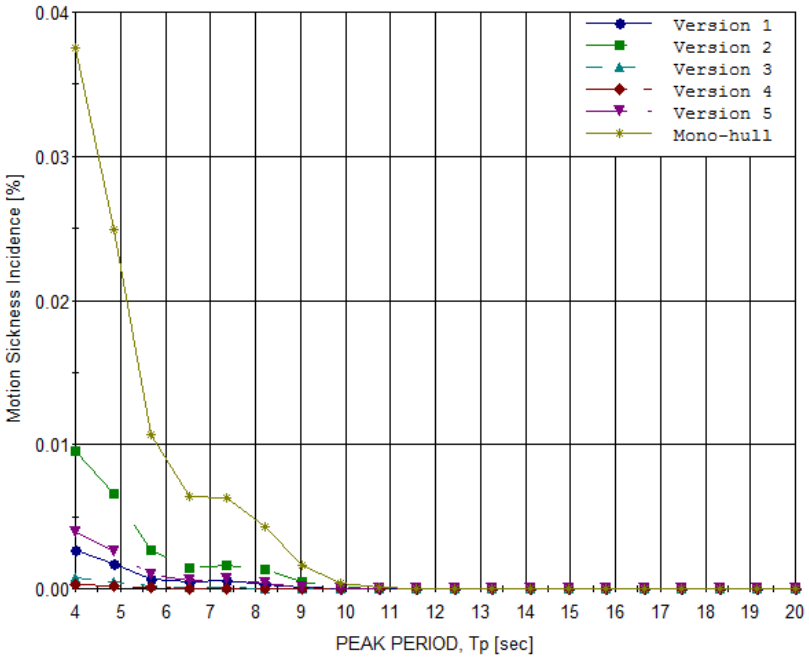

(g) 180 deg heading

Figure A.1: The percentage occurrence of MSI against the peak period, T_p. $H_s = 4$ m. Each vessel has a constant forward speed of 16 knots. The position of the MSI is at the bridge.

B MSI at the recording room, 16 knop

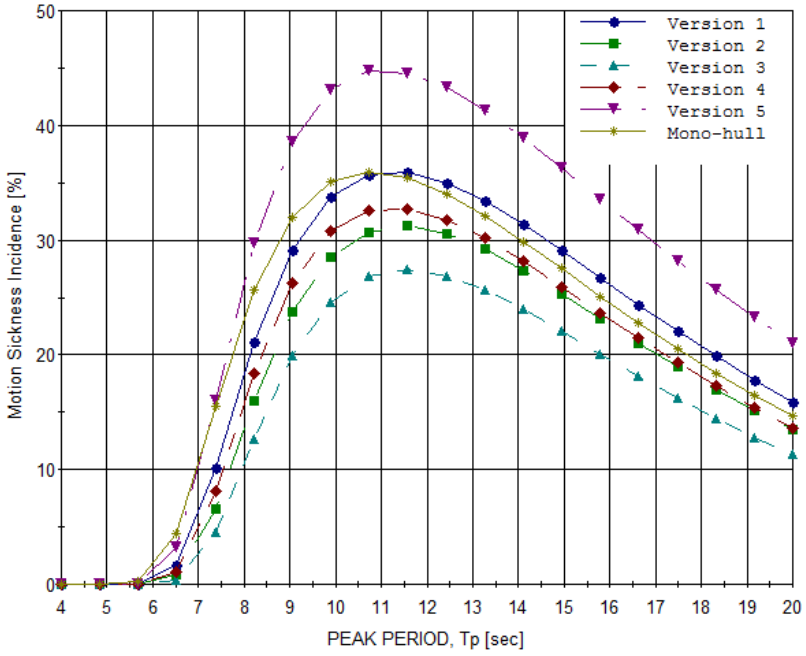

(a) 0 deg heading

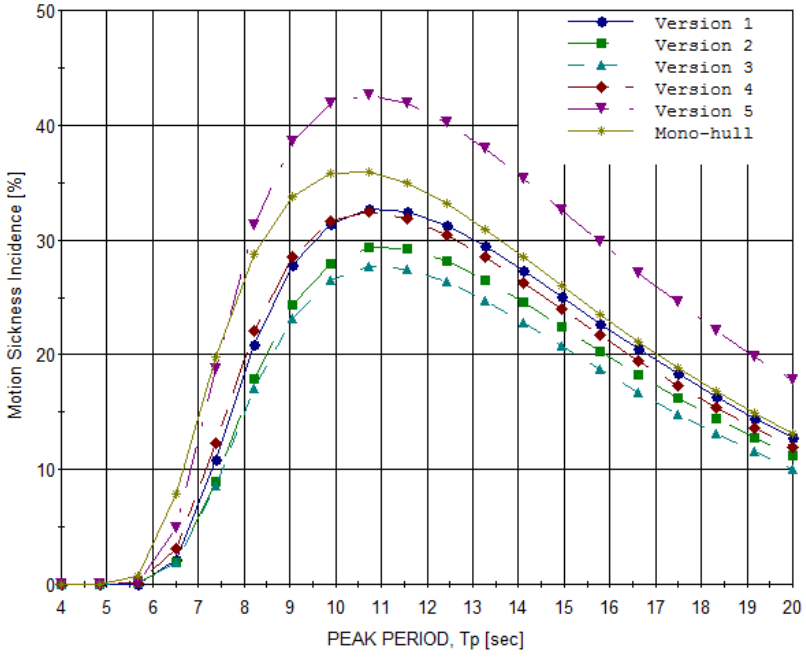

(b) 30 deg heading

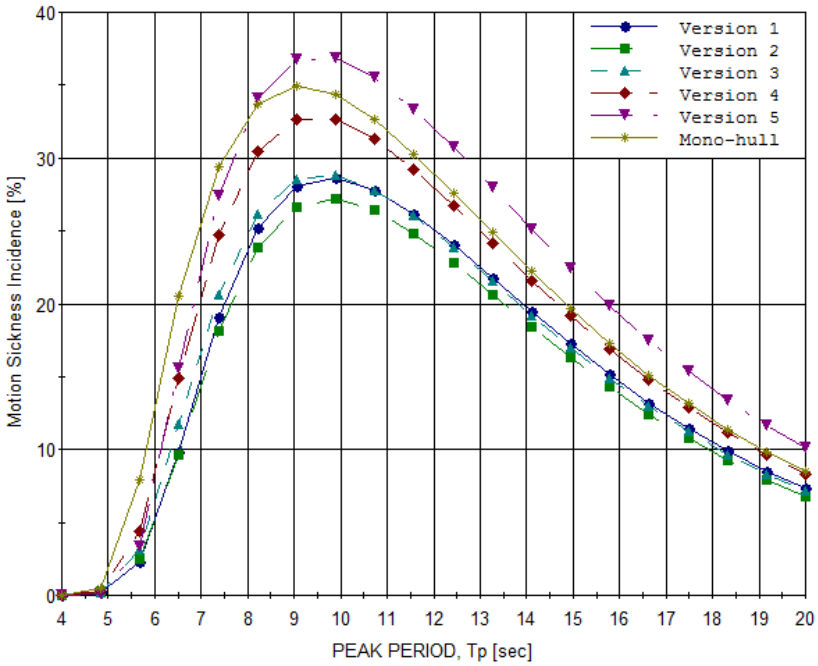

(c) 60 deg heading

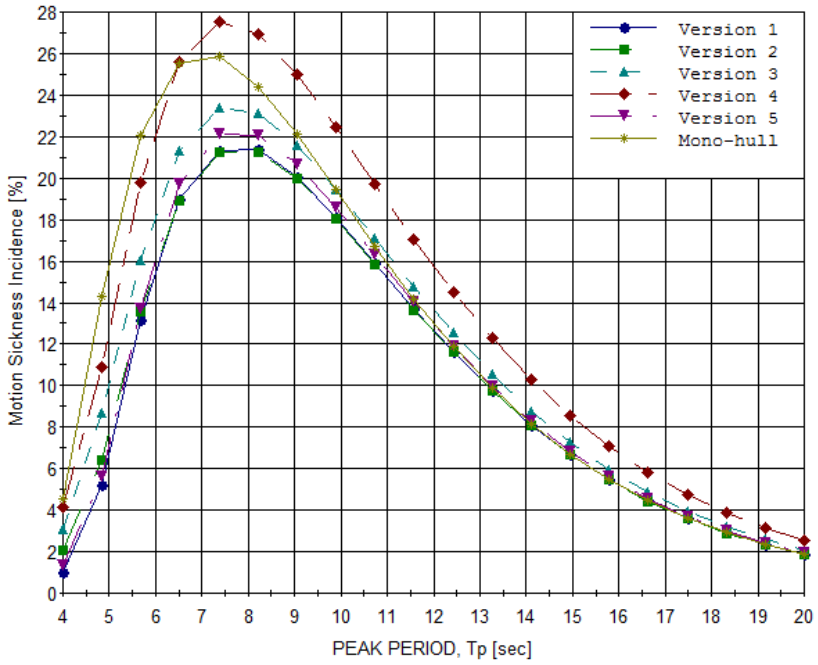

(d) MSI 90 deg

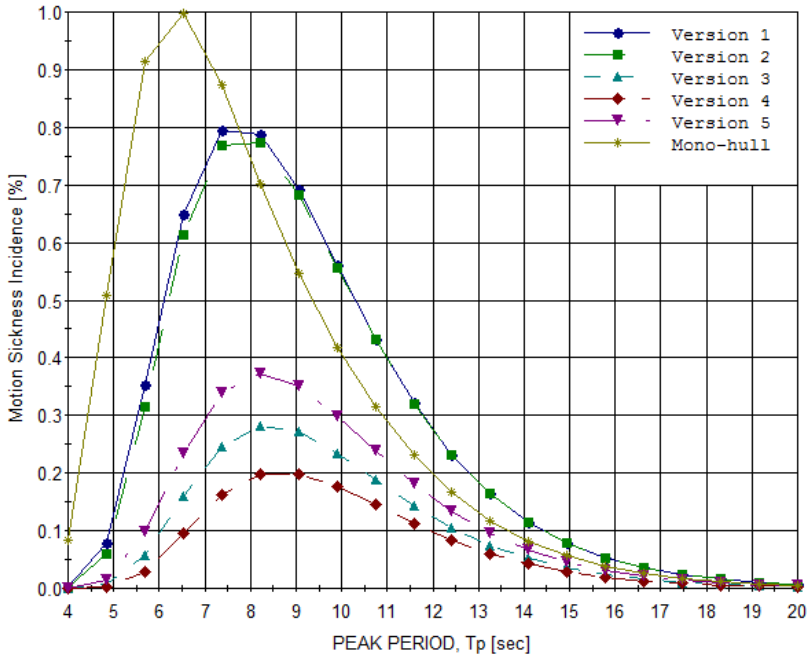

(e) 120 deg heading

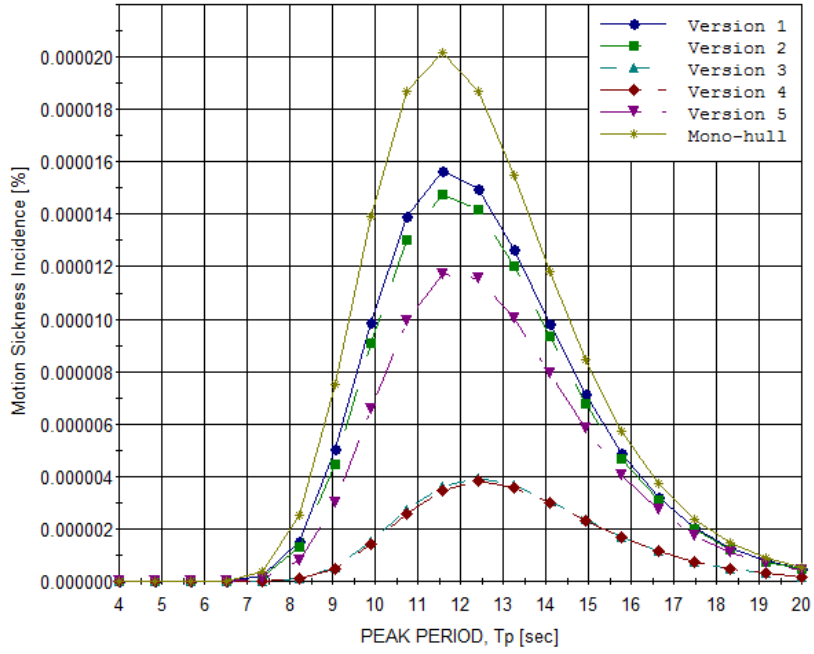

(f) 150 deg heading

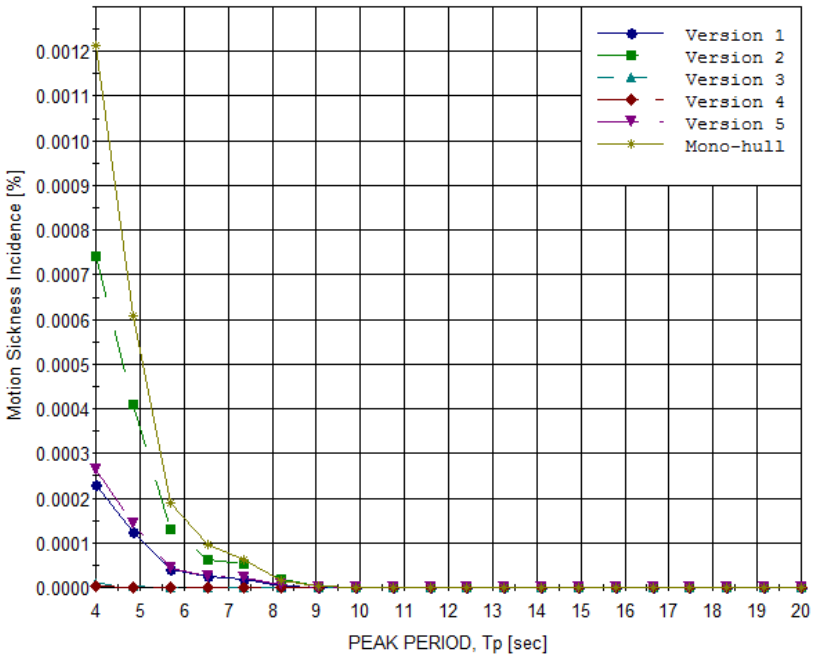

(g) 180 deg heading

Figure B.1: The percentage occurrence of MSI against the peak period, T_p. $H_s = 4$ m. Each vessel has a constant forward speed of 16 knots. The position of the MSI is at the recording room.

C Viscous roll damping

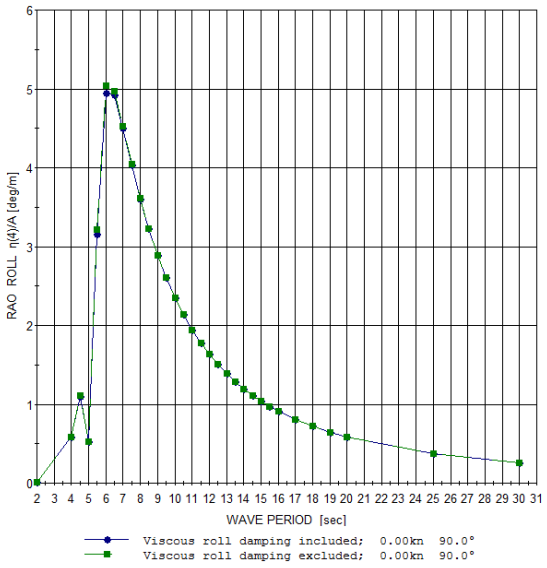

(a) Version 1

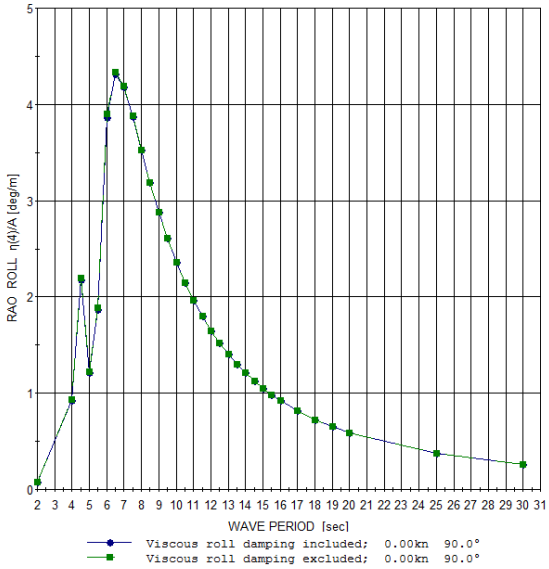

(b) Version 2

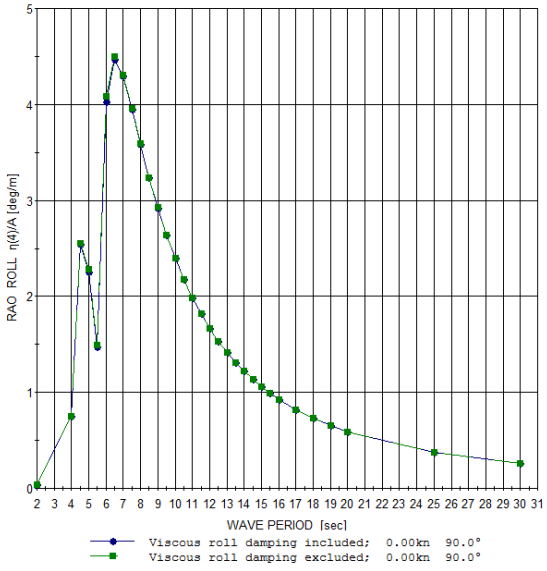

(c) Version 3

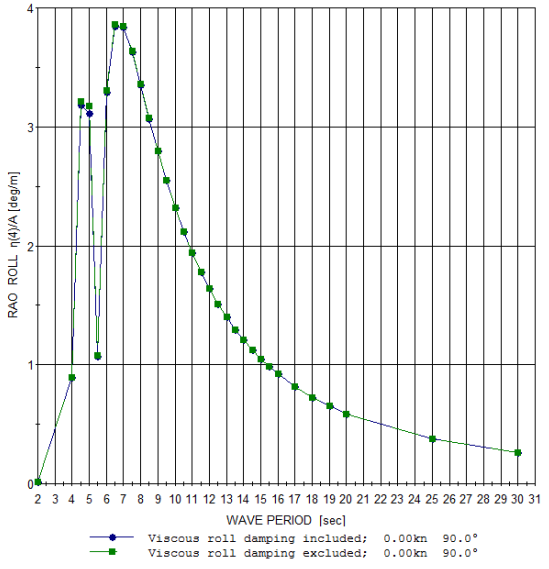

(d) Version 4

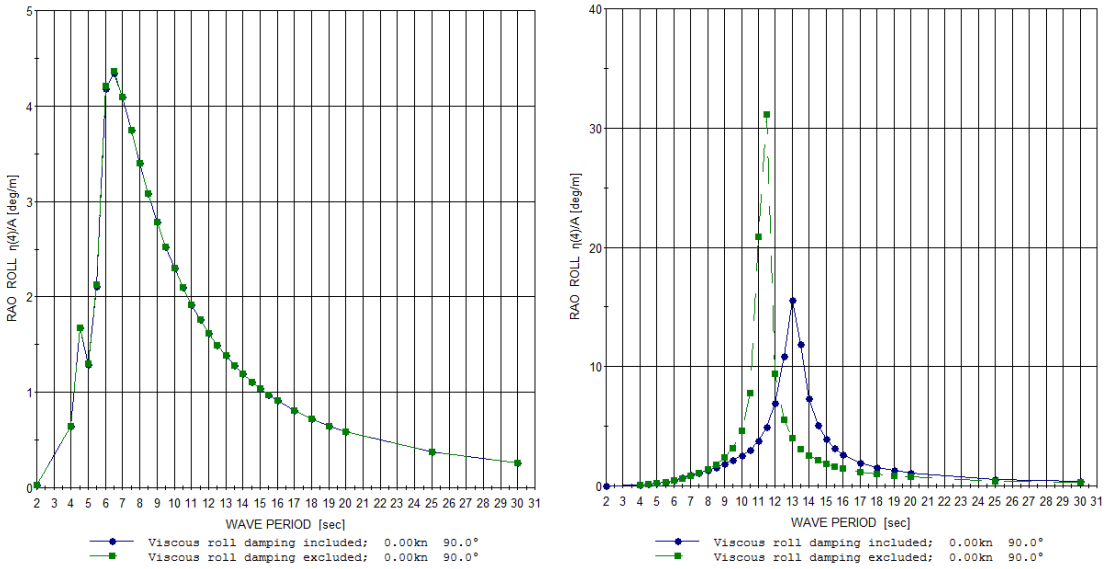

(e) Version 5 **(f)** Mono-hull

Figure C.1: Comparison of roll RAOs when viscous damping is included and excluded

D Pitch RAOs

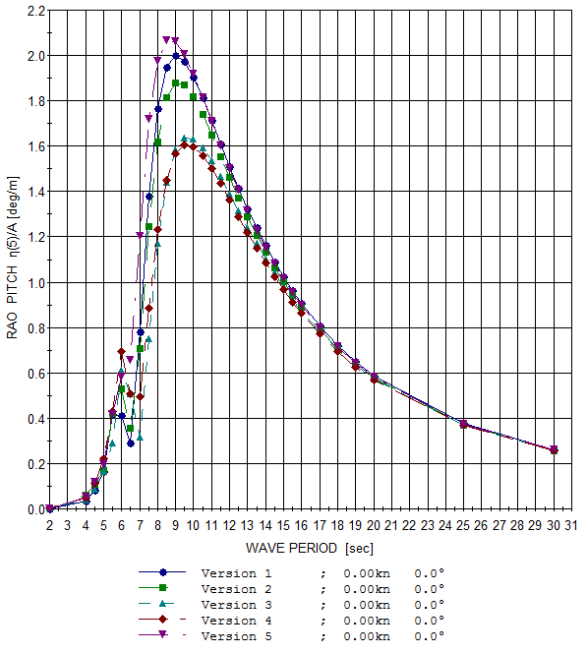

Figure D.1: Pitch RAOs

E Short term statistics of heave velocity

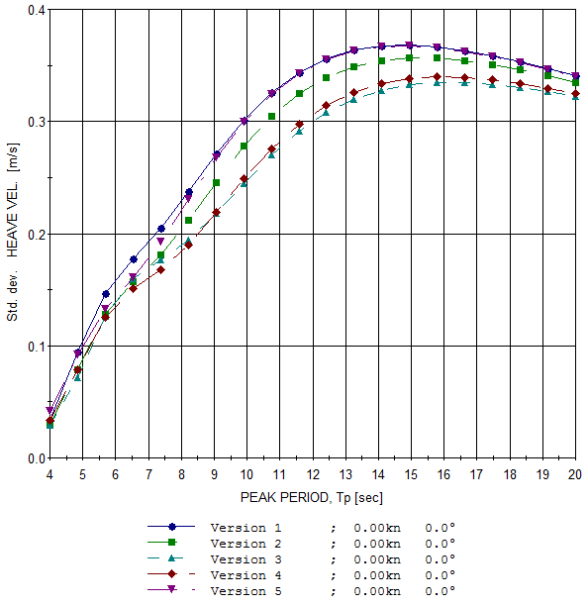

Figure E.1: Heave velocity at 0 knot

F Relative response RAOs

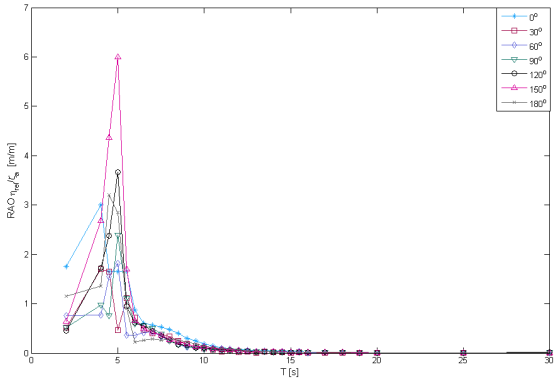

(a) Version 1, 0 knot

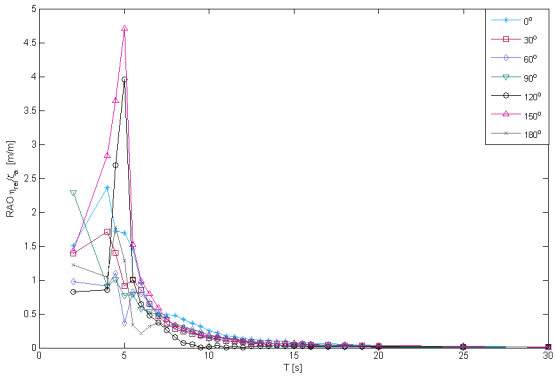

(b) Version 2, 0 knot

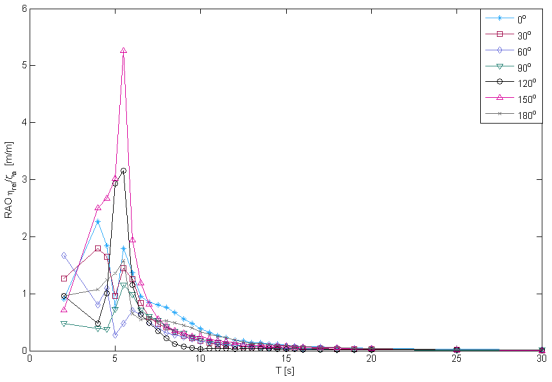

(c) Version 3, 0 knot

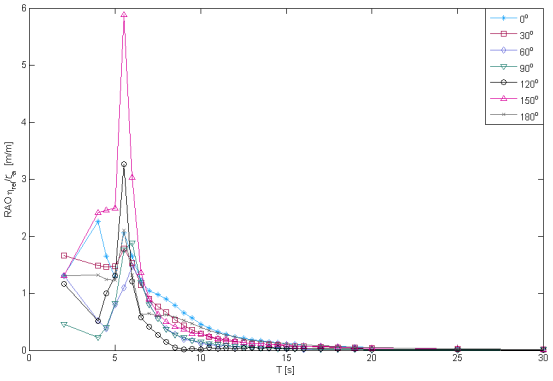

(d) Version 4, 0 knot

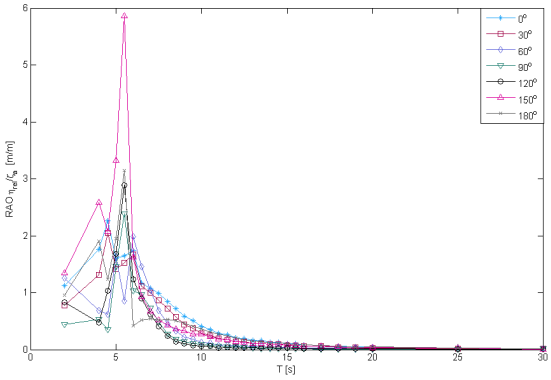

(e) Version 5, 0 knot

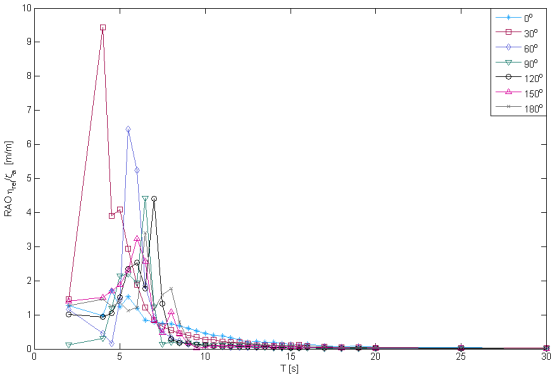

(f) Version 4, 5 knots

Figure F.1: Relative response RAOs, located at the middle position, starboard side

G Relative motion, Veres result

The relative motion between the wave and vessel is presented on the following pages. Note that starboard side is the lee side. 0°, 180° and 90° corresponds to head, following and beam sea, respectively. The main-side hull interaction is not taken into account.

Version 1

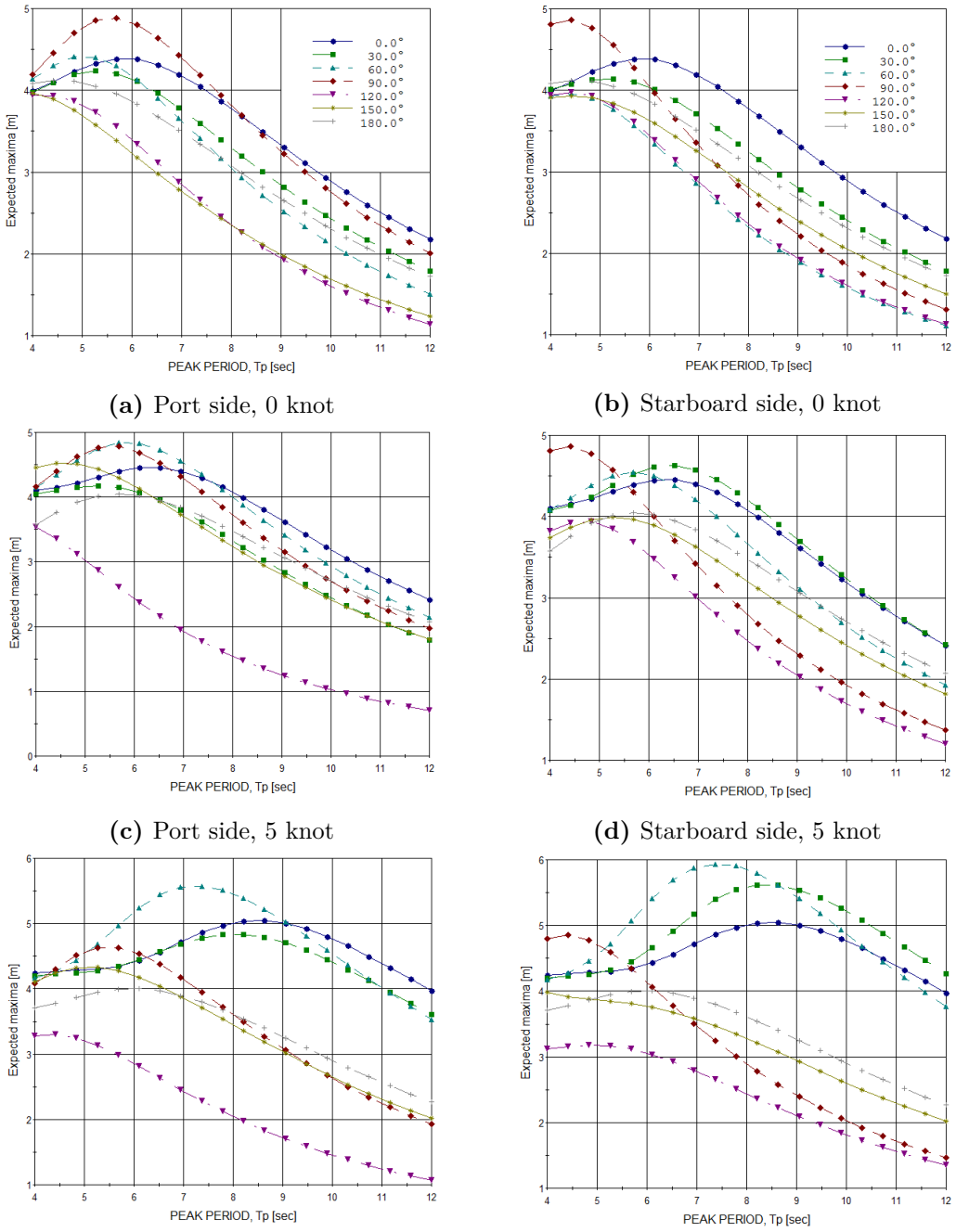

(a) Port side, 0 knot

(b) Starboard side, 0 knot

(c) Port side, 5 knot

(d) Starboard side, 5 knot

(e) Port side, 16 knot

(f) Starboard side, 16 knot

Figure G.1: Expected maxima of relative motion during a 3 hour sea state at different forward speeds. $H_s = 4$ m. Version 1.

Version 2

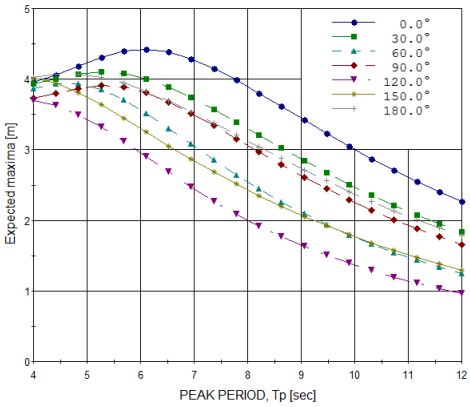

(a) Port side, 0 knot

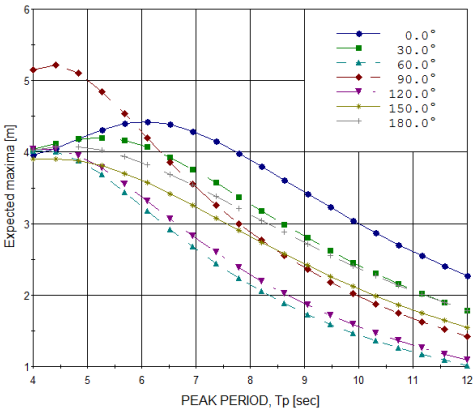

(b) Starboard side, 0 knot

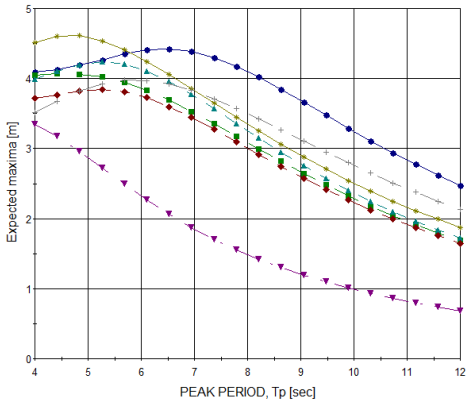

(c) Port side, 5 knot

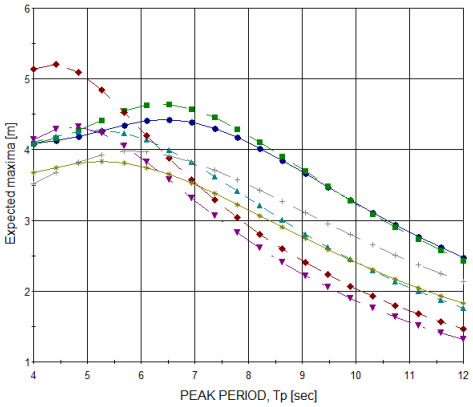

(d) Starboard side, 5 knot

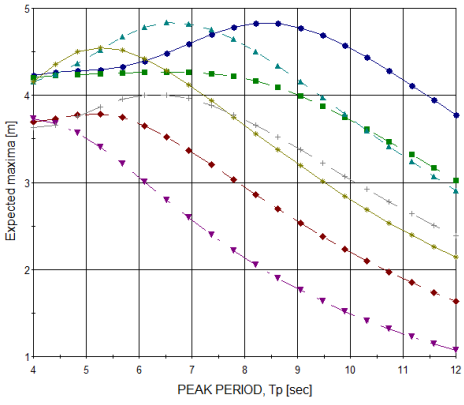

(e) Port side, 16 knot

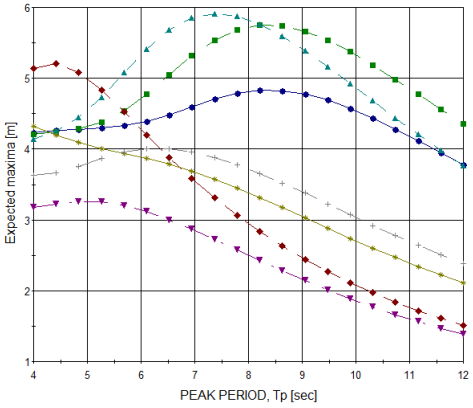

(f) Starboard side, 16 knot

Figure G.2: Expected maxima of relative motion during a 3 hour sea state at different forward speeds. $H_s = 4$ m. Version 2.

Version 3

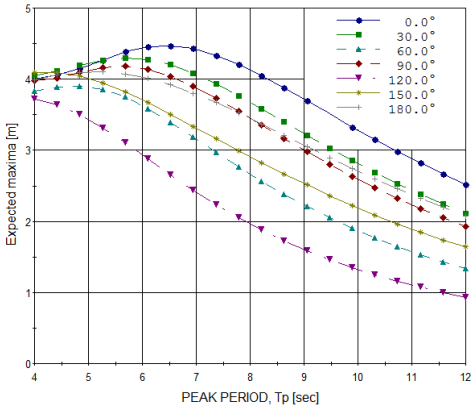

(a) Port side, 0 knot

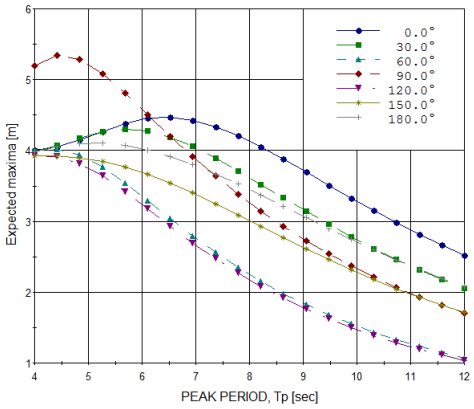

(b) Starboard side, 0 knot

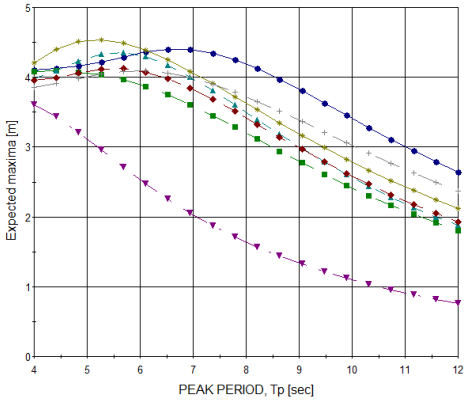

(c) Port side, 5 knot

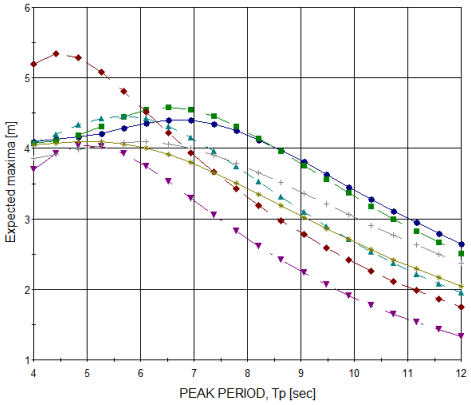

(d) Starboard side, 5 knot

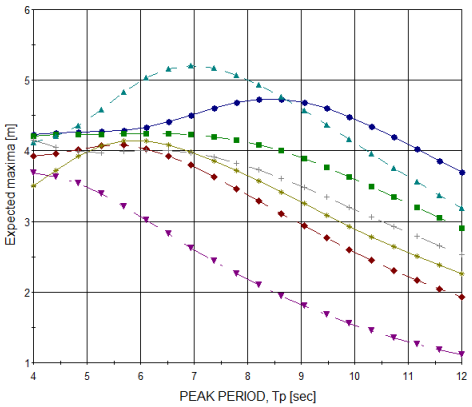

(e) Port side, 16 knot

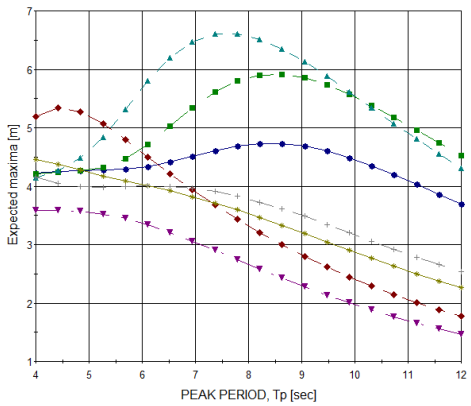

(f) Starboard side, 16 knot

Figure G.3: Expected maxima of relative motion during a 3 hour sea state at different forward speeds. $H_s = 4$ m. Version 3.

Version 4

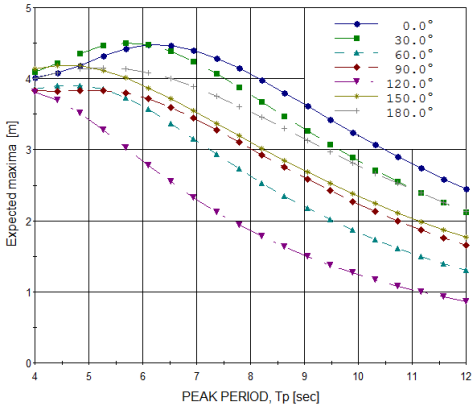

(a) Port side, 0 knot

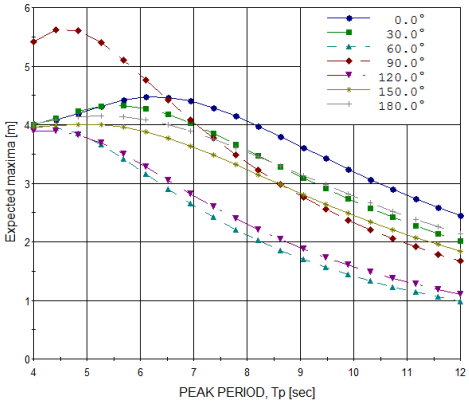

(b) Starboard side, 0 knot

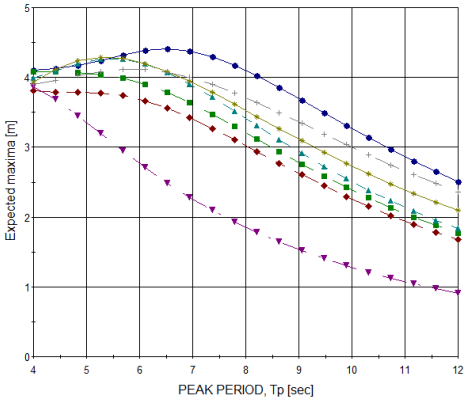

(c) Port side, 5 knot

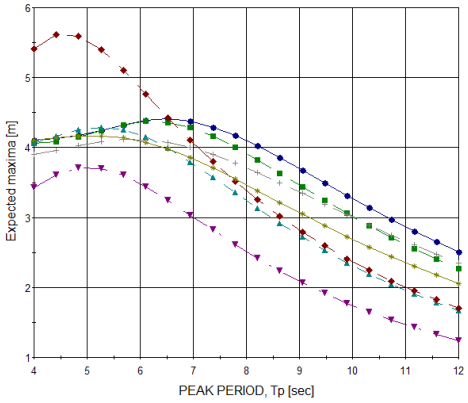

(d) Starboard side, 5 knot

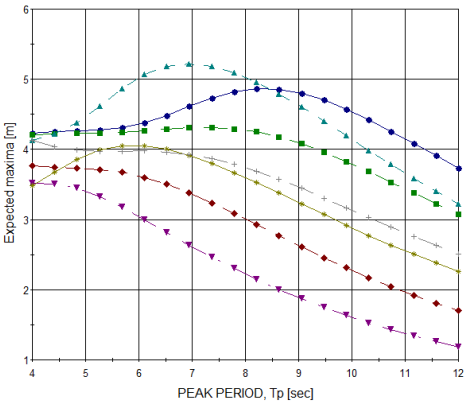

(e) Port side, 16 knot

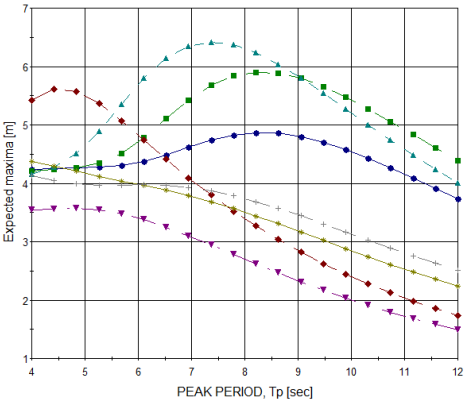

(f) Starboard side, 16 knot

Figure G.4: Expected maxima of relative motion during a 3 hour sea state at different forward speeds. $H_s = 4$ m. Version 4.

Version 5

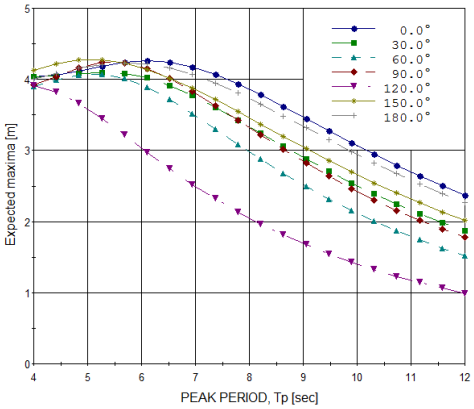

(a) Port side, 0 knot

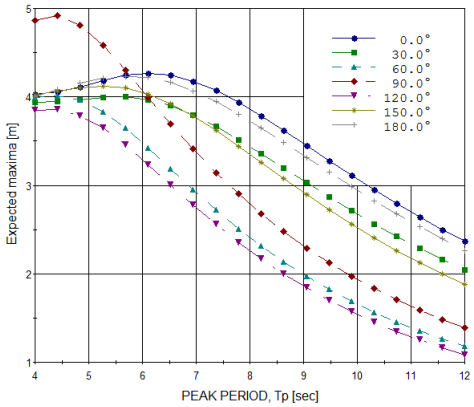

(b) Starboard side, 0 knot

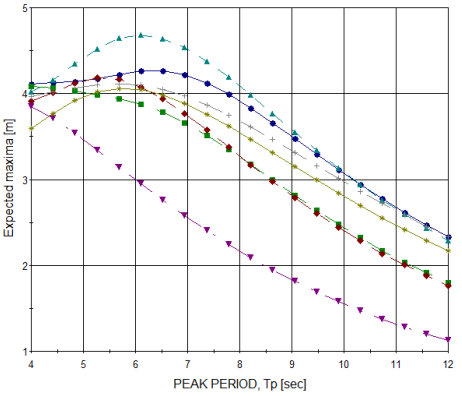

(c) Port side, 5 knot

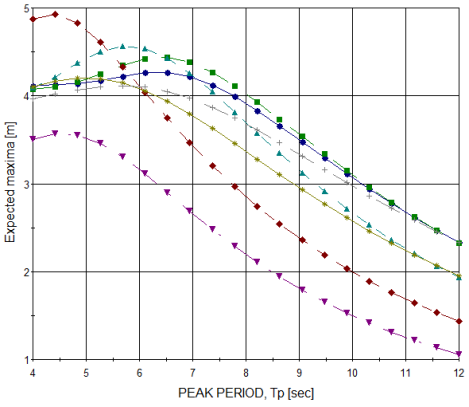

(d) Starboard side, 5 knot

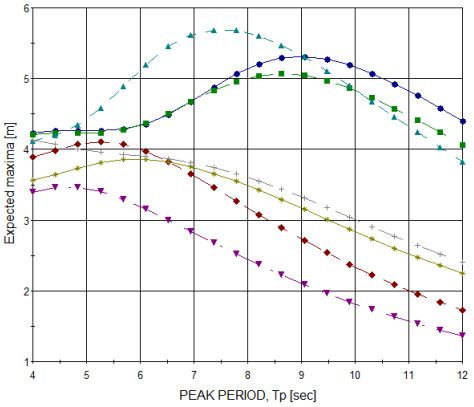

(e) Port side, 16 knot

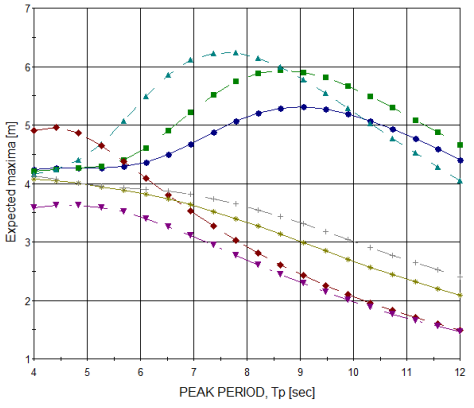

(f) Starboard side, 16 knot

Figure G.5: Expected maxima of relative motion during a 3 hour sea state at different forward speeds. $H_s = 4$ m. Version 5.

H Long-term sea state

Significant wave height (m) (upper limit of interval)	Spectral peak period (s)																		
	3	4	5	6	7	8	9	10	11	12	13	14	15	16	17	18	19	21	22	Sum
1	59	403	1061	1569	1634	1362	982	643	395	232	132	74	41	22	12	7	4	2	2	8636
2	9	212	1233	3223	5106	5814	5284	4102	2846	1821	1098	634	355	194	105	56	30	16	17	32 155
3	0	8	146	831	2295	3896	4707	4456	3531	2452	1543	901	497	263	135	67	33	16	15	25 792
4	0	0	6	85	481	1371	2406	2960	2796	2163	1437	849	458	231	110	50	22	10	7	15 442
5	0	0	0	4	57	315	898	1564	1879	1696	1228	748	398	191	84	35	13	5	3	9118
6	0	0	0	0	3	39	207	571	950	1069	885	575	309	142	58	21	7	2	1	4839
7	0	0	0	0	0	2	27	136	347	528	533	387	217	98	37	12	4	1	0	2329
8	0	0	0	0	0	0	2	20	88	197	261	226	138	64	23	7	2	0	0	1028
9	0	0	0	0	0	0	0	2	15	54	101	111	78	39	14	4	1	0	0	419
10	0	0	0	0	0	0	0	0	2	11	30	45	39	22	8	2	1	0	0	160
11	0	0	0	0	0	0	0	0	0	2	7	15	16	11	5	1	0	0	0	57
12	0	0	0	0	0	0	0	0	0	0	1	4	6	5	2	1	0	0	0	19
13	0	0	0	0	0	0	0	0	0	0	0	1	2	2	1	0	0	0	0	6
14	0	0	0	0	0	0	0	0	0	0	0	0	0	1	0	0	0	0	0	1
15	0	0	0	0	0	0	0	0	0	0	0	0	0	0	0	0	0	0	0	0
Sum	68	623	2446	5712	9576	12 799	14 513	14 454	12 849	10 225	7256	4570	2554	1285	594	263	117	52	45	100 001

Figure H.1: Joint frequency of significant wave height and spectral period. Representative data from the northern North Sea, Faltinsen (1990).